A SYSTEMS ANALYSIS METHODOLOGY FOR DEVELOPING SINGLE EVENT NOISE ABATEMENT PROCEDURES

by

John-Paul Barrington Clarke

S.B., Aeronautics and Astronautics, Massachusetts Institute of Technology, 1991
S.M., Aeronautics and Astronautics, Massachusetts Institute of Technology, 1992

Submitted to the Department of Aeronautics and Astronautics
in partial fulfillment of the requirements for the degree of

Doctor of Science

at the
Massachusetts Institute of Technology
February 1997

Signature of Author_____
Department of Aeronautics and Astronautics
January, 1997

Certified by _____
R. John Hansman, Jr., Ph.D.
Professor of Aeronautics and Astronautics
Chair, Thesis Committee

Certified by _____
Robert W. Simpson, Ph.D.
Professor of Aeronautics and Astronautics, Emeritus

Certified by _____
Ian A. Waitz, Ph.D.
Associate Professor of Aeronautics and Astronautics

Certified by _____
Robert Fricke, Ph.D.
President, Fidge Consulting Group

Accepted by_____
Jaime Peraire, Ph.D.
Associate Professor of Aeronautics and Astronautics
Chair, Department Graduate Committee

A SYSTEMS ANALYSIS METHODOLOGY FOR DEVELOPING SINGLE EVENT NOISE ABATEMENT PROCEDURES

by

John-Paul Barrington Clarke

Submitted to the Department of Aeronautics and Astronautics
in partial fulfillment of the requirements for the degree of
Doctor of Science

ABSTRACT

Advanced flight guidance technologies such as Area Navigation (RNAV) utilizing the Global Positioning System (GPS) offer the potential to reduce the impact of aircraft noise in communities surrounding airports by enabling more flexible approach and departure procedures that reduce noise exposure to the most sensitive areas. This thesis presents a system analysis methodology that incorporates the impact of aircraft noise as a consideration in the design of approach and departure procedures.

The primary tool used in the systems analysis is NOISIM. This tool combines a Flight Simulator, a Noise Model, and a Geographic Information System (GIS) to create a unique rapid prototyping environment in which the user can simulate an aircraft's operation in existing and potential guidance and navigation environments, while simultaneously evaluating the aircraft's noise impact. NOISIM provides a user interface that accurately simulates the interaction between the flight crew and the aircraft and the response of the aircraft to these inputs. The NOISIM GIS, created with United States Geographical Survey (USGS) Land Use and Land Cover data, and United States Census Bureau (USCB) Population Density data, is used to calculate the residential area and population impacted by aircraft noise at specific levels. The combined features of NOISIM provide an environment in which the factors that determine whether a noise abatement procedure is possible, practical, and effective may be considered simultaneously.

NOISIM was used for parametric and case studies of several approach and departure procedure options. These analyzes illustrate the unique simulation capability provided by NOISIM, and provide useful insight into appropriate implementation strategies. Studies of approach procedures indicate that a 3° Decelerating Approach provides significant noise reductions compared to the baseline Instrument Landing System (ILS) Approach, is preferred by pilots to other more complex noise abatement approaches, and allows flexibility in the design of the approach path. Studies of departure procedures indicate that the appropriate noise abatement procedure is heavily dependent on the population distribution, and must be developed on a case by case basis. In a parametric study of the Thrust Cutback Departure, it was observed that the area impacted by noise between 80 and 100 dBA could be minimized by the choice of cutback thrust level. These results illustrate the power of a tool such as NOISIM that may be used to evaluate noise abatement procedures at specific locations, and under different flight conditions.

Thesis Supervisor: R. John Hansman
Title: Professor of Aeronautics and Astronautics

In Memory Of
My Grandmother

Maude Gwendolyn Clarke
1911-1996

Acknowledgments

It isn't often that one gets an opportunity to thank one's colleagues and friends in a medium that will remain in public view, so if I commit a "faux pas" please forgive me.

Let me begin by thanking my thesis advisor Prof. R. John Hansman, the original "good guy." Without his guidance, scolding, and encouragement (one is never sure which it is), my graduate life at MIT would probably not have been as enriching as it was. I must also thank the other members of my thesis committee, Prof. Robert Simpson, Prof. Ian Waitz, and Dr. J. Robert Fricke, for their immeasurable help and guidance along the way.

I would also like to thank Dave Winer and Tom Connor of the FAA, Andy Powell and Kevin Shepherd of NASA Langley, and Nancy Timmerman of Massport. Without their support, monetary and technical, this work would not have been possible.

All the folks in the Aeronautical Systems Laboratory deserve my gratitude for making my graduate life an intellectually fulfilling experience, and most of all, tolerating my loud mouth during discussions. I hope that both the technical discussions and the random arguments will continue with the same volume and intensity.

They say that good friends are better than pocket money, and I can truly say that my friends are worth at least one million dollars each (pity I can't cash them in). Thank you all for everything. All the dinners, domino games, arguments, jokes, and parties made my life wonderful.

My family has been for me, a source of love and support. My parents, are two truly amazing people. Much of what I have achieved is due to their encouragement. My brother Mike has been a tower of strength to me, and is truly a "best friend." I would also like to thank all the members of my extended family. Knowing that I am part of a great tradition, is really a source of inspiration.

Finally, I would like to thank my wife Michelle for all the joy she has brought into my life. No words can express how much she has contributed to this thesis, and I hope that I can be as supportive to her as she was to me.

Table of Contents

List of Figures

List of Tables

1. Introduction

Advanced flight guidance technologies offer the potential to reduce the impact of aircraft noise in communities surrounding airports by allowing pilots to implement approach and departure procedures that reduce noise exposure to the most sensitive areas. This thesis presents a system analysis methodology that incorporates the impact of aircraft noise as a consideration in the design of approach and departure procedures.

1.1 Problem Statement

The impact of aircraft noise in communities is an important consideration in the siting and operation of airports [Smith, 1989; Sperry, 1978]. This is especially the case when residential communities are in close proximity to the airport. The impact of aircraft noise on a community is a function of the amplitude and frequency of the noise produced by the aircraft, the distance between the aircraft and the community, and the local atmospheric conditions. During approach and departure, the aircraft is closer to the community than in any other phase of flight. Since the intensity of noise decreases rapidly with distance, the impact that aircraft noise has on the community will largely be a function of the procedures that are employed during approach and departure.

To mitigate the impact of aircraft noise, certain airports with particularly close or sensitive communities have developed noise abatement procedures. These procedures are modified versions of existing instrument flight procedures, but are often too complex to be performed under Instrument Flight Rules (IFR) as current IFR procedures are limited by the accuracy and coverage of current guidance and navigation systems (see Appendix A). The additional guidance required to perform these noise abatement procedures is provided by the visual ground references available under Visual Meteorological Conditions (VMC).

An example of a visual noise abatement procedure is shown in Figure 1-1. This figure shows the noise abatement approach to runways 13L/R at John F. Kennedy (JFK) International Airport in New York City.

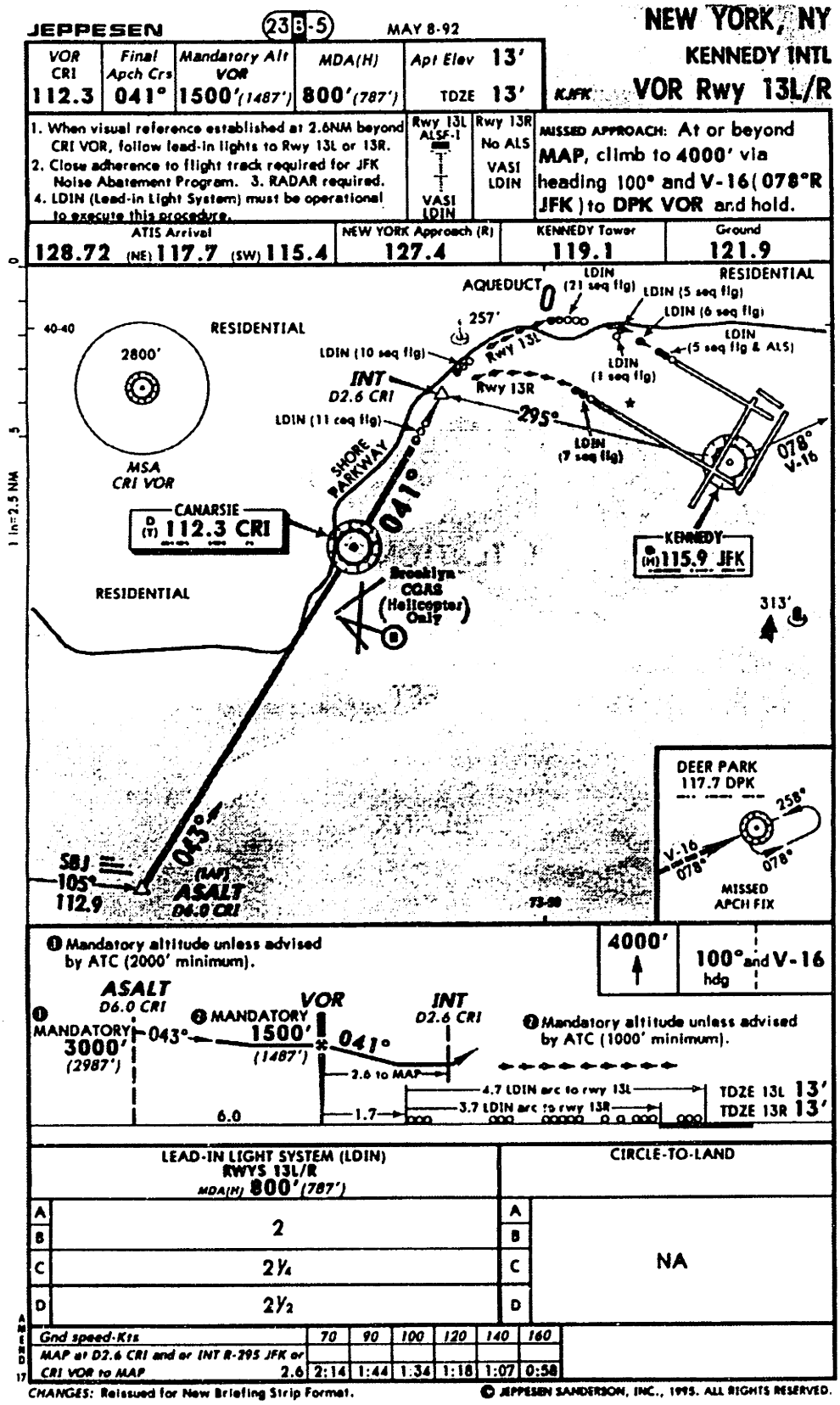

Figure 1-1: Canarsie VOR Approach to Runways 13L/R at JFK
[Reproduced With Permission of Jeppesen Sanderson Inc.; Not For Navigation]

This approach is often referred to as the "Canarsie VOR Approach," because the Canarsie VHF Omni-Range (VOR) navigation aid provides lateral guidance during the initial phases of the approach. During the final phases of the approach, special lead-in lights provide the visual references required to complete the descending turn to the runway. This approach procedure is designed to avoid densely populated residential communities near the airport by flying a tightly curved trajectory that keeps the aircraft as close to Jamaica Bay as possible. The minimum decision altitude (MDA) and visibility for this procedure are indicated at the bottom of the figure. The Canarsie VOR Approach may only be performed under VMC with the ceiling greater than 800 ft. and the visibility greater than 2 nautical miles. During departures from runways 33L/R, the reciprocal runways to runways 13L/R, aircraft perform a noise abatement departure which follows a similar ground track to the Canarsie VOR Approach. Aircraft executing this noise abatement departure turn towards the Canarsie VOR soon after takeoff to avoid the same residential communities as the approach procedure.

Figure 1-2 shows the noise signature around JFK. The marked locations in the figure represent schools or locations scheduled for school construction. The noise impact is depicted in the figure by the shaded regions surrounding the airport. Each region represents noise in two Noise Exposure Forecast (NEF) ranges. The lighter region represents community areas impacted by noise in the 30-40 NEF range, while the darker region represents community areas impacted by noise in the 40-50 NEF range. The noise impact of the Canarsie VOR Approach and Departure can be seen by the curved region in the top-left quadrant of the figure. As the figure shows, many schools are exposed to noise in the 30-40 NEF range. If the Canarsie VOR Approach and Departure Procedures were not used, many of the schools now impacted by noise in the 30-40 NEF range would be impacted by noise in the higher intensity 40-50 NEF range.

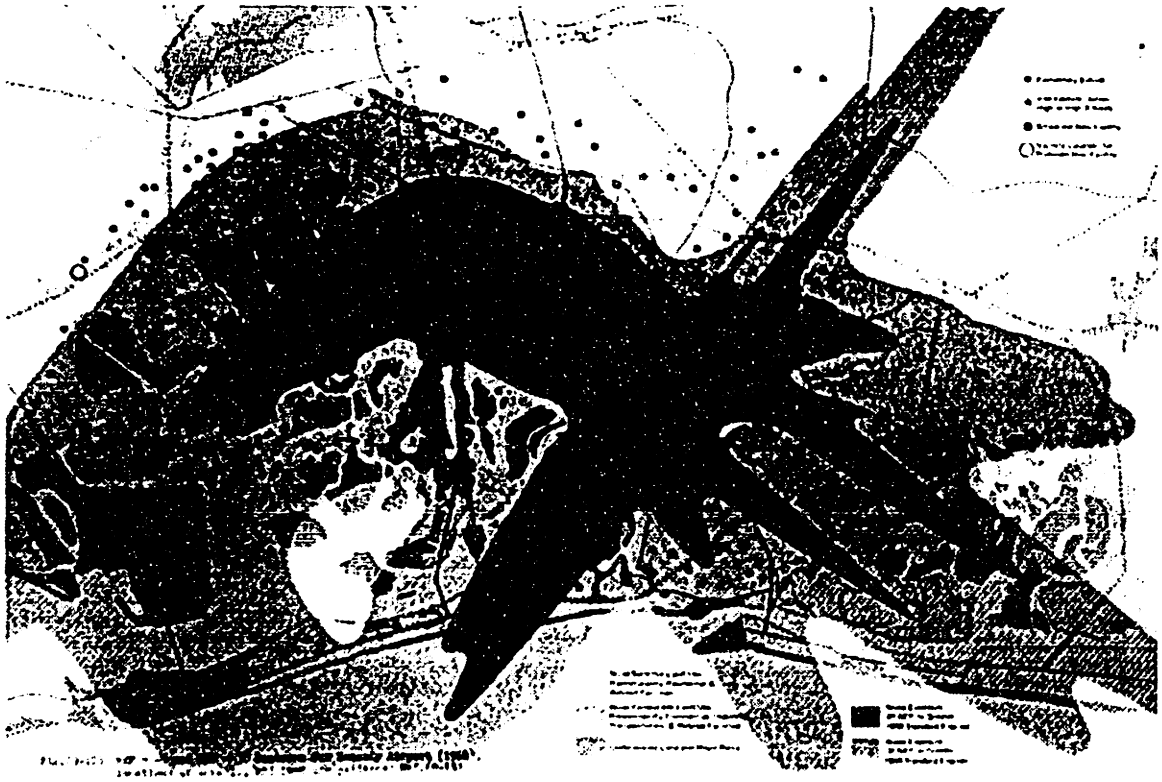

Figure 1-2: Noise Signature Around JFK Airport [Kerrebrock, 1992].

1.2 Technological Opportunity

Recent advances in guidance and navigation technology have given the cockpit crew unprecedented capabilities in the IFR environment (see Appendix B). Area navigation (RNAV) allows pilots to create trajectories using a series of arbitrary reference points or waypoints. The Global Positioning System (GPS) provides accurate position estimates at any location around the world. In combination, these capabilities enable more flexible trajectories that may be adjusted for noise considerations.

The Federal Aviation Administration (FAA) has selected GPS to be the primary means of navigation within the United States after 1998. The accuracy (and thus navigational precision) of GPS varies in time due to factors such as the geometry of the satellites used to calculation position, the deliberate degradation by the system operators to limit the accuracy available to civilian users, and the degradation of the signal by atmospheric effects. At the most basic level, the lateral accuracy of GPS is 100m. Two schemes have been developed to augment the accuracy of GPS within a specific region. The first level of GPS augmentation, the Wide Area Augmentation System (WAAS), is expected to

have 5m accuracy. The second level of augmentation, the Local Area Augmentation System (LAAS) is expected to have 1m accuracy [van Grass et al., 1994; Romrell et al., 1996].

The International Civil Aviation Organization (ICAO), of which the United States is a member state, has recognized the potential benefits of using advanced flight guidance technology to reduce the impact of aircraft noise. ICAO has charged its Noise Abatement Operating Measures Subgroup (NAOMSG) with the following tasks [ICAO, 1993]:

1. Describe effective existing noise abatement operational procedures and strategies.
2. Evaluate the critical components of aircraft flight procedures that can minimize source noise emissions and community exposure.
3. Identify emerging and future airport systems technologies in the fields of flight management, ATC and airport capacity which could also serve to minimize community noise exposure.
4. Conceive new operating procedures to reduce community noise exposure taking account of the emerging and future technologies identified in 3.

This thesis provides a partial response to these tasks.

1.3 Previous Work

1.3.1 Noise Abatement Procedures

Noise abatement procedures have been developed primarily at airports where the population distribution provides an obvious noise abatement solution such as directing the aircraft over a large unpopulated region like a bay or a large river. Many of these procedures are limited to visual conditions because traditional guidance and navigation systems cannot provide the flexibility required to achieve the desired noise benefits while maintaining safety.

Other noise abatement procedures are modifications to standard instrument procedures, and must be designed to meet the constraints placed on them by the guidance and navigation system that is used during the procedure. During departure for example, any noise abatement procedure designed for aircraft that use heading guidance is restricted to a single turn [FAA, 1976]. This limits the applicability of noise abatement procedures for

aircraft using heading guidance to airports where there is an area of low noise sensitivity that may be approximated by one or two straight line segments.

Previous work has shown that significant noise benefits may be achieved during approach by increasing the descent angle of the aircraft [Denery et al., 1975]. The result of that study also showed that the varying performance characteristics of aircraft presents several operational challenges. Other noise abatement strategies have also been studied, but none have found wide acceptance because of operational considerations or restrictions.

1.3.2 Integrated Noise Model

The existing standard for determining the impact of aircraft noise at and around airport is the Integrated Noise Model (INM). This model, developed by the FAA, estimates the average noise exposure at airports over extend periods such as a day or year [Flythe, 1992]. INM is designed as a planning tool to help airport operators dec .de on the appropriate runway configurations to use given a specific mix of aircraft types operating from that airport. INM uses typical approach and departure profiles, empirical in-flight noise data, a user specified mix of aircraft types, and a user specified number of operations, to predict the average impact.

Previous work has shown that the noise impact of a flight procedure is heavily dependent on the detailed characteristics of an aircraft's trajectory [Garbell, 1990], so the primary requirement of a design methodology is the ability to accurately predict the noise impact of new trajectories. The ability of INM to satisfy this requirement is limited by two of it's features. Firstly, INM determines the noise impact using empirical in-flight noise data, so the noise impact of trajectories that are outside the range of trajectories stored in the INM data base must be extrapolated. Secondly, the trajectory of an aircraft can only be described by a limited number of straight line segments. Although the fidelity of INM is useful for planning purposes, these limitations prevent its use in the design and development of new or modified noise abatement procedures.

The need exists therefore, for a methodology to evaluate the effectiveness of proposed noise abatement procedures and, because of the importance of the details of the trajectory, the variation in the noise impact with changes in different flight parameters. To accomplish both of these goals, the design methodology must include aircraft and noise modeling capabilities that can be used in combination to evaluate the noise impact of single approaches and departures (events).

1.4 Scope and Goal of Thesis

This thesis seeks to address the need for a methodology to develop and evaluate the noise impact and operational characteristics of single event noise abatement procedures. The methodology developed draws on the principles of systems analysis, to create tools that may be used in the development and evaluation of these procedures.

This document is divided into seven chapters:

- Chapter 2 gives background on the noise metrics that are used in the thesis.
- Chapter 3 outlines the methodology that was developed.
- Chapter 4 presents an analysis of departure procedures.
- Chapter 5 presents an analysis of approach procedures.
- Chapter 6 presents an analysis of missed approach procedures.
- Chapter 7 summarizes the results of the thesis and suggests areas for future work.

2. Noise Metrics

At any location and instant in time, a complete sound measurement is given by the sound spectra or the mean squared acoustic pressure as a function of frequency. The typical human "hears" sounds in the 20 to 20,000 Hz frequency range. The loudness of a sound depends greatly on the frequency content of that sound, as the sensitivity of the ear varies with frequency. Because of the variation in the sensitivity of the ear, noise of equal pressure at two different frequencies may appear to the listener to be of different loudness.

2.1 Location Specific Metrics

There are a number of metrics that are used to measure the impact of noise at a particular location. These metrics fall into two broad categories. The first category contains metrics that measure the peak instantaneous noise level, while the second category contains metrics that have some correction for the effects of duration. Typically, a metric that measures the peak instantaneous noise level will have a corresponding duration metric which uses the same criteria but with an additional component that incorporates the effects of duration.

The most basic metric is the Sound Pressure Level (SPL). The SPL is ten times the log of the ratio between the sum of the measured mean squared acoustic pressures at all frequencies and the square of the reference acoustic pressure $2 \times 10^{-5}\, N/m^2$. The relationship between the SPL and the acoustic pressure is given by

$$SPL = 10 \cdot \log_{10}\left(\frac{\int_0^{\infty} [P(f)]^2}{[2 \times 10^{-5}]^2} \right), \tag{2-1}$$

where f is the frequency in hertz (Hz), and the SPL is measured in units called decibels (dB).

The fundamental metric used in this thesis is the A-Weighted Sound Pressure Level (AL or L_A). The unit of this metric is also the decibel, but is written as dBA to indicate that the value has undergone an A-weighting. The A-weighting was developed to account for the response of the human ear to noise at different frequencies. In the A-weighting, sound at frequencies where the response of the ear is good is weighted more heavily than sound at frequencies where the response of the ear is poor. Figure 2-1 show the A-weighting versus frequency. As the figure shows, noise between 1,000 and 6,300 Hz are emphasized while noise outside this range are de-emphasized.

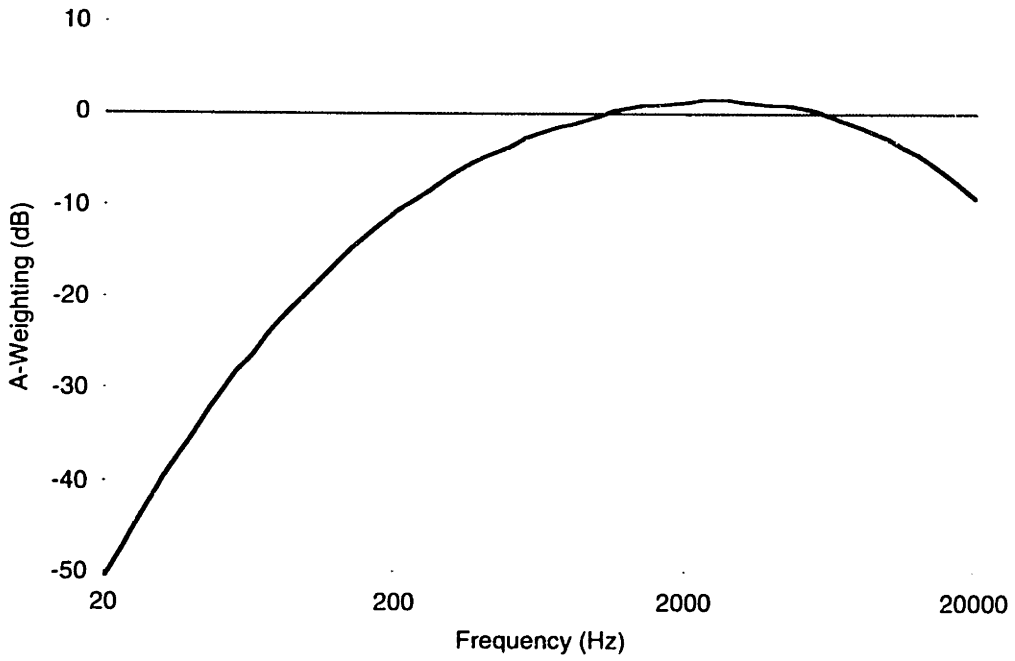

Figure 2-1: A-Weighting versus Frequency.

The weighting values were determined from studies of the relative loudness of noise of equal intensity but different frequency. Research has shown that the A-weighting works well for loudness comparisons at all levels, and is the most widely used for rating sounds at all levels [Ruijgrok, 1993]. It has also been determined that the relationship between the A-weighted sound pressure level and the perceived noise level (the other commonly used measure of peak noise in aviation) may be closely approximated in most cases by

$$L_A = L_{PN} - 14 \text{ dB} \tag{2-2}$$

where L_{PN} is the perceived noise level.

The Sound Exposure Level (SEL or L_{AE}) is the duration counterpart of the A-weighted sound pressure level L_A, and gives some indication of the total amount of acoustic energy received during a single noise event. The SEL is given by the relationship

$$L_{AE} = 10 \log\left[\frac{1}{T_{ref}}\int_0^T 10^{\frac{L_A(t)}{10}}\, dt\right] \tag{2-3}$$

where T_{ref} is a reference time of one second.

In this thesis, the noise impact at a specific location is reported as the peak A-weighted sound pressure level.

2.2 Noise Footprints

A plot of peak A-weighted sound pressure levels in what in commonly referred to as a "noise footprint" describes the noise impact over an entire community. Figure 2-2 shows the noise footprint of the existing noise abatement departure from runway 4R at Logan Airport in Boston. The peak A-weighted sound pressure levels are shown in 10 dBA bands beginning at 60 dBA. The 60 dBA contour is the outermost boundary of the noise footprint. Each of the successively smaller boundaries represent a 10 dBA increase in the peak A-weighted sound pressure level. As the figure shows, during this departure much of the noise is directed over water. Although the footprint provides a qualitative measure of the noise impact, it cannot provide a quantitative measure. Several methods exist to determine a representative noise impact value. These methods involve weighing the area and/or the number of people impacted by different noise levels according to the results of subjective tests. Unfortunately, the impact that noise has on an individual is dependent on several factors including the amplitude of the noise, the frequency content of the noise, and the duration of the noise. Since the noise impact is spread over many different individuals in a community, and the amplitude, frequency, and duration effects vary depending on the location of that individual relative to the aircraft's trajectory, the noise impact is reported in this thesis as the area and/or the population impacted by peak A-weighted sound pressure levels within particular ranges. These values provide basic representative noise impact measures that may be interpreted by the reader using his/her own weighting scheme.

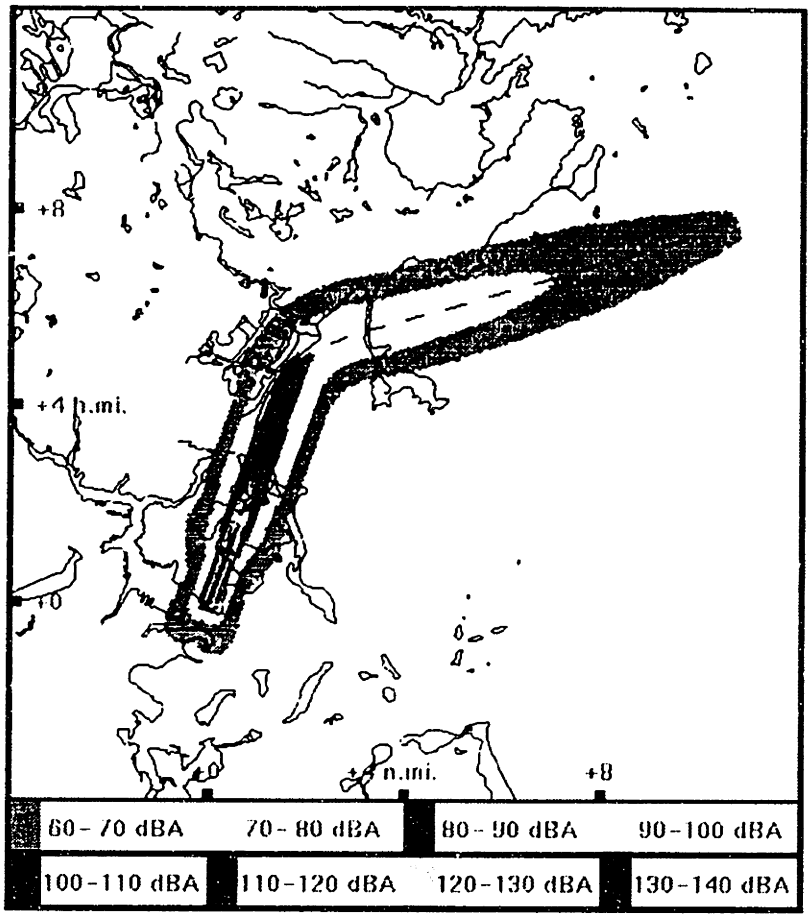

Figure 2-2: Noise Footprint of an Aircraft During Departure

2.3 Noise Thresholds

The acceptable noise level or noise threshold in a community is based on the preferences of that community. Consistent with this, many of the rationales for choosing a threshold value are subjective [Shepherd, 1994]. This thesis does not attempt to recommend acceptable noise thresholds for particular communities, but uses the results of prior studies to establish a representative threshold where aircraft noise begins to interfere with personal conversation and sleep. Most normal conversations are conducted in the 50-60 dBA range, and previous research has shown that the threshold for noise induced sleep disturbances also lies in the 50 to 60 dBA range. It has also been shown that the allowable maximum nighttime A-weighted sound pressure level can be expressed by

$$L_{A\max} = 53.16 + \frac{1}{-0.09 + 0.129N - 0.0018N^2} \tag{2-4}$$

where N is the number of events that occur [Ruijgrok, 1993]. For a single event (N=1) the maximum noise allowable nighttime noise is 80 dBA. In this thesis, 60 dBA is the threshold value above which the noise impact is evaluated. This level represents a lower limit of the threshold for sleep and conversation disturbance.

3. Methodology

This chapter presents the systems analysis methodology that was developed. The chapter begins with a definition of the "system" that was analyzed and the factors that were considered. This is followed by a description of the unique tools that form the basis of the methodology. The chapter concludes with a description of the analysis structure that was used to evaluate the methodology.

3.1 The System

In combination, the aircraft, airport, and the community form a closed system. If flight procedures are the means of operating that system, then the noise abatement procedure represents a way of operating the system with lower noise impact.

To determine the appropriate noise abatement procedure to use, it is necessary to consider several coupled factors:

- Aircraft Performance and Trajectory
- Noise Generated by the Aircraft
- Population Distribution and Density
- Flight Safety and Pilot Acceptance
- Guidance and Navigation Requirements
- Local Atmospheric Conditions

Traditionally these factors have been considered either independently or in subsets. The tools presented below provide a method of incorporating and evaluating these factors simultaneously in a rapid prototyping environment. This approach to developing noise abatement procedures incorporates the coupled relationships that exist between the factors, thus providing a comprehensive method for developing noise abatement solutions.

3.2 NOISIM

The primary tool used in the systems analysis is NOISIM. This tool combines a Flight Simulator, a Noise Model, and a Geographic Information System (GIS) to create a unique rapid prototyping environment in which the user can simulate an aircraft's operation in existing and potential guidance and navigation environments, while simultaneously evaluating the aircraft's noise impact. Figure 3-1 shows the structure of NOISIM.

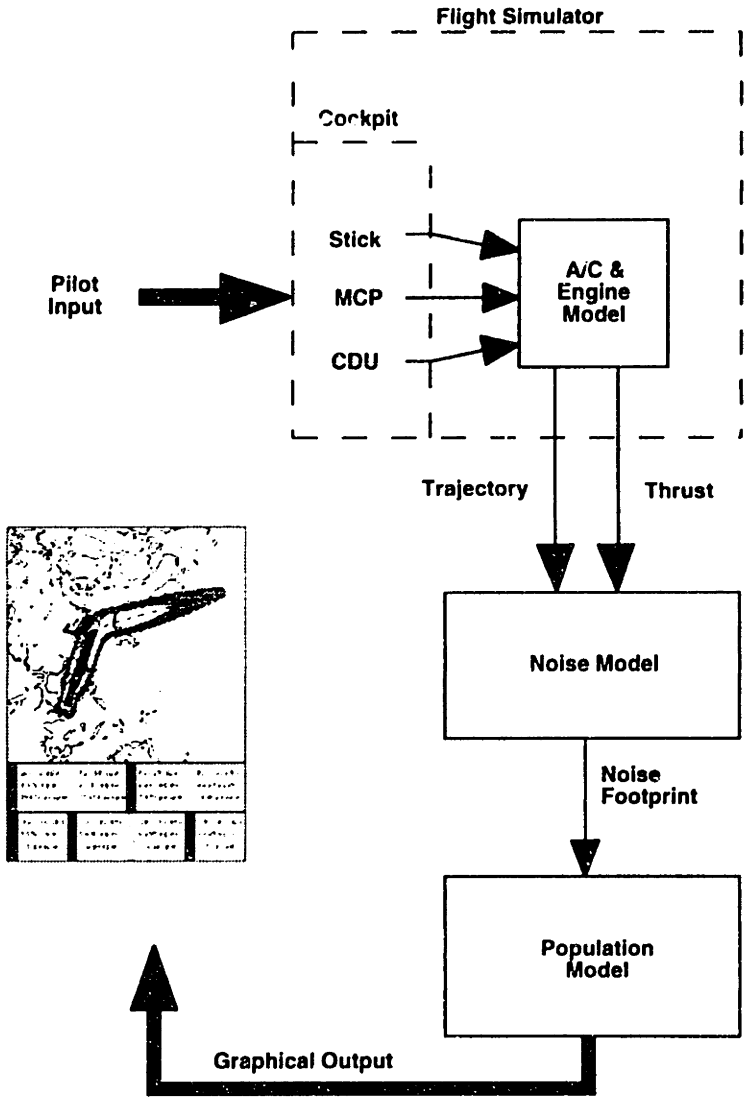

Figure 3-1: NOISIM

The figure shows how the flight simulator, noise model, and GIS are coupled together to determine the noise impact. Pilot input into the flight simulator generates trajectory and thrust profiles that are used by the noise model to determine the noise footprint of the procedure. This footprint is combined with the population distribution and density data of the GIS to determine the noise impact of the procedure. The noise footprint and noise impact are then displayed graphically.

3.2.1 Flight Simulator

The flight simulator component of NOISIM has been developed at the MIT Aeronautical Systems Laboratory using performance data from the Boeing 737 which served as the NASA Advanced Transport Operations (ATOPS) Aircraft [Hansman et al., 1993]. Figure 3-2 shows a diagram of the Flight Simulator. As can be seen, the flight simulator provides all the cockpit interfaces found in an advanced commercial aircraft. The aircraft may be controlled either manually via the sidestick, at the state level via the Mode Control Panel (MCP), or at the trajectory level via the Control Display Unit (CDU).

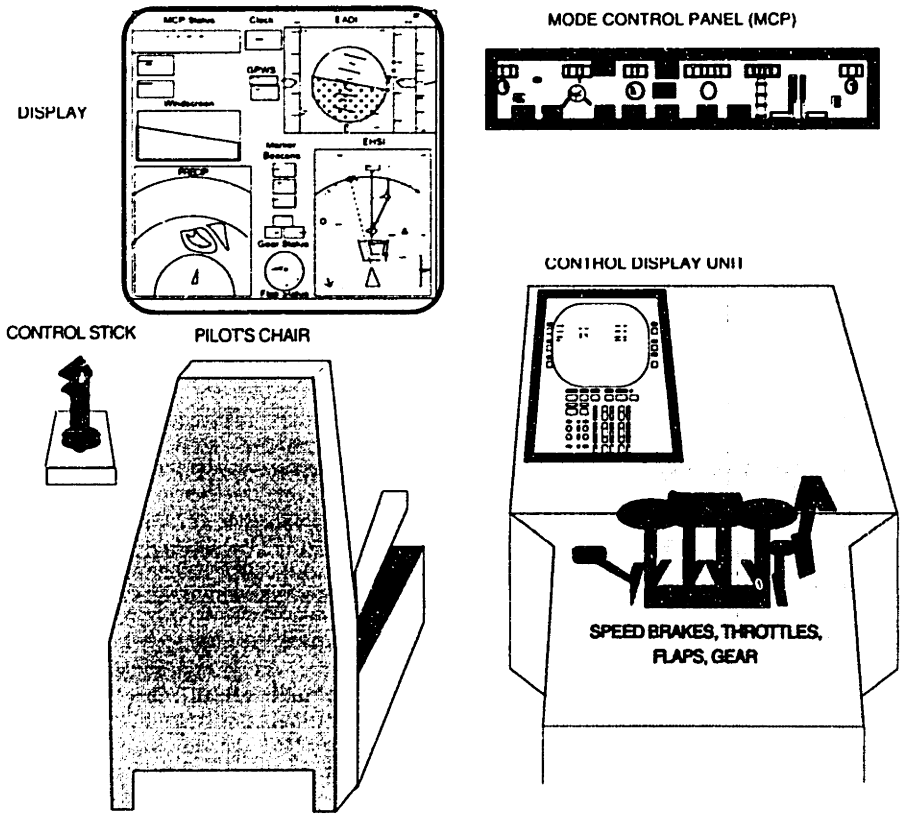

Figure 3-2: Flight Simulator

The Flight Management System (FMS) in the simulator is a software emulation of the FMS system used in many advanced commercial aircraft. The MCP is flight hardware from a Boeing 737-300. The CDU is a replica of the CDU found in the 747-400 cockpit. The response of the FMS to signals from navigation aids is also simulated. The location of these navigation aids were determined from data published by the FAA. In combination , these features allow trajectories to be flown as they would be in an aircraft. The simulator also allows the rapid prototyping of displays that may be required to perform specific procedures.

The engine modeled in the simulator is the Pratt and Whitney JT8D, the engine used on 737-200 aircraft. This engine is a two spool turbofan with mixed exhaust flows. The engine model uses a semi-iterative scheme to determine conditions at each station in the engine. Information about the engine such as the pressure matching condition for mixed flow exhausts, the relationship between the corrected mass flow through the fan and compressors as a function of rotation speed (operating line), and the corrected fuel flow as a function of rotation speed are used to reduce the number of iterations required to solve for the engine operating conditions.

3.2.2 Noise Model

The fan and jet noise generated by the aircraft is determined using the Heidmann and Stone models outlined in the NASA Aircraft Noise Prediction Program (ANOPP) Theoretical Manual [Heidmann, 1975; Stone and Montegani, 1980; Zorumski, 1982]. The fan and jet noise are modeled in one-third octave bands (tertsbands) and in one degree increments from the longitudinal axis of the aircraft. Atmospheric attenuation is modeled as a function of frequency, temperature and humidity [Ruijgrok, 1993]. Excess ground attenuation is modeled using the relationships outlined in SAE 1845 [SAE, 1986].

3.2.3 Geographic Information System

The NOISIM GIS, created with United States Geographical Survey (USGS) Land Use and Land Cover data, and United States Census Bureau (USCB) Population Density data, is used to calculate the residential area and population impacted by aircraft noise at specific levels. The Land Use and Land Cover data are obtained in the Composite Theme Grid (CTG) format [USGS, 1990]. Each grid represent a 200x200m square area on the

surface of the earth. Attributes are provided for each grid that indicate the use of the land, and the type of coverage.

3.2.4 NOISIM Output

Figure 3-3 shows a sample NOISIM output. The figure depicts the noise impact of the existing noise abatement departure from runway 4R at Logan Airport in Boston, Massachusetts. The peak A-weighted sound pressure levels observed in the community during the departure are displayed in a noise footprint overlaid on a map of the area. The lowest noise level that is presented in this example, and in this thesis, is 60 dBA.

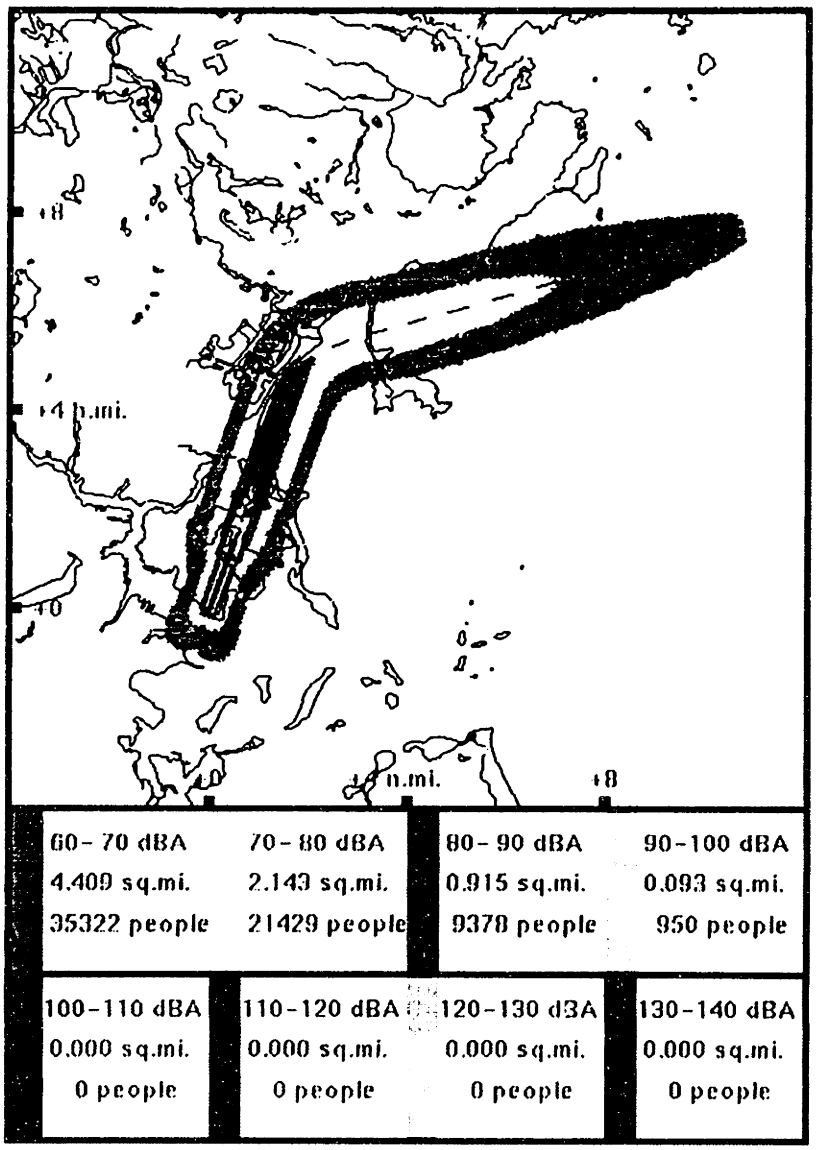

Figure 3-3: Sample NOISIM Output

The values at the bottom of the figure represent the residential area and the number of people impacted by noise in selected noise ranges. Parameters such as the scale of the map, minimum sound pressure level displayed, and size of the sound pressure level bands may be selected by the user. In addition, other metrics may be easily added by the user, as the complete noise spectra in tertsbands is calculated. The combined features of NOISIM create a unique environment in which all the factors that determine whether a noise abatement procedure is possible, practical, and effective, may be considered simultaneously. The noise impact results presented are representative of realistic flight conditions, population distributions, and population densities. Further details of NOISIM are presented in Appendix C.

3.2.5 NOISIM Validation

The noise impact calculated by NOISIM for the departure from runway 4R at Logan Airport was compared to noise measurements for the same aircraft and engine type (737-200 with JT8D engines) at two noise monitoring stations operated by the Massachusetts Port Authority (Massport) [Timmerman, 1993]. The results of that comparison are shown in Table 3-1. As the table shows, the calculated peak noise levels are in agreement with the measured levels.

Table 3-1: Peak A-weighted Sound Pressure Levels at Two Massport Noise Monitoring Stations (Measured and Calculated).

	Measured	NOISIM
Peak Noise at Station 1 (dBA)	96	95.6
Peak Noise at Station 2 (dBA)	91	90.4

The time history of the unweighted sound pressure level at station 1 was also compared. The results of that comparison is shown in Table 3-2. As the table shows, the time history of both the measured and calculated sound pressure levels are in agreement.

Table 3-2: Time History of Peak A-weighted Sound Pressure Levels at a Single Massport Noise Monitoring Station (Measured and Calculated).

	Measured	NOISIM
Time Noise > 90 dB (sec)	5	6.7
Time Noise > 80 dB (sec)	18	18.9

It should be noted that NOISIM was validated for a limited number of cases, and its accuracy may not be as good as indicated in Tables 3-1 and 3-2.

3.3 Noise Boundaries

Certain noise sensitive communities have established maximum noise levels for aircraft operation. A method has been developed to define a virtual region around the noise sensitive community, such that if an aircraft is outside this region, the noise level at all points in the noise sensitive community will not exceed the maximum allowed level. The surface of this region is the "Noise Boundary" for that noise sensitive community. This boundary is determined *a priori*, and defines the region in space (similar to terrain) from which aircraft must be excluded. Figure 3-4 shows an example of a noise boundary along the departure path of an aircraft. Since aircraft cannot penetrate the noise boundary, trajectories must either climb or turn to avoid the region.

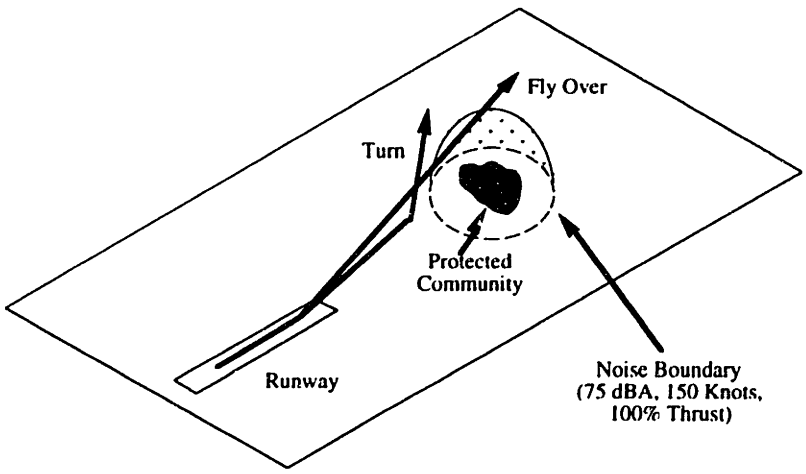

Figure 3-4: Example of Noise Boundary

These noise boundaries are developed using the principles of acoustic reciprocity and linear superposition. This approach to the noise problem may be utilized in cases where

there are specific location that must be protected from noise in preference to other locations. This method was not used in the analyses performed in this thesis, as the cases selected for study did not require its use. However, a detailed description of the method is presented in Appendix D.

3.4 Structure of Analysis

The analyses presented in the following chapters illustrate the unique simulation capability provided by NOISIM, and provide useful insight into appropriate implementation strategies. Approach, departure, and missed approach procedures were analyzed independently, and are presented in separate chapters. Each analysis was divided into two phases. In the first phase, generic studies were done to quantify the relative benefits of the available noise abatement options. In the second phase, case studies were performed to address the issues and constraints that are specific to a particular airport or group of airports. The results and insights gained during the generic studies were utilized in the cases studies.

4. Analysis of Approach Procedures

This chapter presents an analysis of approach procedures. The first section presents a generic study of three approach procedures. The second and third sections present case studies of approaches to two major metropolitan airports. All three studies illustrate how NOISIM may be used in both generic and site specific analyses.

4.1 Generic Study of Approach Procedures

This section presents the results of a generic study of three approach procedures: the baseline ILS Approach, the Vertically Segmented Approach, and the 3° Decelerating Approach. The Vertically Segmented Approach and the 3° Decelerating Approach are noise abatement procedures. In the study, the noise impact of all three procedures was evaluated. Pilot acceptance of the noise abatement procedures was also evaluated, and the noise abatement approach that provided the best combination of noise reduction and pilot acceptance was determined.

The aircraft simulated in the analysis was a 737-200 with two JT8D turbofans. The weight of the aircraft was assumed to be 90,000 lb. and the atmospheric conditions were assumed to be the same as those in the standard U.S. atmosphere.

4.1.1 ILS Approach

The ILS is the primary means of landing guidance in commercial aircraft. Although the ILS is designed to provide guidance in low visibility, commercial aircraft typically perform the ILS Approach regardless of the weather conditions. Figure 4-1 shows an example of the approach profile for an aircraft using ILS guidance. The ILS Approach is divided into three segments: the initial approach, the intermediate approach, and the final approach.

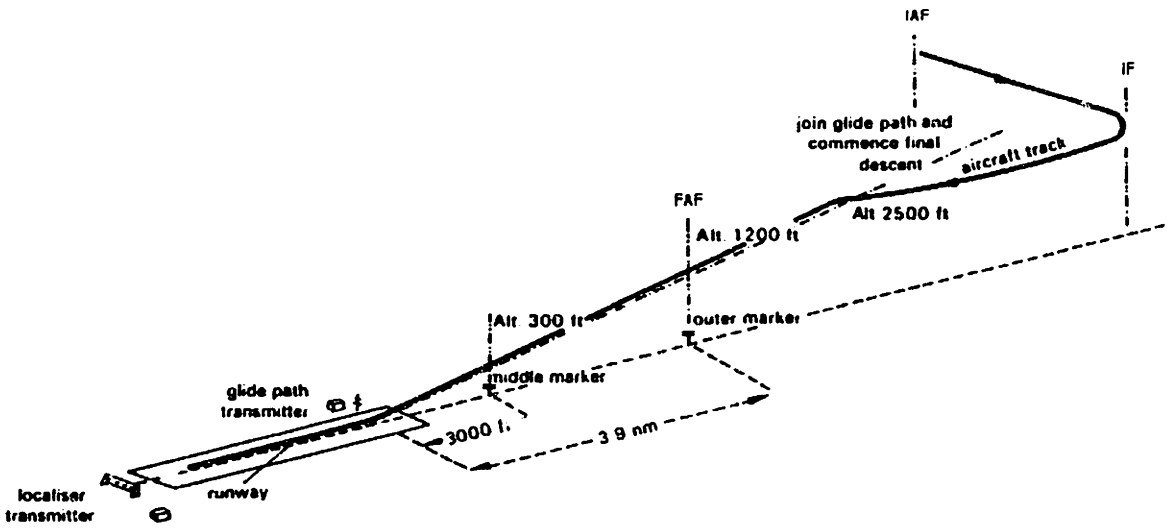

Figure 4-1: Approach Profile with ILS Guidance [Kendal, 1987]

The final approach segment is the segment preceding touchdown, where the aircraft is descending the 3° glide slope to the runway. The Final Approach Fix (FAF) marks the start of the final approach segment and the end of the intermediate segment. The farthest the FAF can be from the runway is the point where the aircraft intercepts the glide slope. Often times however, the FAF is located closer to the runway at the location of the Outer Marker (OM) Beacon. Marker beacons broadcast vertical signals at known locations along the final approach segment. The OM is the farthest such beacon from the runway. A second beacon, the Middle Marker (MM) is placed between the OM and the runway. At some airports, a third beacon, the Inner Marker (IM), is placed between the MM and the runway. These signals provide audible and visible cues to the flight crew. Pilots use these cues to cross check the aircraft's altitude versus distance to the runway. They also provide cues to the flight crew to abandon the approach if the runway is not visible. The exact location of each beacon is related to the accuracy of the particular ILS in use and local geography

The intermediate segment is the segment immediately preceding the FAF where the aircraft is flying along the extended centerline of the runway and adjusting its configuration and speed for the final approach segment [FAA, 1976]. The Intermediate Fix (IF) marks the start of the intermediate segment and the end of the initial approach segment. Aircraft typically decelerate to an intermediate speed which they maintain until they reach the FAF.

The initial approach segment is the segment immediately preceding the IF. The start of the initial approach segment is indicated by the Initial Approach Fix (IAF). The initial approach is often at some angle relative to the intermediate segment. The initial approach segment is the preferred routing by which aircraft are brought into the area of ILS coverage.

The ILS consists of two independent and orthogonal beams that are used for lateral and vertical guidance. Both beams combine to provide guidance within a narrow angular corridor centered on a nominal final approach path inclined at 3° to the plane of the runway (Figure 4-2). The lateral guidance is provided by the localizer and the vertical guidance is provided by the glide slope. The localizer provides guidance along the intermediate and final approach segments, while the glide slope only provides guidance along the final approach segment. The localizer provides guidance in the region which extends 2 degrees to the right and 2 degrees to the left of the extended centerline. The glide slope provides guidance in the region which extends 0.7 degrees above and 0.7 degrees below the final approach path.

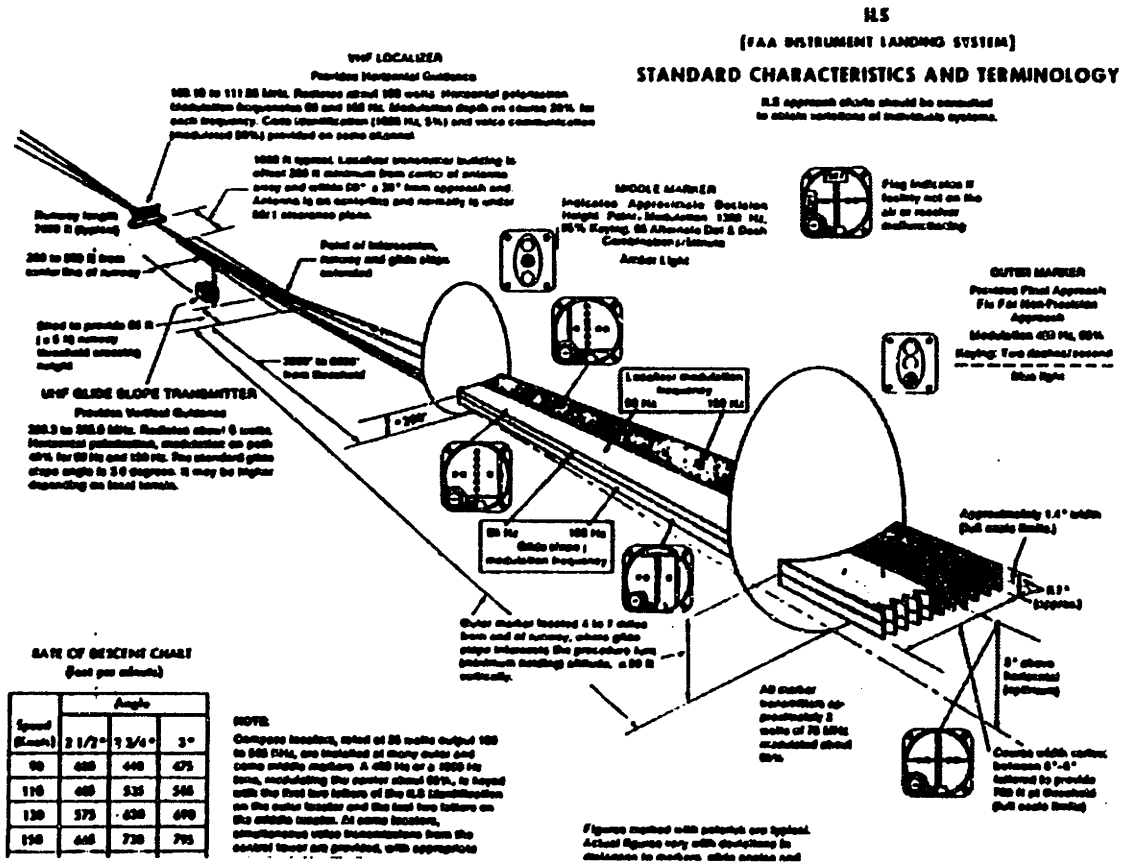

Figure 4-2: Instrument Landing System [FAA, 1994b]

The construction of the ILS has a significant effect on the noise impact of aircraft that use the system for approach guidance. Figure 4-3 shows the details of the ILS construction. The glide slope is composed of two signals of distinct frequency but equal strength. One signal has a frequency of 90 Hz and the second signal has a frequency of 150 Hz. The difference in frequency modulation is used by an onboard receiver to determine the angular deviation from the desired path. The signals are constructed so that when the aircraft is on the desired path, it is half way between the two signals and will receive equal modulation from each. As the aircraft deviates from the desired path, it will receive more modulation of one frequency than another. The difference in the amount of modulation from each signal is correlated to the angular deviation from the desired path, and thus may be used as a measure of that deviation.

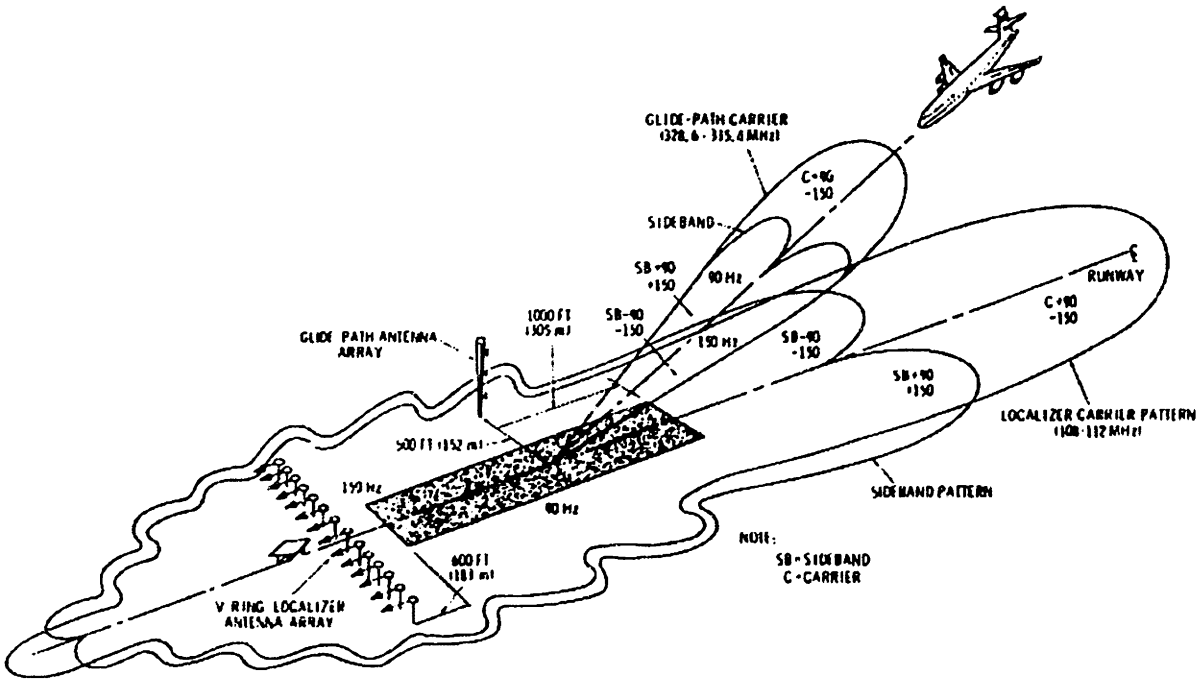

Figure 4-3: Composition of the ILS [?]

Although the glide slope is designed with only two signals, the presence of a ground plane directly below it causes some radiation to be reflected above the nominal approach path. If the path that the aircraft is on is an integer multiple of the nominal approach path (6°, 9°, 12°, etc.), the pathology of the glide slope is such that the ILS receiver onboard the aircraft will indicate that the aircraft is on the nominal approach path. In Figure 4-4 for example, aircraft located at point A and point B would indicate no path deviation.

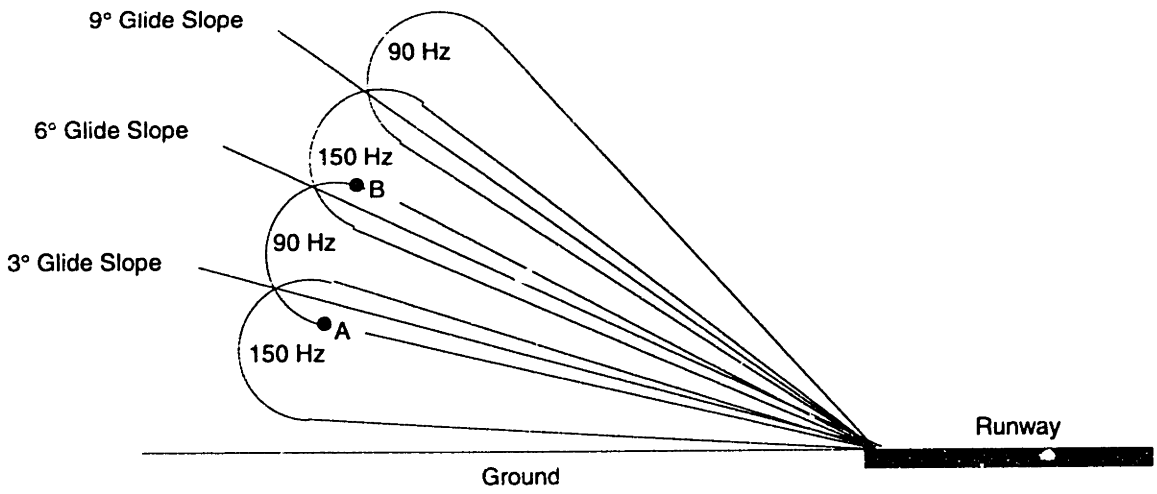

Figure 4-4: Secondary Glide Slopes due to Reflections from Ground.

To prevent confusion, aircraft are required to intercept the glide slope from below so that the 3° nominal path is always the first path that the aircraft encounters. This 3° path is referred to as the "true" glide slope and the other paths are referred to as "false" glide slopes. A typical glide slope signal extends to 3,000 feet above the extended centerline of the runway at a distance of 10 nautical miles from the runway threshold, so the glide slope construction forces aircraft closer to the communities along the approach path to the runway. Although the thrust levels are lower than during departure, the close proximity to the ground required by this procedure causes significant noise impact on those communities along the approach path.

The ILS construction also impacts the lateral trajectory of an aircraft during approach. At many airports, air traffic controllers vector aircraft to intercept the localizer at some point between the intermediate fix and the final approach fix (Figure 4-5). To satisfy the requirement that the aircraft intercept the glide slope from below, the aircraft descends to the altitude at which it will intercept the glide slope before commencing the turn. This increases the time the aircraft spends at low altitude and the thrust of the aircraft, thus also increasing the noise impact.

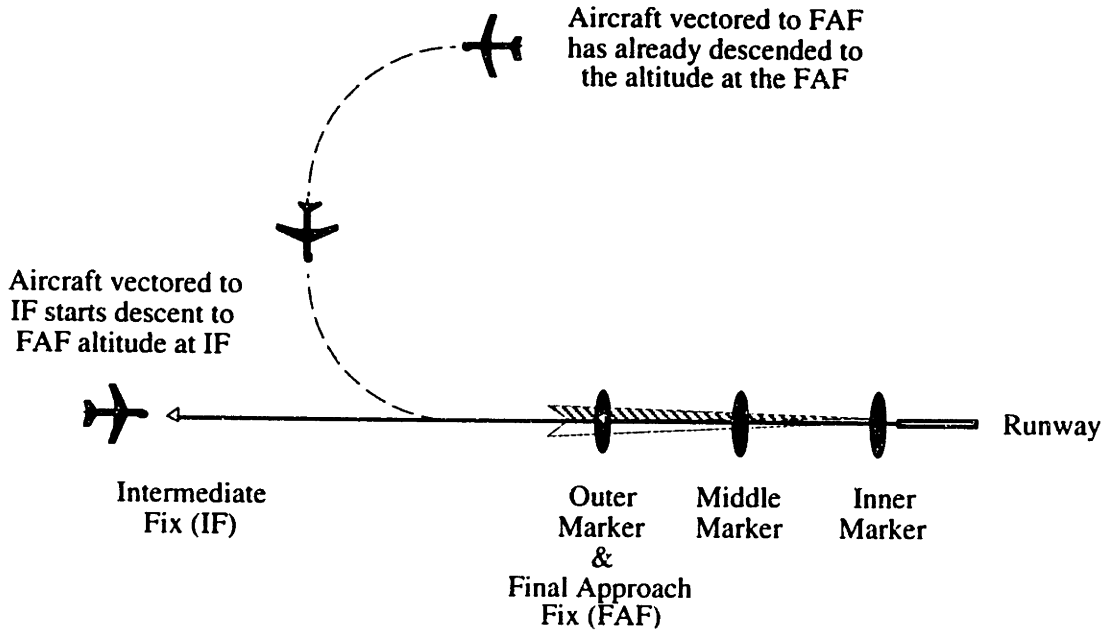

Figure 4-5: Low Altitude Vectoring of Aircraft.

4.1.2 Vertically Segmented Approach

Previous work has indicated that significant noise benefits may be achieved through the use of a Vertically Segmented Approach [Denery et. al., 1975]. In this procedure, the aircraft descends at a steeper than normal angle (greater than 3°) and intercepts the 3° glide slope from above. This approach varies both the angle of descent and the thrust. Increasing the angle of descent increases the aircraft's height above the ground at all points along the track before the point where the aircraft intercepts the 3° glide slope. This increases the distance between the aircraft and the community. The steeper descent also reduces the thrust required, thus reducing the noise produced by the aircraft.

Figure 4-6 shows the profile of the Vertically Segmented Approach that was evaluated in this study. As the figure shows, the transition between the first and second segments occurs at 1,000 ft. above the runway, and the first segment of the approach is a 5° descent. The 1,000 ft. height for the transition between segments was selected based on the results Denery's work and pilot interviews. The 5° first segment descent angle was selected to increase the number of aircraft that could descend at that angle in the minimum certified landing flap setting, and to prevent the aircraft from entering the sensitive range of the 6° false glide slope.

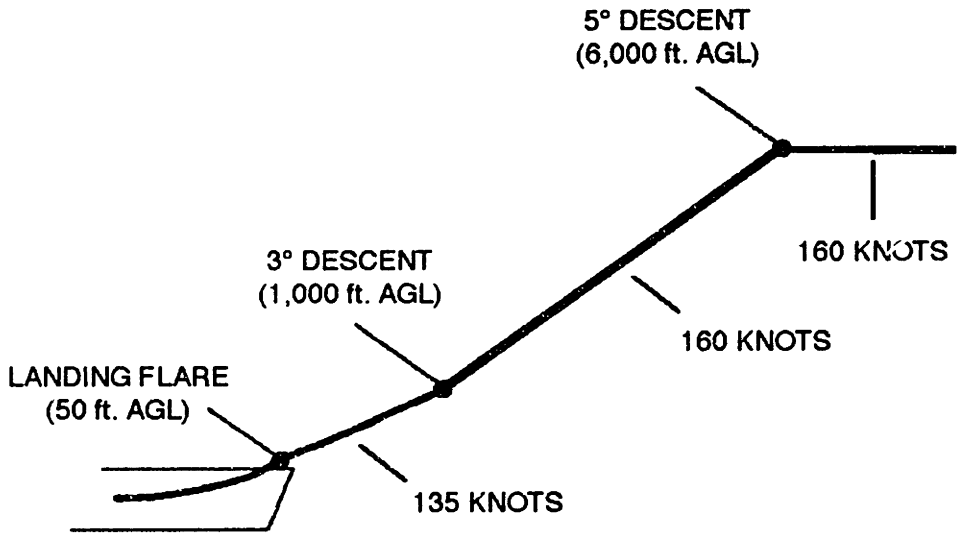

Figure 4-6: Vertically Segmented Approach.

Studies by Denery et al. concluded that one of the challenges faced by the Vertically Segmented Approach is the limited descent performance of some aircraft. In those studies, it was determined that the lowest descent angle of the aircraft in service at that time (1975) varied between 3.0° and 7.5°. These results were based on the assumption that the aircraft would descend the first segment in zero winds with its flaps at the minimum landing flap setting, its landing gear extended, and with a 1° to 2° margin included for flight path control. For aircraft with a descent angle shallower than 5°, a 5° descent could be maintained either through a greater than minimal landing flap setting or by eliminating the 1° to 2° flight path control margin. In a tailwind or in icing conditions however, these aircraft would be unable to maintain the required 5° descent. To provide adequate margins for tailwinds, wind uncertainties, and icing conditions, these aircraft would be required to descend at a shallower angle from further away to intercept the 3° segment at the same location. Unfortunately, these aircraft would be traveling through the wake vortices created by aircraft on the 5° descent as wake vortices propagate down and away from an aircraft. To prevent wave vortex interactions, the separation requirements would need to be increased. Increasing the separation requirements would decrease the landing rate.

A second challenges faced by the Vertically Segmented Approach is the ability of the flight crews to distinguish between the false glide slopes and the true glide slope. In flight tests performed by Denery et al., this difficulty was overcome by installing special indicator lights that were triggered using altimeter information. Although the RNAV-

GPS structure could eliminate the need for special equipment, the continued presence of the ILS in the cockpit could create confusion for the flight crew.

In the Vertically Segmented Approach evaluated, the aircraft intercepts the 5° first segment 6,000 feet above the runway at a speed of 160 knots, 25 knots above the final approach speed of 135 knots. The aircraft maintains that speed until it intercepts the 3° second segment at 1,000 ft. above the runway altitude. During the transition to the second segment, the speed is reduced to the final approach speed. All thrust changes during the transition are performed by the autothrottles. The higher speed during the first segment and the speed reduction in the transition was included in the procedure to avoid the rapid thrust increase that would be required to maintain the same speed throughout the transition.

4.1.3 Decelerating Approach

In the standard ILS Approach, the aircraft flies along the extended centerline of the runway at low altitudes for extended periods. As previously outlined, the primary reasons for this are the range and construction of the ILS. Because the RNAV structure is not restricted in this way, it may be used to create a straight or curved approach path that is outside the range of the ILS. If the aircraft begins its decent to the runway along a 3° descent path (straight or curved) at a higher altitude and at higher speeds than the ILS Approach, the speed reductions that are usually performed during the intermediate approach segment can be achieved during the descent by reducing the thrust to idle, maintaining a constant 3° flight path angle, and allowing the drag forces to decelerate the aircraft.

Figure 4-7 shows the profile of the 3° Decelerating Approach that was evaluated. In this approach, the aircraft intercepts a virtual glide slope 6,000 feet above the runway at a speed of 250 knots. During the transition to the 3° descent path, the thrust is set to idle and the aircraft is allowed to decelerate during the descent. The first three flap extensions (5°, 10°, 15°) are performed at 15 knots below the maximum speed allowed for the new flap setting, while the other flap extensions (20°, 25°, 30°) are performed at 10 knots below the maximum allowed speed. No slats or speed brakes were used during this approach. The landing gear is extended at the same time that the final flap extension is performed. The final approach speed of 135 knots is achieved 500 ft. above the runway. At that time, the autothrottles re-engaged and the remainder of the final approach

proceeds as normal. For the evaluation, the approach was constructed using two waypoints.

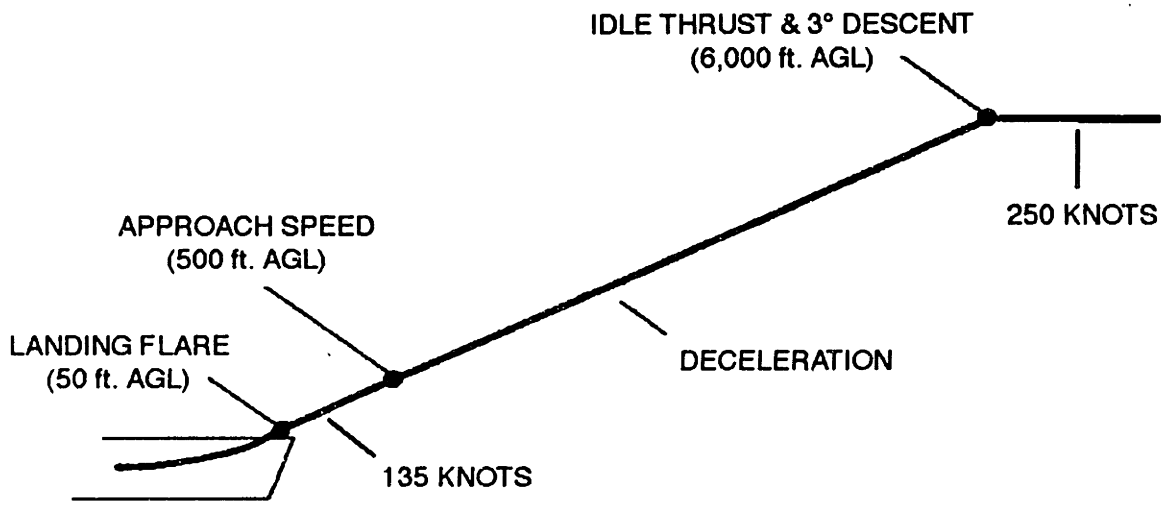

Figure 4-7: 3° Decelerating Approach

Unlike the Vertically Segmented Approach, the 3° descent is well within the operational envelope of all aircraft, and has adequate margins to deal with wind uncertainties. In the 3° descent, the flight crew can compensate for the tailwind by decreasing the pitch of the aircraft to maintain the desired 3° descent, and performing a more aggressive flap extension schedule to maintain the deceleration rate. They may also use speed brakes to decelerate the aircraft. In a headwind, the flight crew can increase the pitch of the aircraft to maintain the 3° descent, and perform a less aggressive flap extension schedule to maintain the deceleration rate. They may also enter the 3° descent at a constant speed of 250 knots and delay the time that the thrust is reduced to idle to compensate for the higher deceleration rate that accompanies a headwind.

4.1.4 Noise Impact of Approach Procedures

This section presents a comparison of the noise impact of the three procedures described above. All three approaches were simulated on NOISIM using RNAV. Figure 4-8 shows the airport-community used in the study. The airport is located in the midst of an area of uniform population density. The runway threshold is situated at the boundary of the airport. The airport is assumed to be sufficiently large that all the noise produced on the airport side of the boundary at the threshold is contained within the airport.

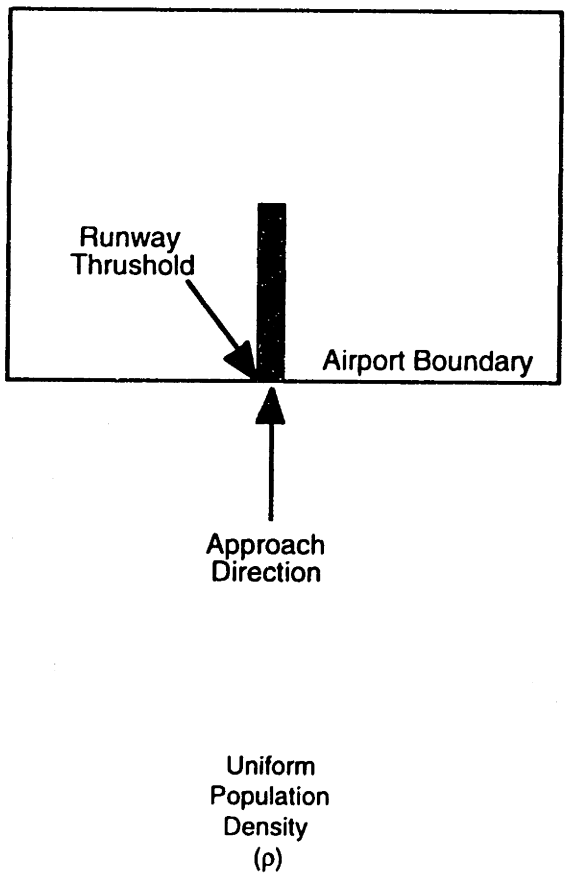

Figure 4-8: Airport-Community Geometry in Vertical Approach Study

4.1.4.1 Noise Impact of ILS Approach

Table 4-1 shows the simulation sequence during the evaluation of the ILS Approach procedure depicted in Figure 4-1. the results of this simulation are used in this section as the benchmark noise impact values.

Table 4-1: Simulation Sequence During the Evaluation of the ILS Approach.

Distance to Threshold (n.mi.)	Height AGL (ft.)	Speed (knots)	Event
25	6,000	250	Simulation Commenced
21	6,000	210	Descent to 2,500 ft. Idle Thrust & Constant Speed
12	2,500	210	Deceleration to 135 knots Idle Thrust
6	2,500	160	Glide Slope Intercepted Final Approach
5	2,000	135	Autothottles Re-Engaged
0	50	135	Landing Flare

Figure 4-9 shows the noise footprint and noise impact of the baseline ILS Approach. As the figure shows, much of the noise impact during approach occurs during the intermediate and final approach segments. The first area exposed to noise greater than 70 dBA is approximately 6.5 nautical miles from the runway threshold. This is near the location where the aircraft begins the final approach segment

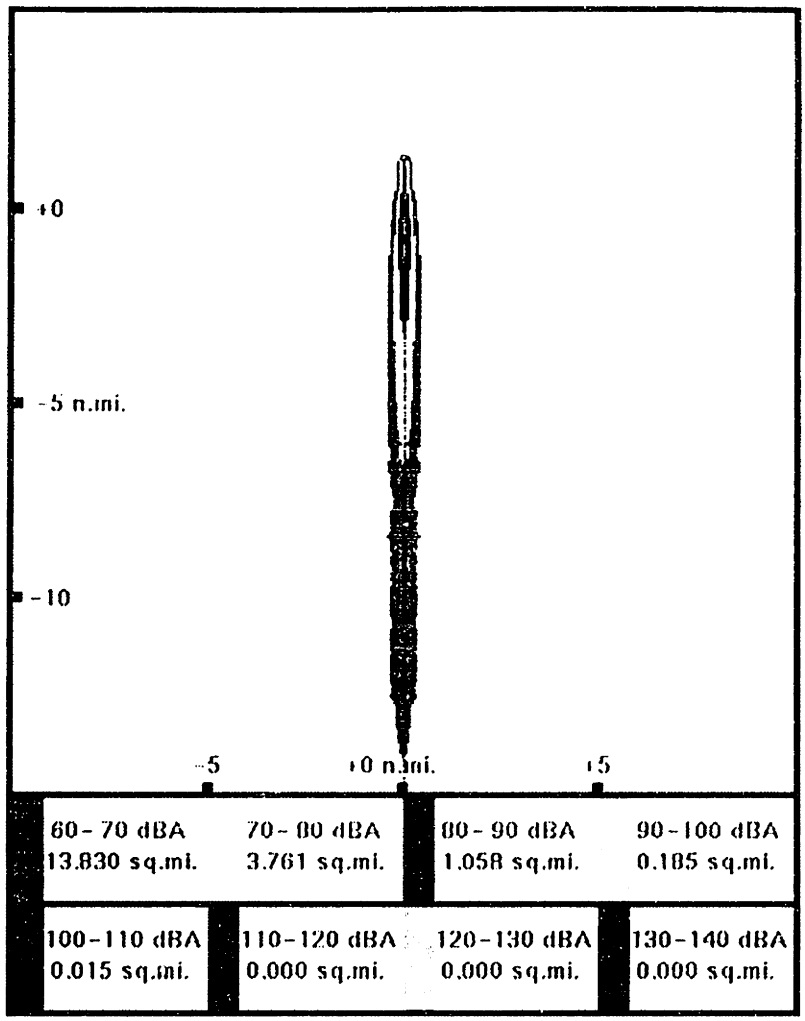

Figure 4-9: Footprint and Impact of ILS Approach in Figure 4-1.

4.1.4.2 Noise Impact of Vertically Segmented Approach

Table 4-2 shows the noise impact for the Vertically Segmented Approach. There are significant (greater than 40%) reductions in the area exposed to 60-80 dBA noise. The results also indicate that there is a modest reduction in the area exposed to 80-90 dBA noise, with a negligible decrease in the area exposed to 90-100 dBA noise.

Table 4-2: Impact of Vertically Segmented Approach in 10 dBA Bands.

Noise (dBA)	Impact Area (sq.mi.)	Change (sq.mi.)	Change (%)
60-70	5.39	-8.44	-61.0
70-80	2.093	-1.668	-44.3
80-90	0.842	-0.216	-20.4
90-100	0.178	-0.007	-3.8

4.1.4.3 Noise Impact of 3° Decelerating Approach

Table 4-3 shows the noise impact of the simulated 3° Decelerating Approach. There are significant (greater than 40%) reductions in the area exposed to noise between 60 and 90 dBA. The results also indicated that there is a negligible decrease in the area exposed to 90-100 dBA noise. This is consistent with the fact that the last 500 ft. that the aircraft descends is unchanged in either of the three approaches.

Table 4-3: Impacts of 3° Decelerating Approach in 10 dBA Band.

Noise (dBA)	Impact Area (sq.mi.)	Change (sq.mi.)	Change (%)
60-70	5.691	-8.139	-58.9
70-80	1.637	-2.124	-56.5
80-90	0.595	-0.463	-43.8
90-100	0.178	-0.007	-3.8

4.1.4.4 Comparison of Results

Figure 4-10 shows the noise footprints of the ILS Approach, Vertically Segmented Approach, and the 3° Decelerating Approach. The figure illustrates the significant reductions in the area exposed to noise between 60 and 80 dBA in both noise abatement approaches in comparison to the ILS Approach. It also illustrates the differences in the "aspect ratio" of the noise footprints, as the footprint of the Vertically Segmented Approach is slightly shorter and wider than the 3° Decelerating Approach. Even with this difference, the area exposed to noise above 60 dBA is nearly equal. In the Vertically Segmented Approach, both the angle of descent and the thrust were changed to values

that were favorable to noise reduction. In the 3° Decelerating Approach, only the thrust was changed.

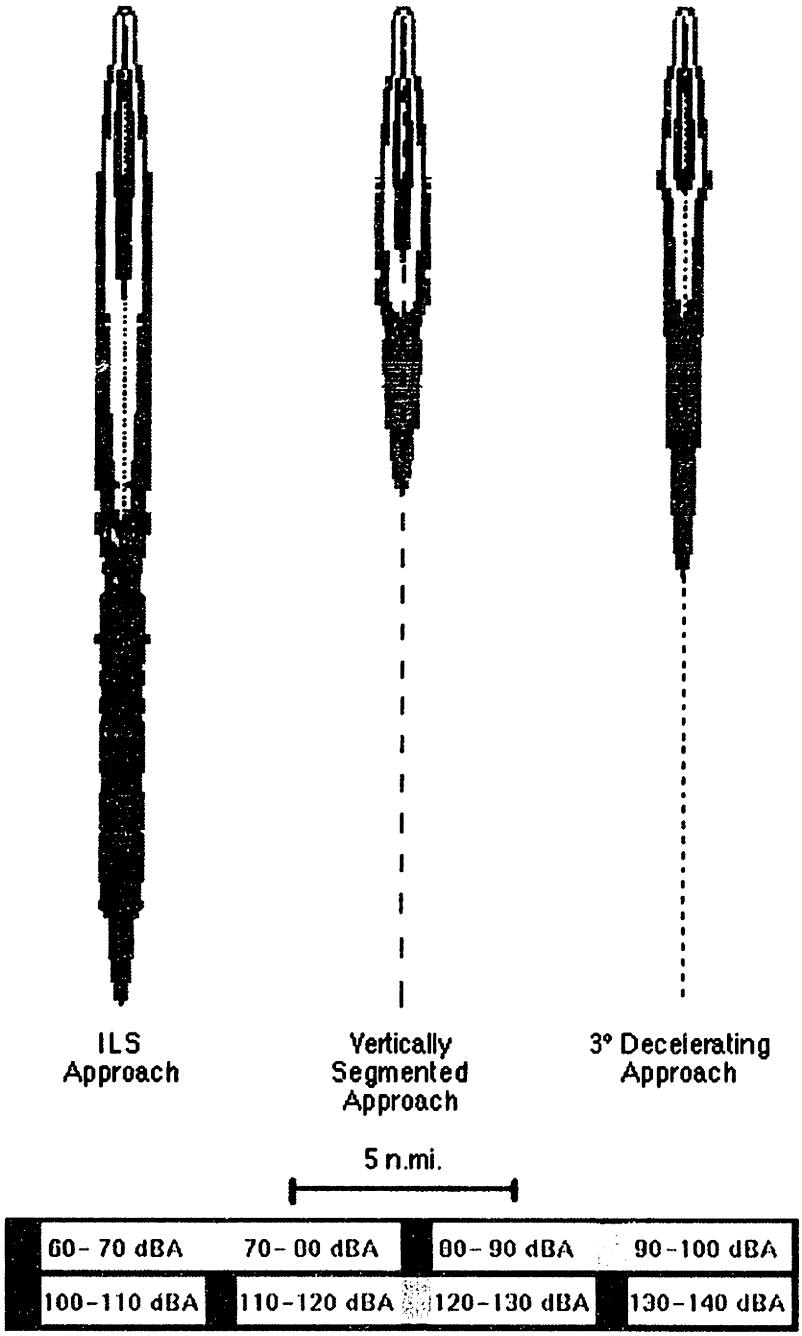

Figure 4-10: Footprints of ILS, Segmented, and 3° Decelerating Approaches.

Figure 4-11 shows the noise impact of the three procedures in 10 dBA bands. As the figure shows, both the Vertically Segmented Approach and the 3° Decelerating Approach provide significant reductions in the area exposed to noise between 60 and 80 dBA. The

3° Decelerating Approach provides more of a reduction in the area impacted by 80-90 dBA noise than the Vertically Segmented Approach.

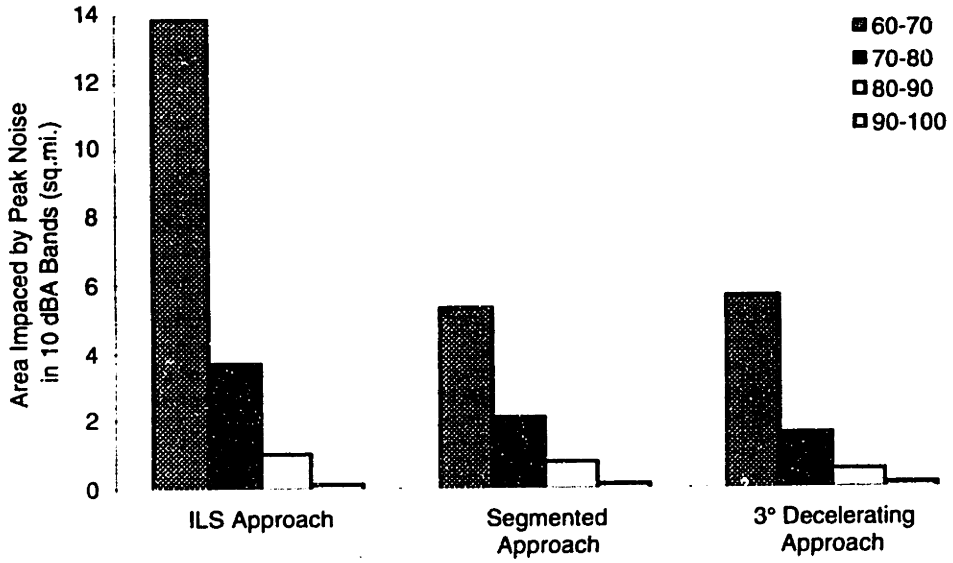

Figure 4-11: Impact of ILS, Segmented, and 3° Decelerating Approaches.

Figure 4-12 shows the total noise impact of the three procedures. As the figure shows, the area impacted by noise greater than 60 dBA is marginally lower during the 3° Decelerating Approach than during the Vertically Segmented Approach, although the area impacted by noise between 60 and 70 dBA is actually greater during the 3° Decelerating Approach than during the Vertically Segmented Approach. This illustrates the effectiveness of the 3° approach in reducing the noise between 70 and 90 dBA in comparison to the Vertically Segmented Approach.

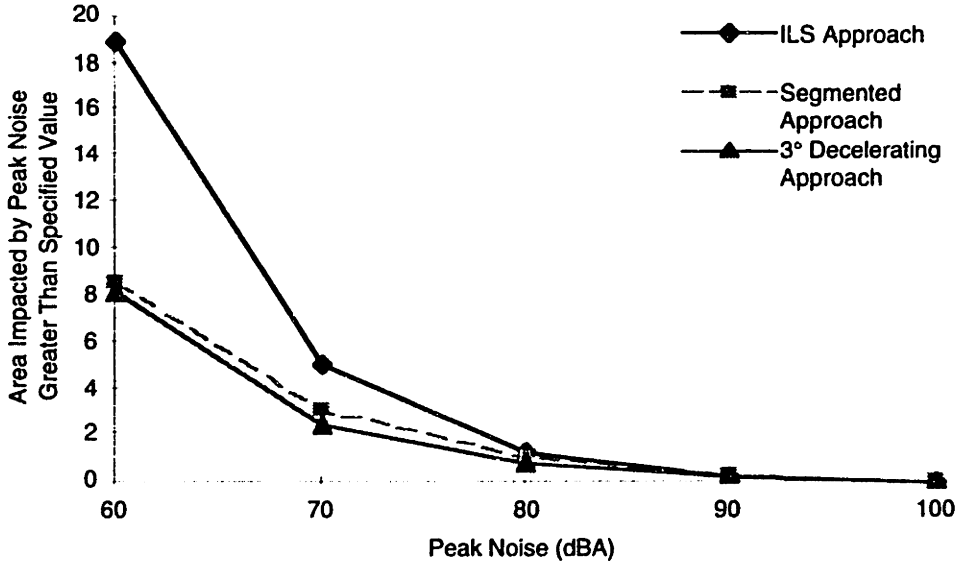

Figure 4-12: Total Impact of ILS, Segmented, and 3° Decelerating Approaches.

4.1.5 Flight Simulator Study of Pilot Acceptance

The acceptability of a flight procedure to the pilot community is an important factor in the implementation of flight procedures. Since the Vertically Segmented Approach and the 3° Decelerating Approach had comparable noise impact, pilot acceptance was evaluated in a Flight Simulator study to determine the approach that provided the best combination of noise reduction and pilot acceptance.

4.1.5.1 Subjects

Four pilots participated in the simulator study. Two of the pilots were airline captains with "glass cockpit" experience, and the other 2 pilots were certified instrument flight instructors.

4.1.5.2 Scenarios

Each subject performed a total of 9 approaches. Of the 9 approaches, 3 were Vertically Segmented Approaches, 3 were 3° Decelerating Approaches, and 3 were ILS Approaches. Before each approach, subjects were presented with an approach chart that was similar in format to existing Jeppesen Sanderson Charts. Subjects were allowed as much time as they required to familiarize themselves with the details of the approach.

4.1.5.3 Wind Conditions

Each approach procedure was performed in zero wind, a tailwind of 20 knots, and windshear conditions.

4.1.5.4 Prototype Approach Charts

Prototype approach charts were developed for 9 runways at 3 airports. Below are the three prototype approach charts for the ILS, Vertically Segmented, and 3° Decelerating Approaches to runway 31R at JFK

Figure 4-13 shows the prototype approach chart for the ILS Approach. The IF for this approach is LORAC, and the FAF (and OM) is GRIMM. Aircraft performing this ILS Approach are required to descend to an altitude of 3,000 ft. before reaching LORAC. At LORAC the aircraft turns onto the localizer. When the aircraft reaches MALDE, it descends to an altitude of 1900 ft. The aircraft intercepts the glide slope before reaching the OM GRIMM, and enters the final approach.

Figure 4-14 shows the prototype approach chart for the Vertically Segmented Approach. Unlike the example in Figure 4-6, the 5° segment of this approach begins 10.5 n.mi. from the runway threshold at an altitude of 5,000 ft. As designed, aircraft that are performing the Vertically Segmented Approach are not required to change their lateral trajectory, as the lateral trajectory of this approach is identical to the lateral trajectory of the ILS Approach.

Figure 4-15 shows the prototype approach chart for the 3° Decelerating Approach. As the figure shows, the 3° Decelerating Approach begins 15.5 n.mi. from the runway threshold at an altitude of 5,000 ft. Pilots were instructed to begin the 3° Decelerating Approach at a specific speed above the final approach speed. The speed was selected based on the performance characteristics of the 737-200 used in the simulation.

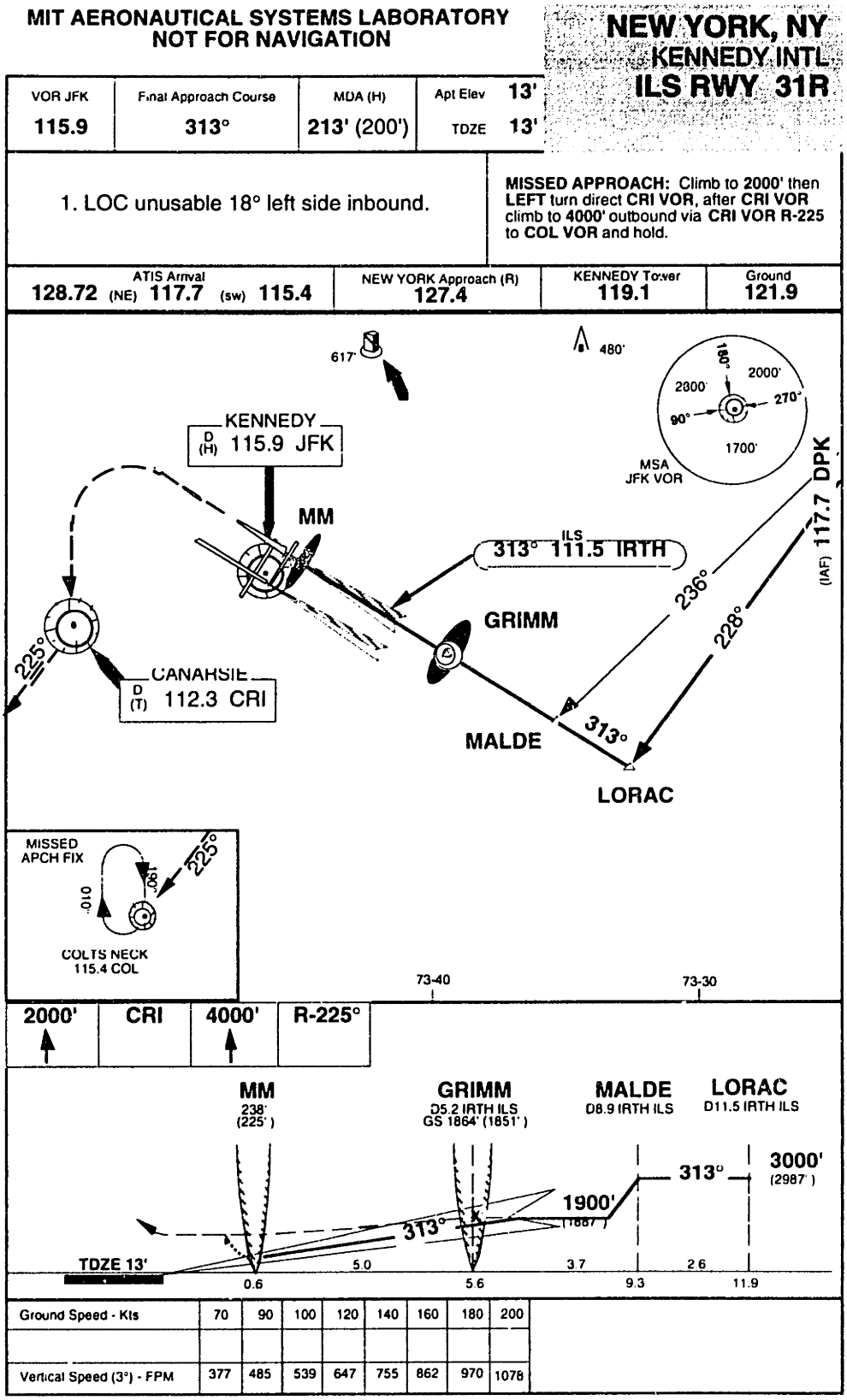

Figure 4-13: Prototype Approach Chart for ILS Approach to JFK Runway 31R.

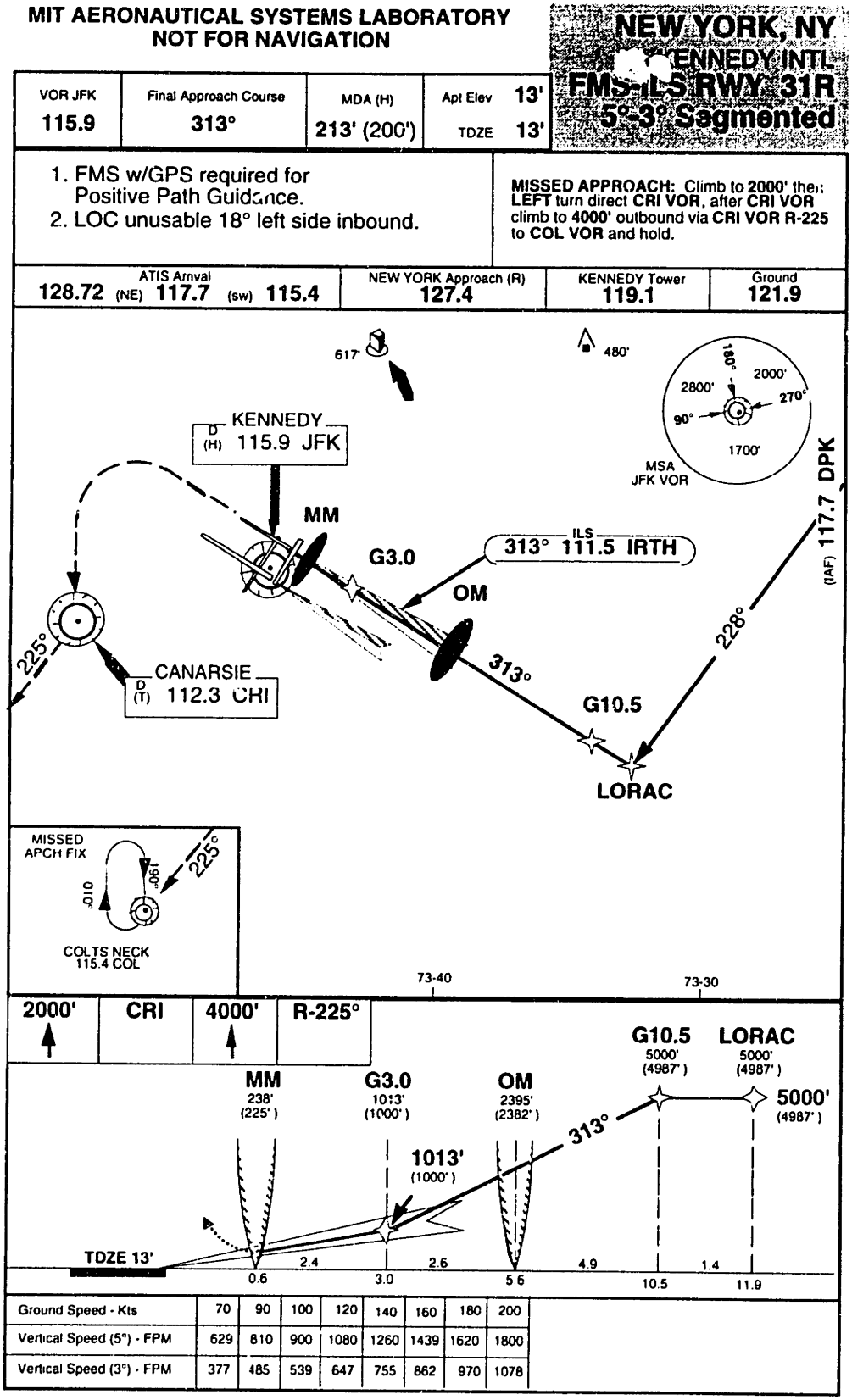

Figure 4-14: Prototype Approach Chart for Vertically Segmented Approach to JFK Runway 31R.

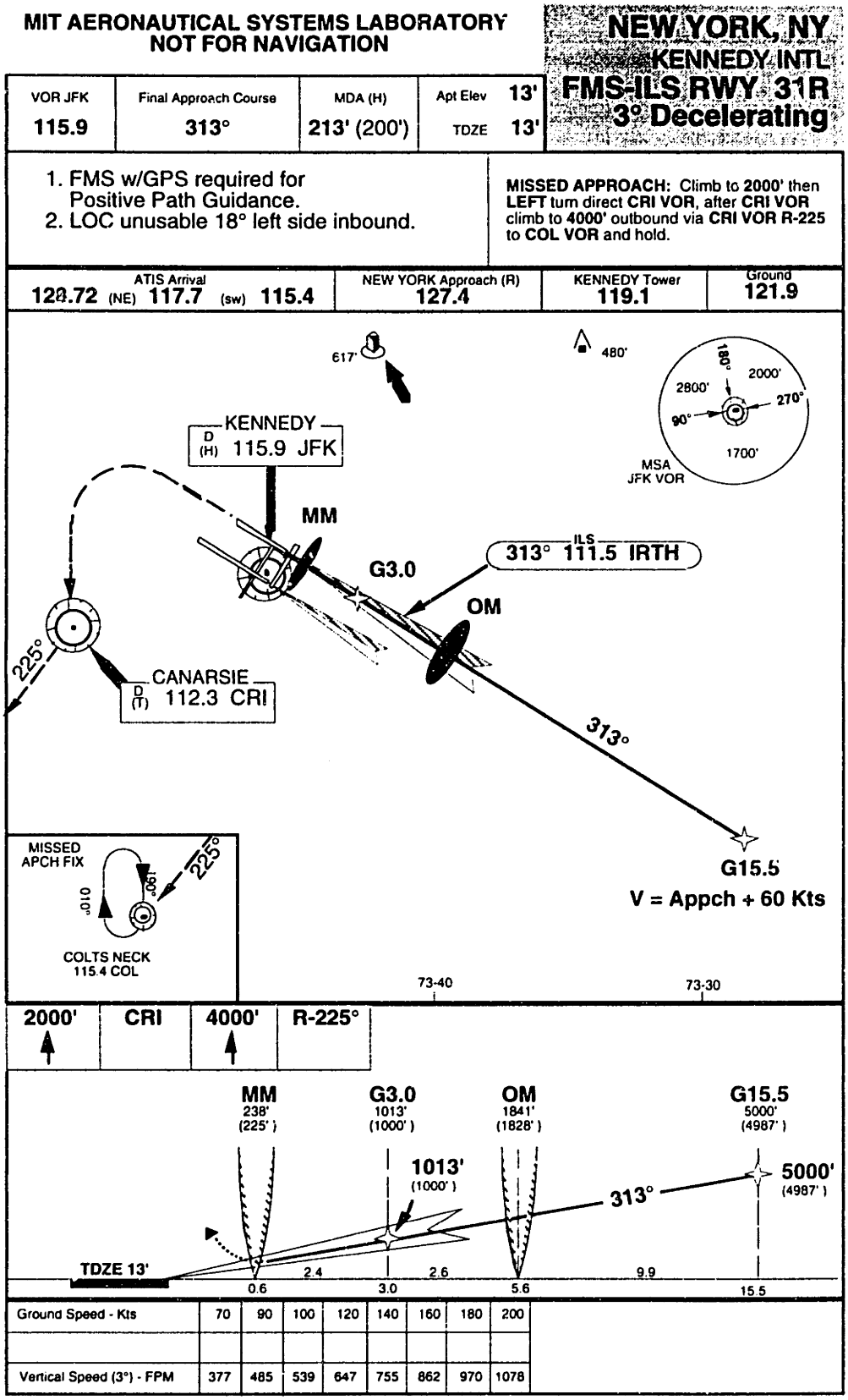

Figure 4-15: Prototype Approach Chart for 3° Decelerating Approach to JFK Runway 31R.

4.1.5.5 Prototype Display

Positive path guidance is required during the first segment of the Vertically Segmented Approach when the aircraft is above the ILS. A prototype Attitude Direction Indicator (ADI) display was developed to provide this positive path guidance. Figure 4-16 shows the prototype ADI display during the transition from the 5° segment to the 3° glide slope in the Vertically Segmented Approach. Apart from a single modification, the display is the typical ADI found in advanced commercial cockpits such as the 747-400.

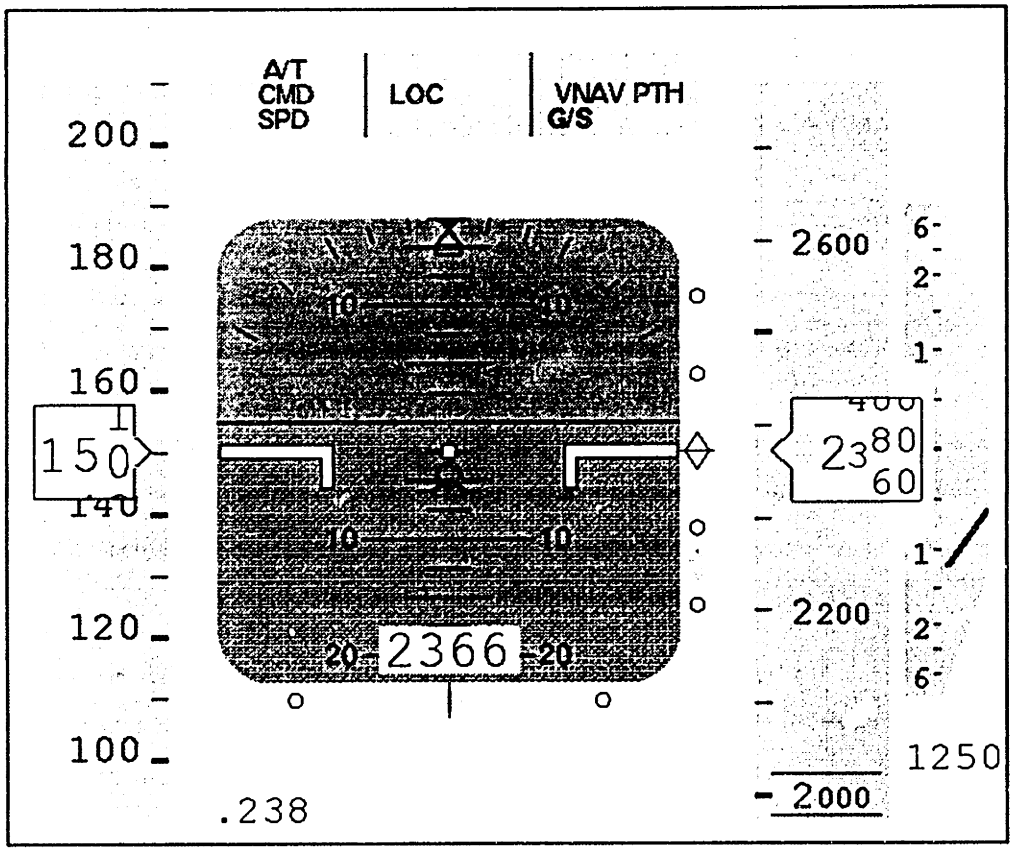

Figure 4-16: Prototype Display Developed for Pilot Evaluation of Alternative Procedures.

In the center of the display is the artificial horizon. The two filled diamonds below and to the right of the artificial horizon indicate the localizer and glide slope deviations respectively. The hollow diamond above the filled glide slope diamond is the modification made to the display. This second vertical deviation indicator has been added to provide an indication of the deviation from the desired path when the aircraft is outside effective ILS coverage. As the figure shows, the aircraft is centered on the hollow diamond while the filled glide slope diamond is below. This indicates that the aircraft is on the 5° segment and descending toward the glide slope. To the left of the

artificial horizon is the airspeed indicator. The number above the speed indicator is the airspeed selected in the FMS. Immediately to the right of the artificial horizon is the altitude indicator. The number above the altitude indicator is the altitude that is selected in the FMS. To the extreme right of the artificial horizon is the vertical speed indicator. The boxes above the artificial horizon indicate from left to right: the components of the FMS that are active, the lateral mode of the FMS, and the vertical mode of the FMS. At the time this image was recorded, both the autopilot and autothrottles were on, the aircraft was using the localizer for lateral guidance, and was using VNAV for vertical guidance. The G/S below the VNAV indication shows that the glide slope is armed for automatic transition when the aircraft is within glide slope coverage.

4.1.5.6 Results

All subjects completed their 9 approaches without incident. When queried about their preference for a noise abatement procedure, all the pilots selected the 3° Decelerating Approach. When queried about their rationale for choosing the 3° Decelerating Approach in preference to the Vertically Segmented Approach, all the pilots indicated that they preferred the stabilized flight path of the 3° Decelerating Approach. They also indicated that they disliked the Vertically Segmented Approach because of the higher descent rates and the proximity of the transition to the ground.

Pilots were also asked to compare the difficulty of the 3° decelerating approach to the difficulty of the Vertically Segmented Approach. Figure 4-17 shows the rating scale that was used. The average ranking for the 3° Decelerating Approach procedure was 5.5, and the standard deviation was 0.33.

1	2	3	4	5	6	7
Extremely Harder	Much Harder	Somewhat Harder	Neutral	Somewhat Easier	Much Easier	Extremely Easier

Figure 4-17: Rating Scale for Comparison of Noise Abatement Approach Procedures.

When queried about the difficulty of the 3° Decelerating Approach in comparison to the ILS Approach, none of the pilots indicated that the 3° Decelerating Approach was more difficult.

These results indicate that, of the two noise abatement procedures that were studied, the 3° Decelerating Approach provides the best combination of noise reduction and pilot acceptance. Based on these result, the 3° Decelerating Approach was evaluated in two case studies. The results of those case studies are presented in the following sections.

4.2 Case Study of Logan Runway 22L

4.2.1 ILS Approach

Figure 4-18 shows the ILS Approach to runway 22L at Logan Airport (BOS). Because Logan is adjacent to many residential communities in the Boston metropolitan area, there are densely populated communities along the ILS Approach to that runway. Although there is some noise relief because approximately 2 nautical miles (between 2 and 4 n.mi. from the runway threshold) of the final approach segment is over water, much of the noise impact occurs along the initial and intermediate approach which is between 4 and 12 nautical miles from the runway threshold. For this approach, the initial approach fix is WAXEN, the intermediate fix is WYANE, and the final approach fix is LINDY. An aircraft on ILS Approach to runway 22L, first flies to WAXEN. The aircraft descends to an altitude of 3,000 ft. before reaching that fix. From WAXEN, the aircraft flies at a constant altitude of 3,000 and a heading of 192° until it intercepts the localizer. At this point, the aircraft turns onto the final approach course. When the aircraft reaches WYANE, it descends to an altitude of 1,700 ft. and is configured for landing. Before reaching LYNDY, the aircraft intercepts the glide slope and begins its final descent to the runway.

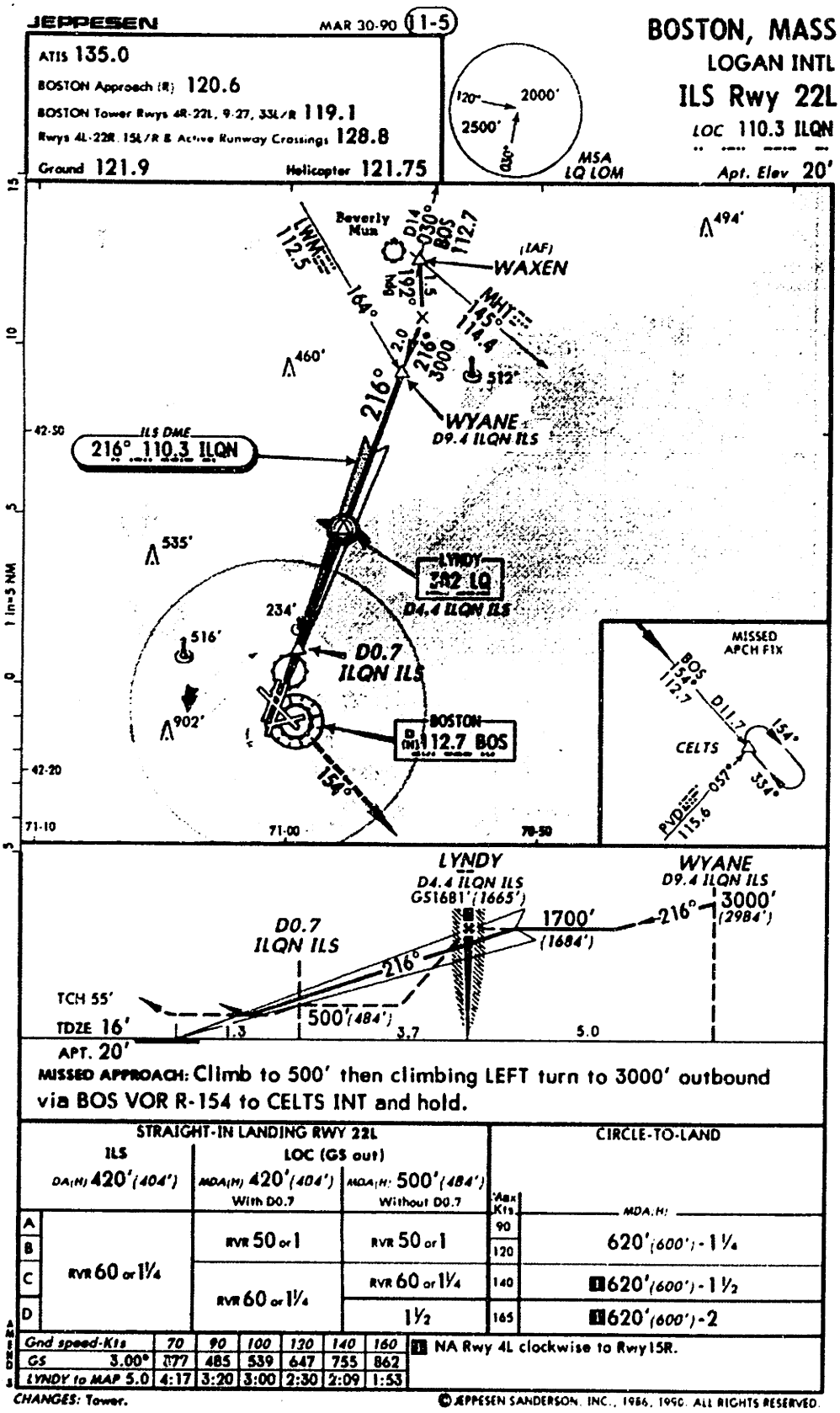

Figure 4-18: ILS Approach to BOS Runway 22L.
[Reproduced With Permission of Jeppesen Sanderson Inc.; Not For Navigation]

Figure 4-19 shows the noise footprint, area impacted, and population impacted during the ILS Approach to runway 22L. This simulation illustrates the ability of NOISIM to evaluate the noise impact of a flight procedure as it is actually flown. The simulation begins with the aircraft descending from an altitude of 11,000 ft. at the Manchester VOR (MHT) to WAXEN. During the descent, ATC requests that the aircraft decelerate to 210 knots before WAXEN and maintain that speed until it reaches WYANE. At WYANE, ATC requests that the aircraft decelerate to 170 knots and maintain that speed until it reaches LYNDY, where it should decelerate to its final approach speed of 135 knots. As the figure illustrates, the requirement that aircraft descend to 3,000 ft. and then to 1,700 ft. during the intermediate segment has a significant noise impact on communities north of the airport. Two distinct areas are impacted by aircraft noise generated during the initial and intermediate segments. The first area impacted, the area furthest from the runway, is the area near WAXEN and WAYNE where the aircraft is intercepting the localizer at 3,000 ft. and 210 knots. The noise impact in this area is in the 60-70 dBA range. The second area impacted is the area between WYANE and LYNDY. The noise impact in this area is between 60 and 90 dBA, a significant increase over the noise impact in the first area. The gap in the noise footprint between the first and second areas occurs when the aircraft is in idle descent from 3,000 to 1,700 ft.

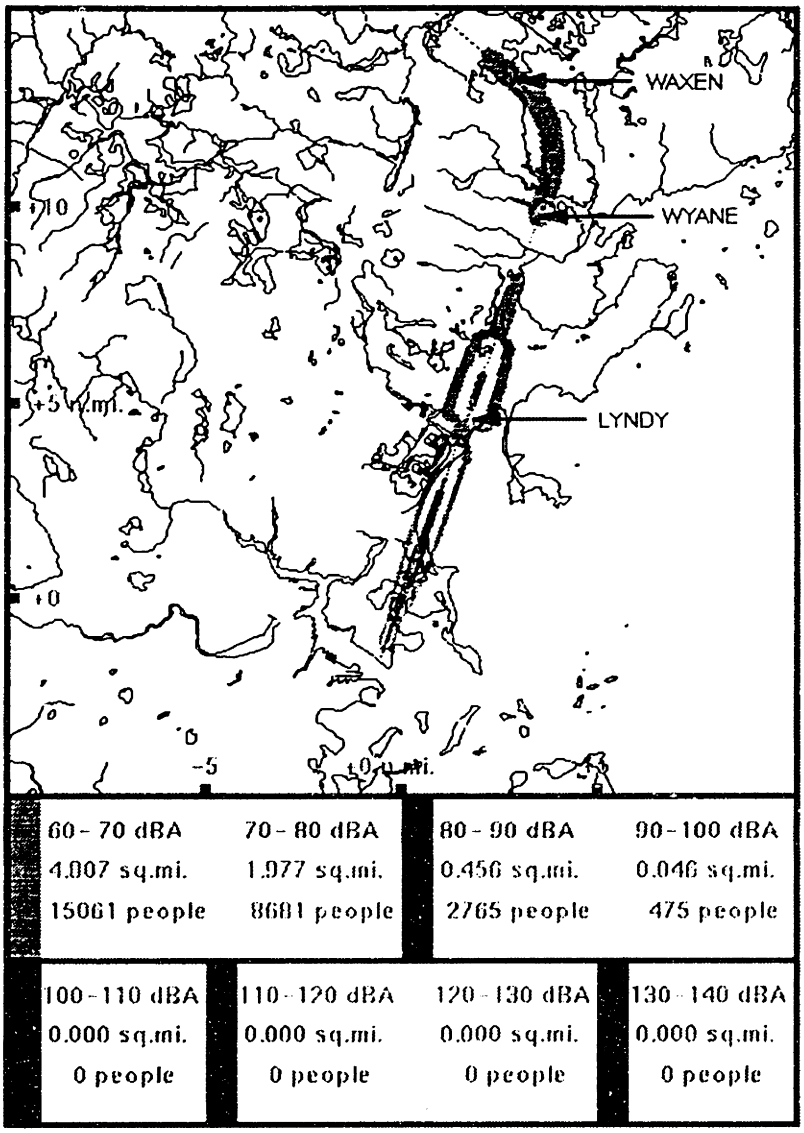

Figure 4-19: Footprint and Impact of ILS Approach to BOS Runway 22L.

4.2.2 3° Decelerating Approach

Figure 4-20 shows the noise footprint and noise impact of a 3° Decelerating Approach to the runway 22L. As the figure shows, much of the noise impact that occurs during the initial and intermediate segments of the ILS Approach is significantly reduced through the use of this procedure.

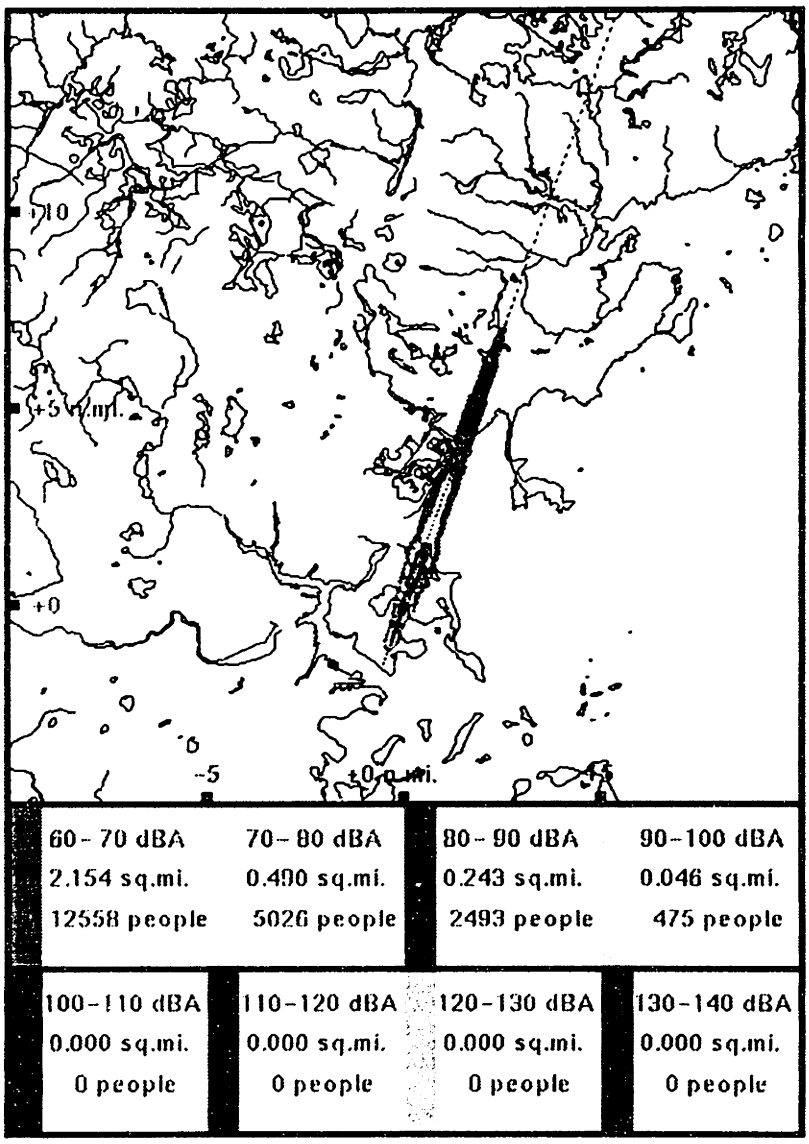

Figure 4-20: Footprint and Impact of 3° Decelerating Approach to BOS Runway 22L.

4.2.3 Comparison of Approaches

Figure 4-21 shows the noise impact of the ILS Approach and the 3° Decelerating Approach to runway 22L in 10 dBA bands. As the figure shows, the number of people impacted by noise in each of the 10 dBA bands between 60 and 80 dBA, is reduced by approximately 3,000. There is also a slight decrease in the number of people impacted by noise between 80 and 90 dBA, and no change in the number of people impacted by noise between 90 and 100 dBA.

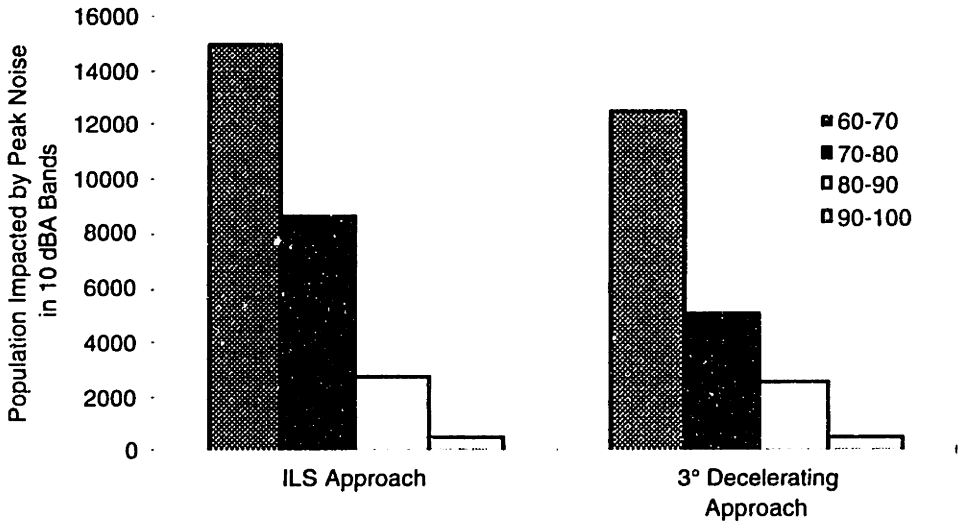

Figure 4-21: Impact of ILS and 3° Decelerating Approach to BOS Runway 22L, in 10 dBA Bands.

Figure 4-22 shows the total noise impact of the ILS Approach and the 3° Decelerating Approach to runway 22L. As the figure shows, when the 3° Decelerating Approach was used instead of the ILS Approach, the number of people impacted by noise greater than 60 dBA was reduced from 26,982 to 20,552, a 24% reduction.

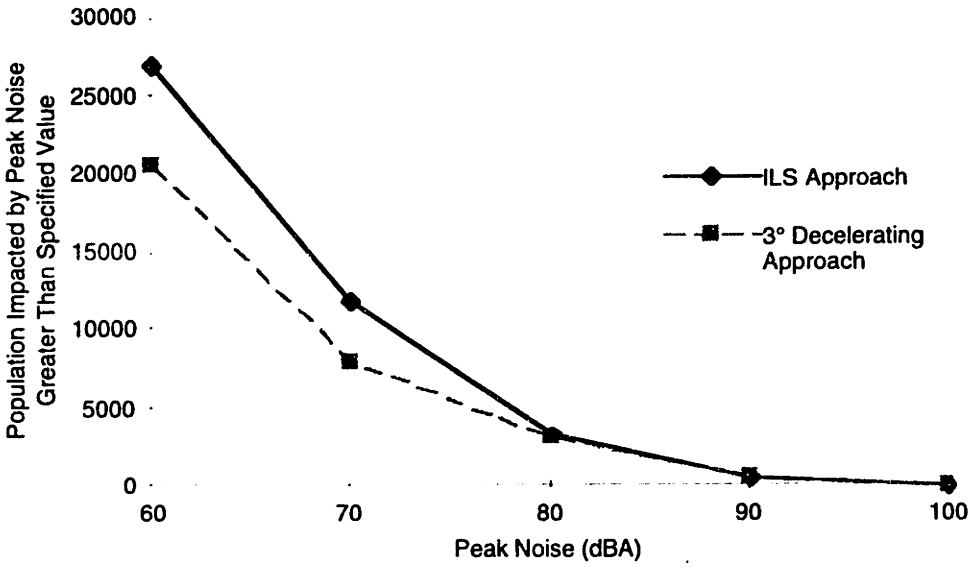

Figure 4-22: Total Impact of ILS and 3° Decelerating Approach to BOS Runway 22L.

4.3 Case Study of Kennedy Runway 13L

4.3.1 ILS Approach

Figure 4-23 shows the ILS Approach to Kennedy (JFK) runway 13L. To avoid conflicts with traffic departing and approaching Newark and La Guardia Airports, aircraft that are performing the ILS Approach are vectored towards the fix TELEX from the south at low altitude to intercept the ILS at an altitude of 2,000 ft. Low altitude vectoring has an adverse effect on the noise impact in communities, as the aircraft is closer to the community over a greater portion of it's trajectory. Figure 4-19 shows the noise impact for the ILS Approach to runway 13L. As the figure shows, the communities near TELEX are heavily impacted during the turn onto the final approach.

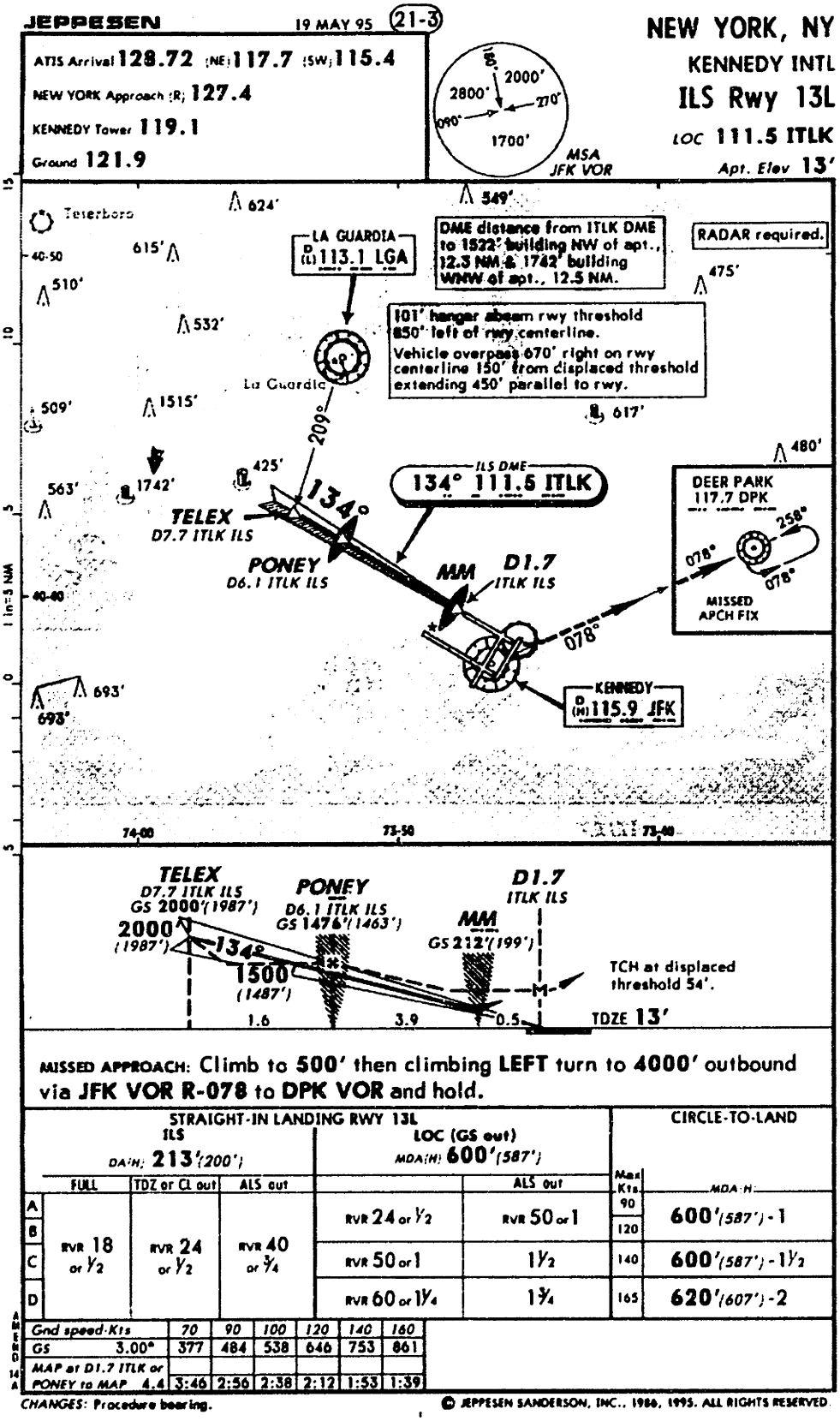

Figure 4-23: ILS Approach to JFK Runway 13L.
[Reproduced With Permission of Jeppesen Sanderson Inc.; Not For Navigation]

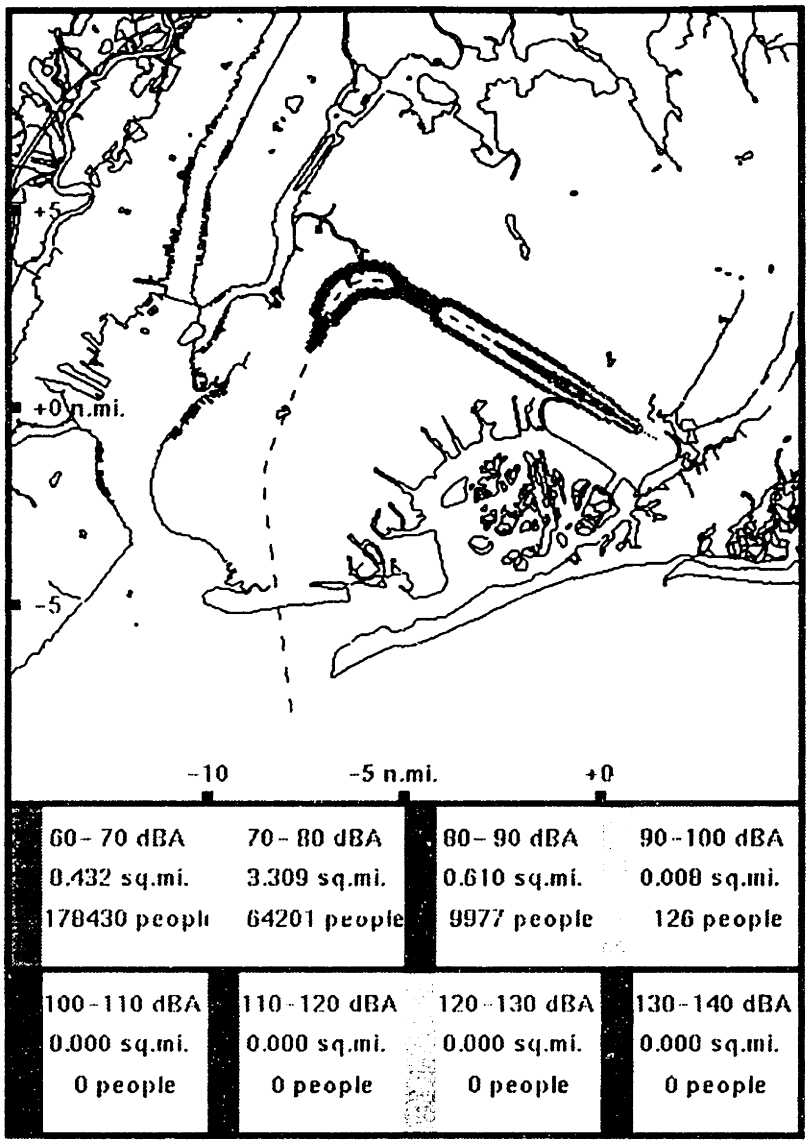

Figure 4-24: Footprint and Impact of ILS Approach to JFK Runway 13L.

4.3.2 Canarsie VOR Approach

In VMC, aircraft on approach to runway 13L currently perform a visual noise abatement approach that uses the Canarsie VOR (CRI) for guidance during the initial phases. Figure 4-25 shows the Canarsie VOR Approach. Aircraft fly to CRI from the fix ASALT via the inbound 043° radial, descending from 3,000 ft. to 1,500 ft. altitude. From CRI, the aircraft begins a descent while flying along the outbound 041° radial. If the aircraft descends below 800 ft. without seeing the runway lead in lights that mark the curved approach to the runway, then a missed approach is executed at 2.6 nautical miles from CRI. The minimum visibility required to perform this approach procedure is 2 nautical

miles. The total distance from the first lead in light to the runway threshold is 4.7 nautical miles. At the first lead in light, the aircraft is less than 800 ft. above the runway altitude, thus most of the curved portion of the approach must be performed at the same altitude or in a shallow descent. Figure 4-26 shows the noise impact of the Canarsie VOR Approach. In the simulation, the aircraft thrust was idle from ASALT until the aircraft was midway through the turn onto the runway centerline. At that time, the autothrottles were re-engaged to maintain the approach speed.

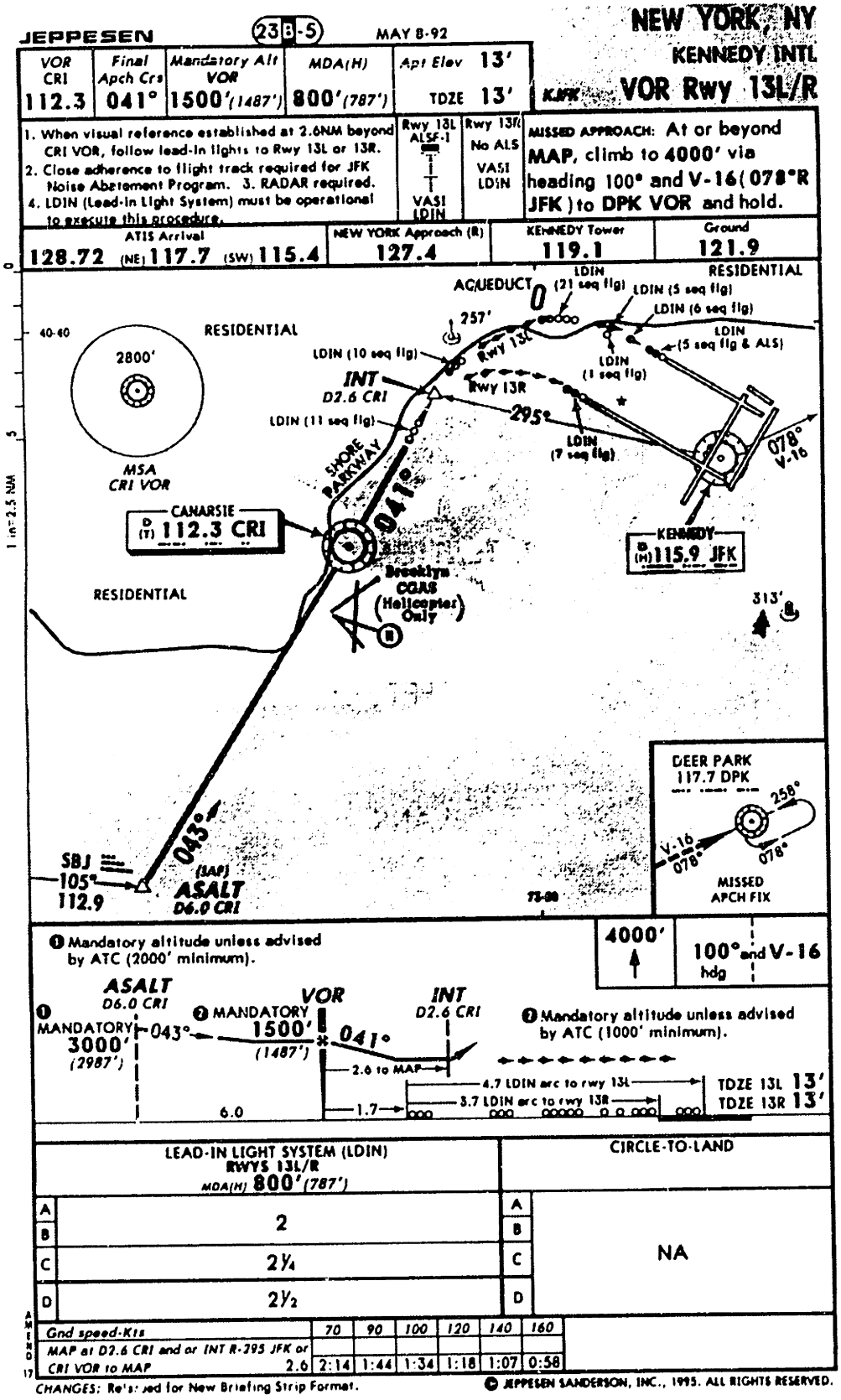

Figure 4-25: Canarsie VOR Approach to JFK Runway 13L.
[Reproduced With Permission of Jeppesen Sanderson Inc.; Not For Navigation]

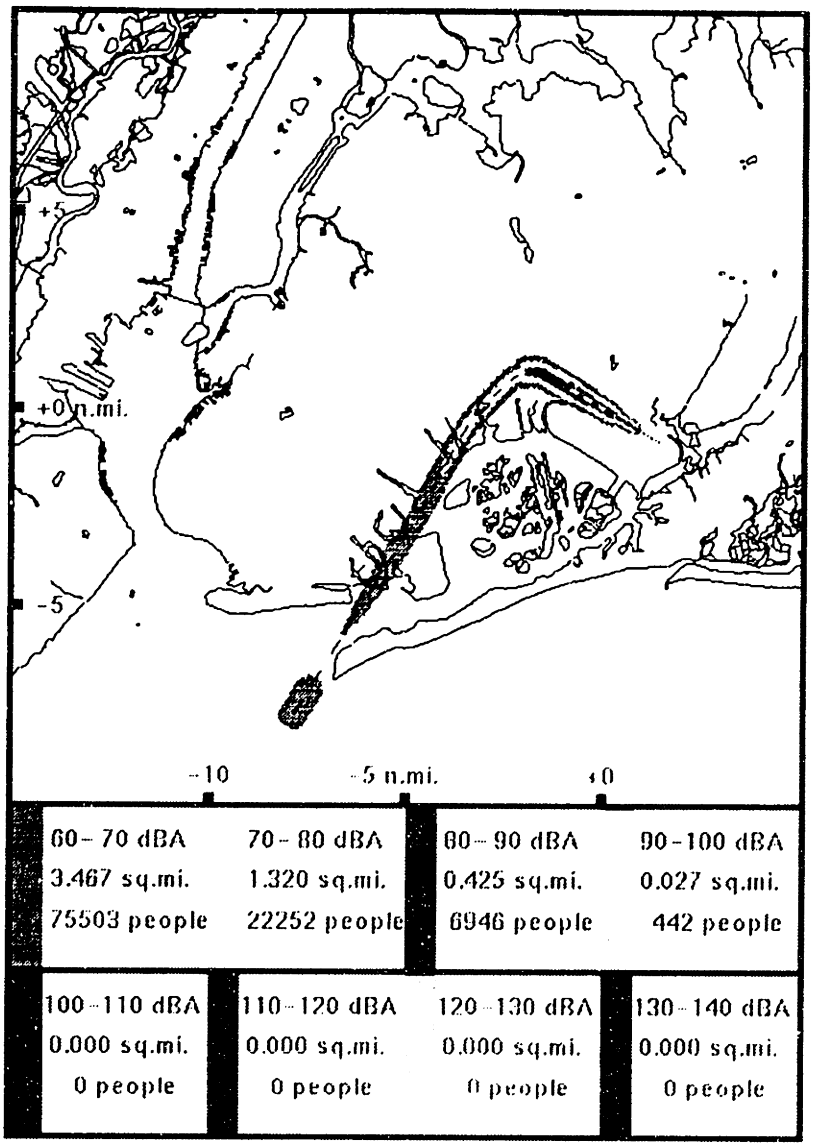

Figure 4-26: Footprint and Impact of Canarsie VOR Approach to JFK Runway 13L.

4.3.3 3° Decelerating Approach

As discussed earlier, aircraft that perform the ILS Approach during IMC have a significant noise impact on the communities under their flight path. A 3° Decelerating Approach with a single turn at an altitude of 2,000 ft. was developed to reduce the noise impact in these communities. This approach has a very similar ground track to the ILS Approach, but the aircraft is in an idle descent throughout the approach, with no level segments at constant speed. Figure 4-27 shows the noise impact of the 3° Decelerating Approach.

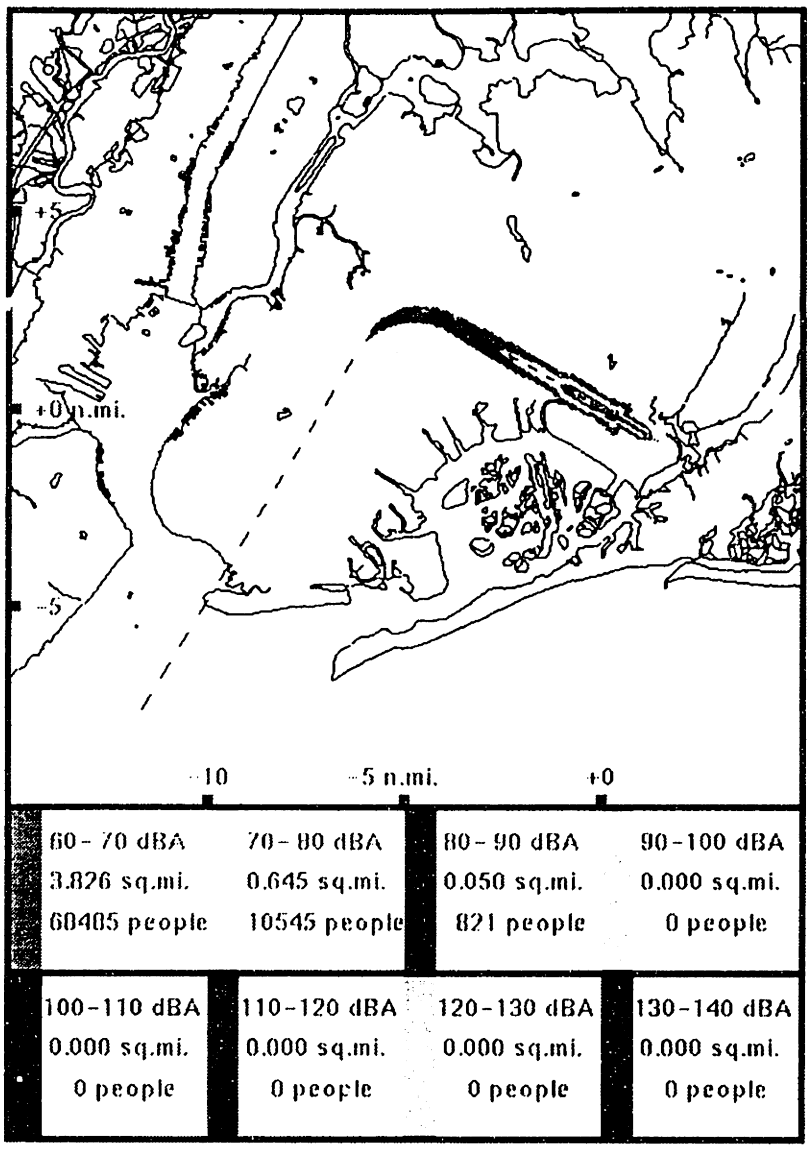

Figure 4-27: Footprint and Impact of 3° Decelerating Approach to JFK Runway 13L

4.3.4 Comparison of Approaches

Figure 4-28 shows the noise impact of the ILS, Canarsie VOR, and 3° Decelerating Approaches in 10 dBA bands. As the figure shows, in the three 10 dBA bands between 60 and 90 dBA, the 3° Decelerating Approach generates the least noise impact.

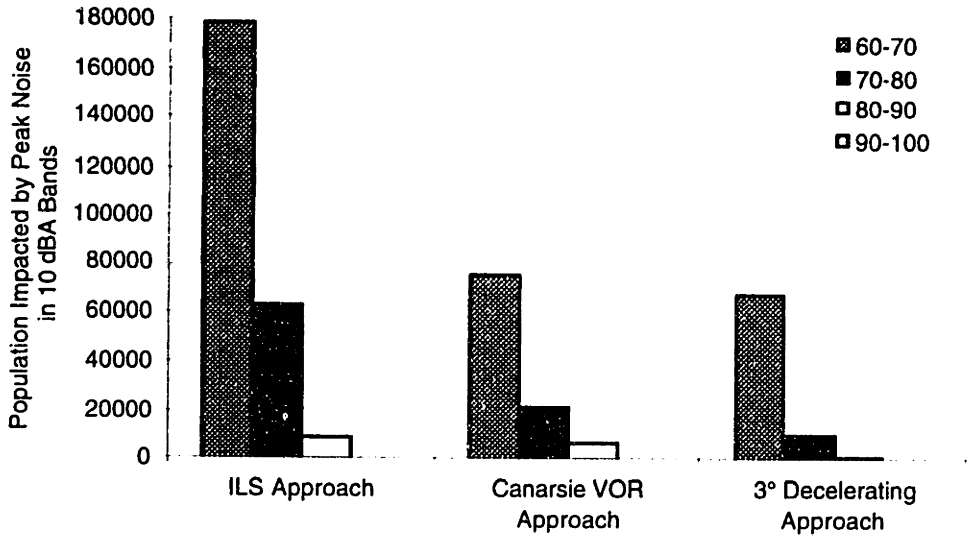

Figure 4-28: Impact of ILS, Canarsie VOR, and 3° Decelerating Approaches to JFK Runway 13L, in 10 dBA Bands.

Figure 4-29 shows the total noise impact of the ILS, Canarsie VOR, and 3° Decelerating Approaches. As the figure shows, both the Canarsie VOR Approach and the 3° Decelerating Approach have significantly lower impact than the ILS Approach. When the 3° Decelerating Approach was used instead of the existing ILS Approach, the number of people impacted by noise greater than 60 dBA was reduced from 252,734 to 79,851, a 68% reduction.

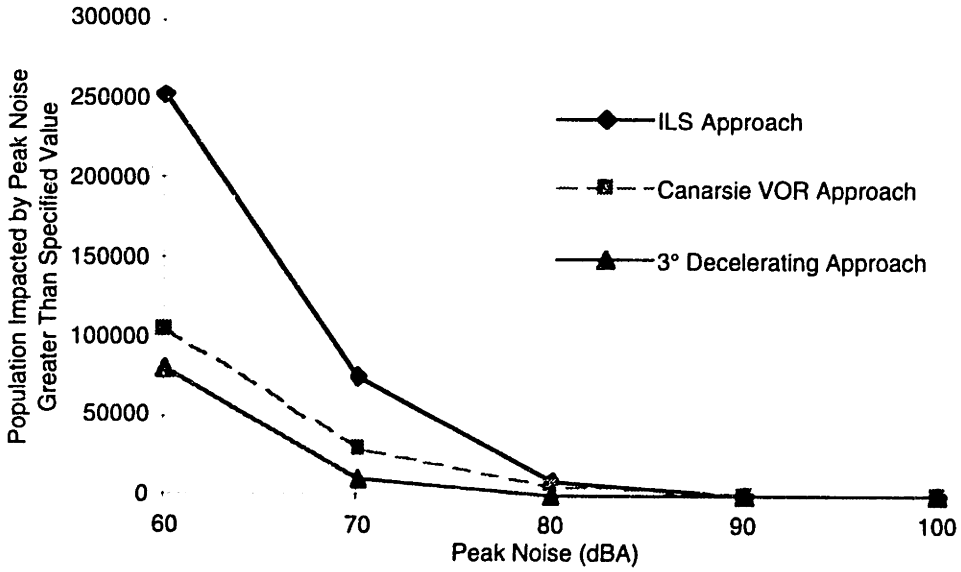

Figure 4-29: Total Impact of ILS, Canarsie VOR and 3° Decelerating Approaches to JFK Runway 13L.

5. Analysis of Departure Procedures

This chapter presents an analysis of departure procedures. The first and second sections present generic studies of procedures composed of vertical and lateral maneuvers, respectively. These studies illustrate how NOISIM may be used to evaluate and compare noise abatement options. The third section presents a case study of the departure procedure from runway 4R at Logan Airport in Boston. This study illustrates how NOISIM may be used to combine different noise abatement options into a single noise abatement procedure, quantify the benefits of that procedure, and determine the sensitivity of the noise benefit to changes in the level of navigational precision.

The aircraft simulated in the analysis was a 737-200 with two JT8D turbofans. The weight of the aircraft was assumed to be 90,000 lb. and the atmospheric conditions were assumed to be the same as those in the standard U.S. atmosphere.

5.1 Generic Study of Vertical Maneuvers

This section presents the results of a generic study of departure procedures composed primarily of vertical maneuvers. Figure 5-1 shows the airport-community geometry used in the study. The airport is assumed to be located in the midst of an area of uniform population density, and is assumed to be sufficiently large that any noise behind the vertical plane defined by the boundary at the departure end of the runway is contained within the airport's boundaries. The distance between the start of the runway and the boundary at the departure end of the runway in 2 statute miles (10,560 ft.), a typical distance at many airports.

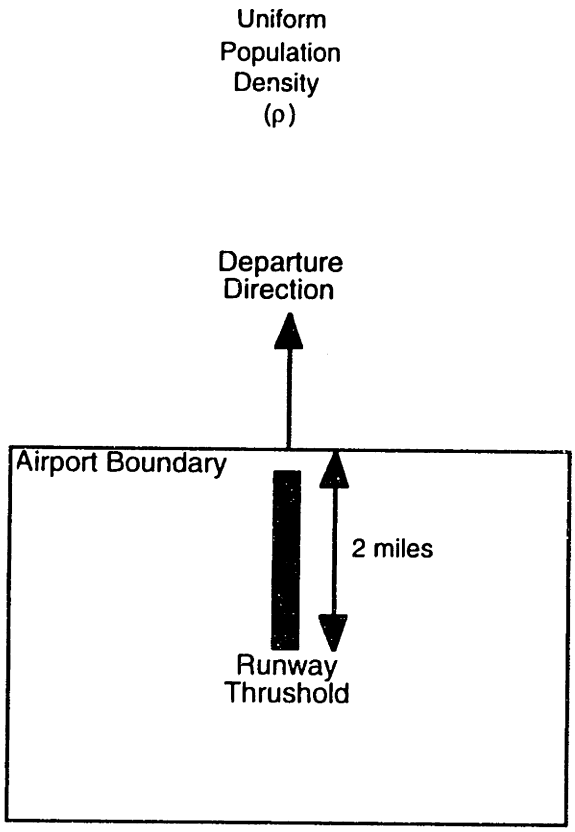

Figure 5-1: Airport-Community Geometry in Vertical Analysis.

Five procedures were evaluated in the study. The first, the Baseline Departure, consists of a full thrust takeoff with derated thrust climb. The second, the Derated Thrust Departure, has been developed to address engine maintenance concerns. The third, the Unrestricted Climb Speed Departure, has been proposed as a method of increasing airline efficiency. The fourth and fifth procedures, the Thrust Cutback Departure and ICAO Noise Abatement Departure, are noise abatement procedures.

5.1.1 Baseline Departure

Figure 5-2 shows the profile of the Baseline Departure, a full thrust takeoff with reduced thrust climb. In the Baseline Departure, the maximum available thrust level is selected at the start of the takeoff roll. Immediately after takeoff, the landing gear is retracted and the aircraft accelerates to its initial climb speed. In this study, the initial climb speed is assumed to be 170 knots.

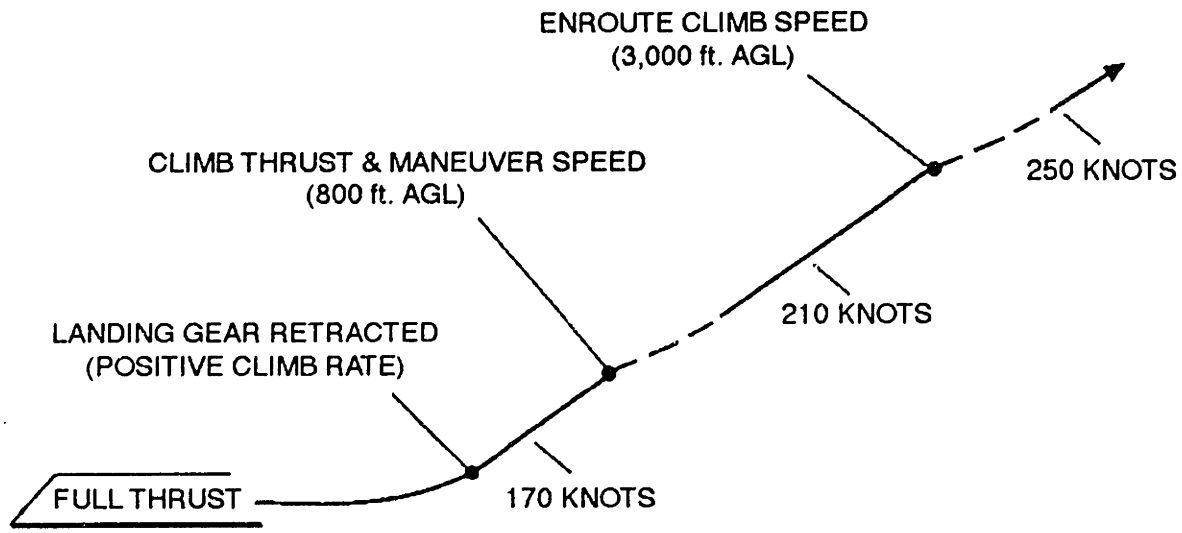

Figure 5-2: Baseline Departure

When the aircraft is 800 feet above the ground, the thrust is reduced to climb thrust (approximately 80% of the maximum available thrust) and the aircraft accelerates to its maneuver speed. The actual value of the maneuver speed varies with the weight of the aircraft and the atmospheric conditions, but the value used in this analysis is 210 knots. When the aircraft is 3,000 feet above the runway, it accelerates to the enroute climb speed. The enroute climb speed used in this analysis is 250 knots, the maximum indicated airspeed allowed below an altitude of 10,000 feet in the United States.

5.1.1.1 Noise Impact of Baseline Departure

Figure 5-3 shows the noise footprint and noise impact of the Baseline Departure. The decrease in the width of the footprint between 2 and 3 nautical miles from the runway threshold represents the thrust reduction to climb thrust at 800 ft. above the runway. The noise footprint and noise impact are used in the parametric studies that follow as a baseline.

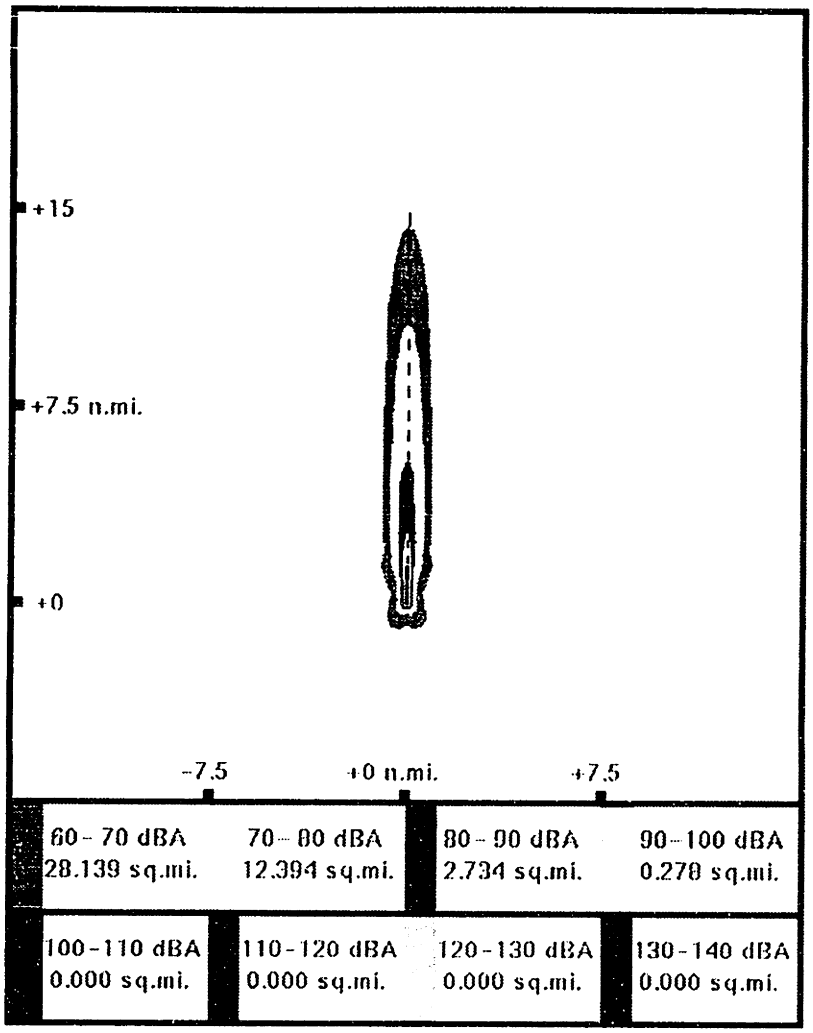

Figure 5-3: Footprint and Impact of Full Thrust Takeoff.

5.1.2 Derated Thrust Departure

The Derated Thrust Departure has been developed to address engine maintenance concerns. The wear on a gas turbine engine is a function of the length of time that the engine operates at elevated temperatures [Pratt and Whitney, 1974]. At maximum thrust, the turbine inlet temperature is near the maximum level that can be maintained with cooling. Even then, the length of time that an engine may operate at its maximum thrust level is restricted. Previous work has demonstrated that the mean time between maintenance checks may be increased through the use of lower thrust during takeoff [Midkiff, 1993].

The takeoff thrust level during the derated thrust departure is set by balanced field length and climb gradient requirements. The balanced field length is the distance required for

an aircraft to accelerate to V_1 (the takeoff decision speed) and then either continue the takeoff on a single engine or decelerate to a complete stop using brakes only. The acceleration distance is proportional to the thrust and the deceleration distance depends on the runway braking conditions. The thrust level that satisfies the balanced field length requirement is the thrust at which the balanced field length is equal to the length of the runway being used. The climb gradient requirement is set by the height of the obstacles and terrain along the departure path. The thrust level that satisfies the climb gradient requirement is the thrust at which the aircraft will safely avoid those obstacles. The minimum thrust that may be used during takeoff is the greater of the two thrust levels.

5.1.2.1 Noise Impact of Derated Thrust Departure

Figure 5-4 shows the noise footprints of the Derated Thrust Departure at 80 and 90% takeoff thrust, along with the noise footprint of the Baseline Departure. As the figure shows, the length of the noise contours increase with decreasing takeoff thrust. These increases are especially significant at the higher noise intensities, as the level of annoyance is in general proportional to the noise intensity.

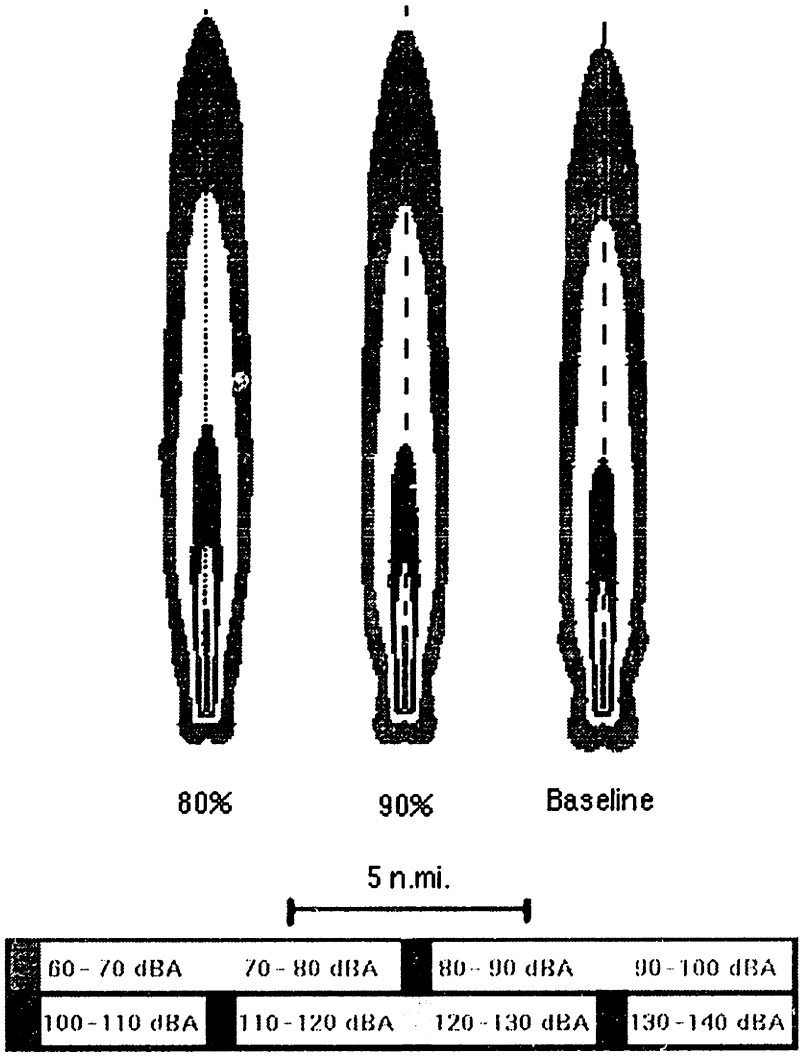

Figure 5-4: Footprints of Derated Thrust Departure at 80 and 90% Takeoff Thrust, and Baseline Departure.

Figure 5-5 shows the noise impact of the Derated Thrust Departure versus takeoff thrust level, in 10 dBA bands relative to the Baseline Departure. During both Derated Thrust Departures, the area exposed to noise in the 4 sound level bands is increased. The greatest relative change occurs in the 90-100 dBA band. During the Derated Thrust Departure at 90% takeoff thrust, the area impacted by 90-100 dBA noise is increased by 55%. During the Derated Thrust Departure at 80% takeoff thrust, the area impacted by 90-100 dBA noise is increased by 145%. These results illustrate the rapid increase in the high intensity noise impact with decreasing takeoff thrust levels. Since the communities impacted by the highest intensity noise are closest to the runway, the number of people impacted by the highest intensity noise is dependent on the population distribution and density immediately adjacent to a specific runway. Using the GIS component of

NOISIM for parametric investigations of the relationship between the noise impact and the derated thrust level during takeoff from a specific runway, allows the noise impact to be incorporated as a factor in the selection of the derated thrust level.

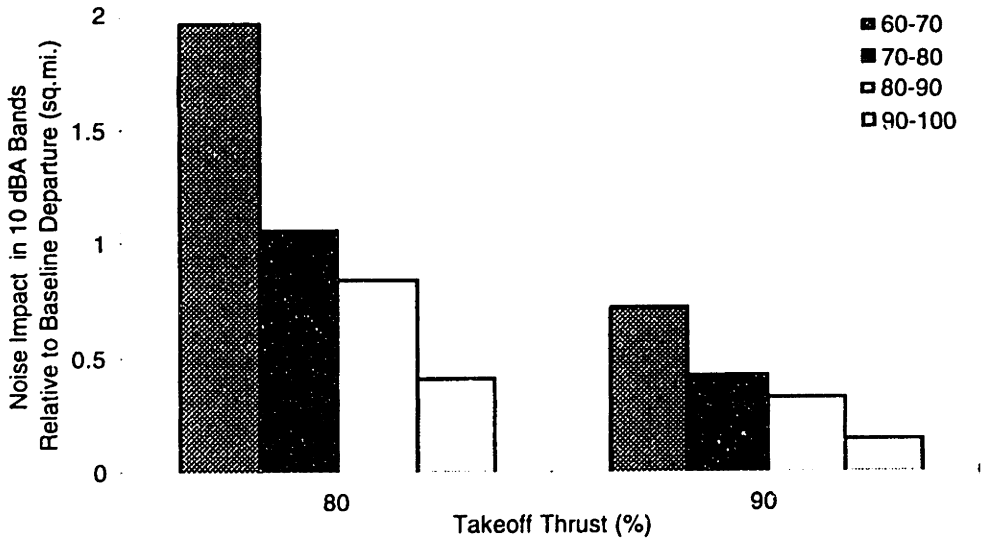

Figure 5-5: Impact of Derated Thrust Departure vs. Takeoff Thrust Level, in 10 dBA Bands Relative to Baseline Departure

5.1.3 Unrestricted Climb Speed Departure

The proposals of the RTCA Free Flight Implementation Task Force include the removal of the indicated airspeed limit of 250 knots below 10,000 feet and allowing aircraft to accelerate to their enroute cruising speed in controlled airspace [RTCA, 1995]. Figure 5-6 shows the noise footprints of the Unrestricted Climb Speed Departure with enroute climb speeds of 275 and 300 knots, along with the noise footprint of the Baseline Departure (250 knots). As the figure shows, increasing the enroute climb speed increases the size of the 60 and 70 dBA contours, but does not affect the 80 and 90 dBA contours. The figure also shows that most of the increase in the noise impact occurs at distances between 10 and 17 miles from the runway.

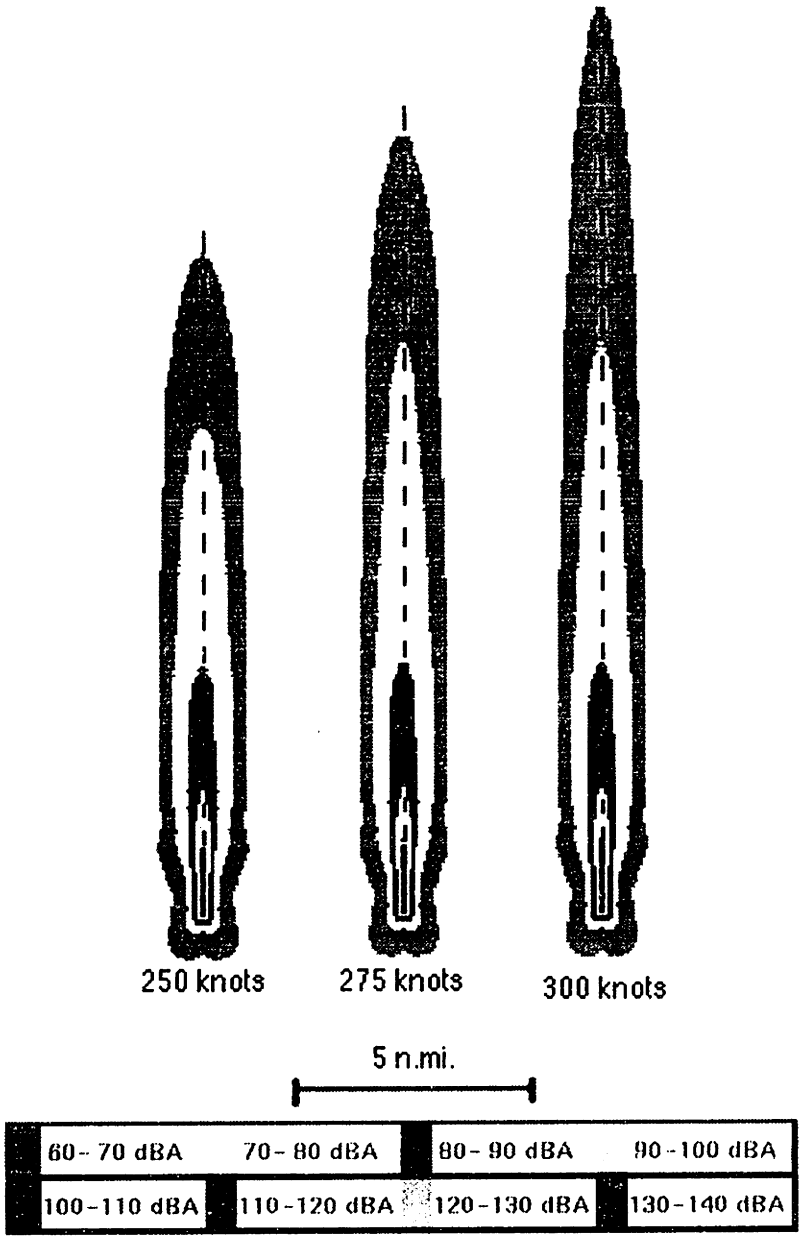

Figure 5-6: Footprints of Unrestricted Climb Speed Departure with Enroute Climb Speed of 275 and 300 knots, and Baseline Departure.

Figure 5-7 shows the noise impact of the Unrestricted Climb Speed Departure versus enroute climb speed, in 10 dBA bands relative to the Baseline Departure. As the figure shows, there are no changes in the area impacted by noise greater than 80 dBA. This is expected, since the height that the aircraft accelerates to the enroute climb speed is greater than the distance at which the noise intensity drops to 80 dBA. There are however, increases in the area impacted by noise below 80 dBA. If the aircraft accelerates to an enroute climb speed of 275 knots, the area impacted by 60-80 dBA

noise is increased by 16%. If the aircraft accelerates to an enroute climb speed of 300 knots, the area impacted by 60-80 dBA noise is increased by 24%. The increase in the area impacted by 60-80 dBA noise is the result of both the longer period over which the aircraft climb rate is decreased during acceleration, and the lower climb rate at higher enroute climb speeds. The actual population impacted however, depends on the population distribution in the communities around the airport, so evaluation of the noise impact of this proposal at a specific runway, requires a tool such as NOISIM.

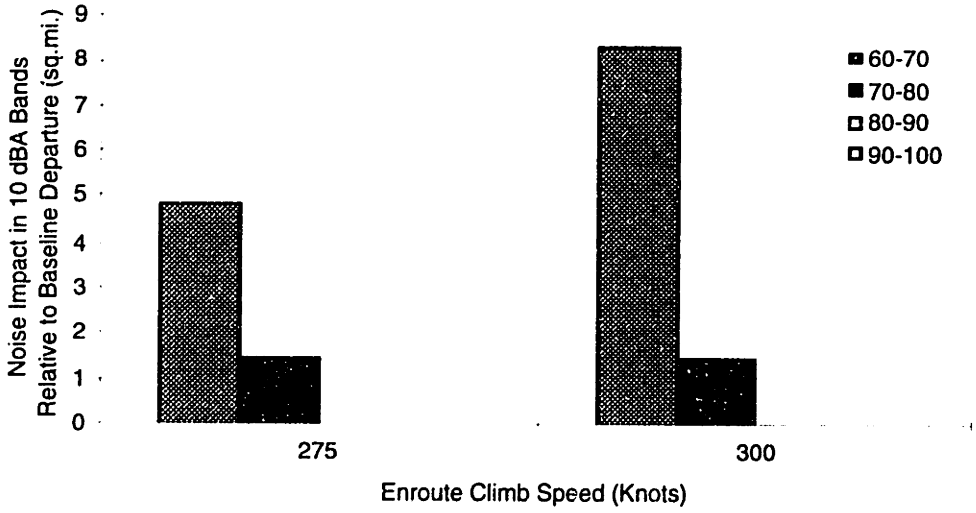

Figure 5-7: Impact of Unrestricted Climb Speed Departure vs. Climb Speed, in 10 dBA Bands Relative to Baseline Departure.

5.1.4 Thrust Cutback Departure

The Thrust Cutback Departure is designed to reduce the noise impact at a specific location. In the Thrust Cutback Departure, the initial thrust reduction in not accompanied by an acceleration to the maneuver speed. Instead, the thrust is reduced to a lower level that the climb thrust, and the speed of the aircraft is maintained at the initial climb speed. At a higher altitude, climb thrust is resumed and the aircraft accelerates to its maneuver speed, and then to its enroute climb speed. Figure 5-8 shows an example profile of the Thrust Cutback Departure. In this example, the aircraft thrust is reduced at 800 feet above the runway and the speed is maintained at 170 knots. At 2,000 feet above the runway, climb thrust is resumed and the aircraft accelerates to its maneuver speed of 210 knots. At 3,000 feet above the runway, the aircraft accelerates to its enroute climb speed of 250 knots.

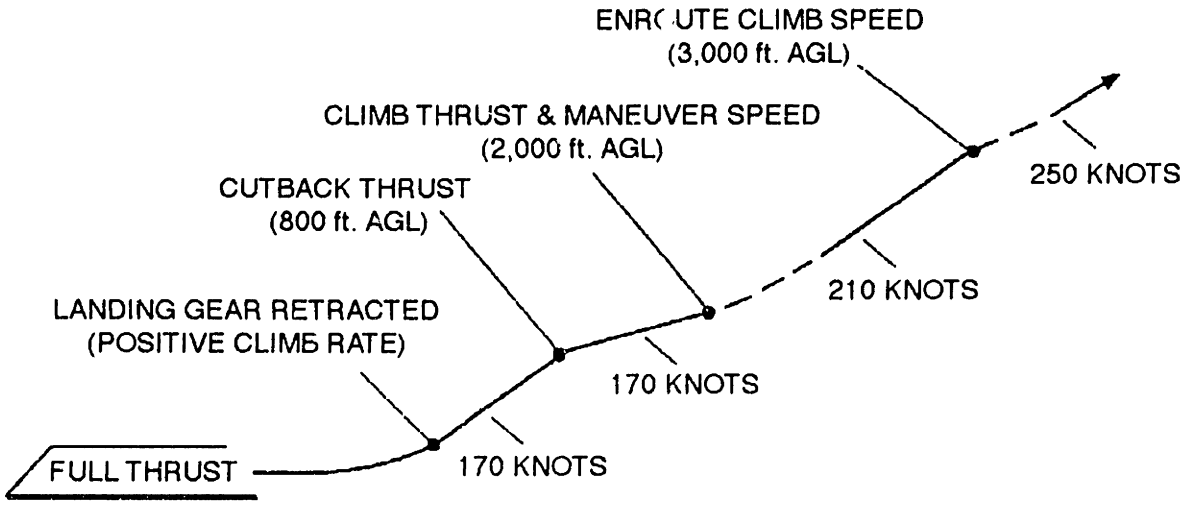

Figure 5-8: Thrust Cutback Departure.

If the height at which the cutback begins is fixed, the two parameters that determine the characteristics of the Thrust Cutback Departure are the thrust level during the cutback and the height that climb thrust is resumed. The effects of changes in these parameters on the noise impact of the Thrust Cutback Departure were investigated, and the results are presented below.

5.1.4.1 Thrust Level During Cutback

Figure 5-9 shows the noise footprints of the Thrust Cutback Departure with cutback to 50, 60, and 70% thrust at 800 ft. and climb thrust resumed at 2,000 ft. above the runway, along with the noise footprint of the Baseline Departure. As the figure shows, the length of the 90 dBA contour decreases with decreasing cutback thrust, while the length of the 60, 70, and 80 dBA contours increases with decreasing cutback thrust. The figure also shows that during the thrust cutback, the width of the 60, 70, and 80 dBA contours is less than the corresponding width during the Baseline Departure. In the case of the 80 dBA contour, this decrease in width results in a separation of the 80-90 dBA footprint. The portion furthest away from the runway represents the noise impact after climb thrust is resumed.

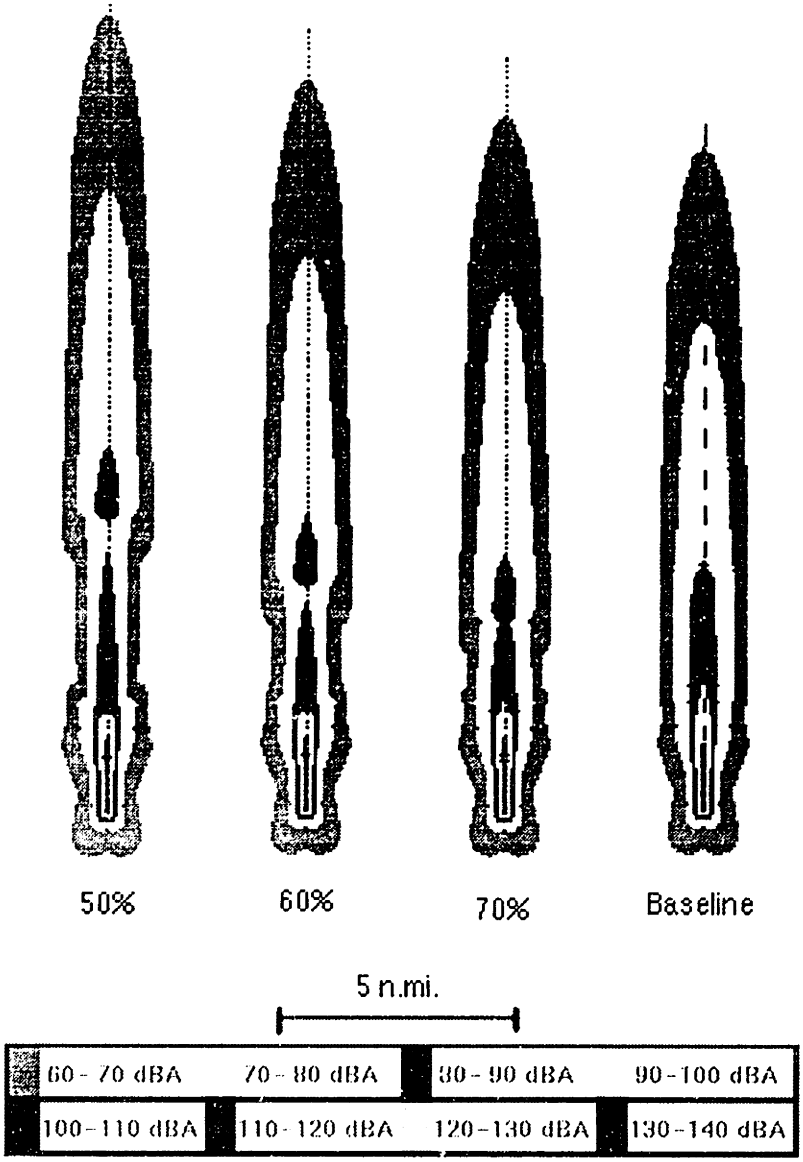

Figure 5-9: Footprints of Thrust Cutback Departure at 50, 60, and 70% Cutback Thrust, and Baseline Departure.

Figure 5-10 shows the noise impact of the Thrust Cutback Departure versus cutback thrust level, in 10 dBA bands relative to the Baseline Departure. The figure illustrates the trade between increases in low intensity noise and decreases in high intensity noise that occurs during the Thrust Cutback Departure. If the thrust is cutback to 50% thrust, the area impacted by 60-80 dBA noise is increased by 21%, while the area impacted by 80-100 dBA noise is decreased by 2%. If the thrust is cutback to 60% thrust, the area impacted by 60-80 dBA noise is increased by 10%, while the area impacted by 80-100 dBA noise is decreased by 20%. If the thrust is cutback to 70% thrust, the area impacted by 60-80 dBA noise is increased by 6%, while the area impacted by 80-100 dBA noise is

decreased by 14%. These results show that the greatest reduction in the area impacted by 80-100 dBA noise does not occur at the lowest cutback thrust, but at a specific intermediary thrust level. This indicates that, during a Thrust Cutback Departure, the area exposed to noise above 80 dBA may be minimized by the choice of cutback thrust level.

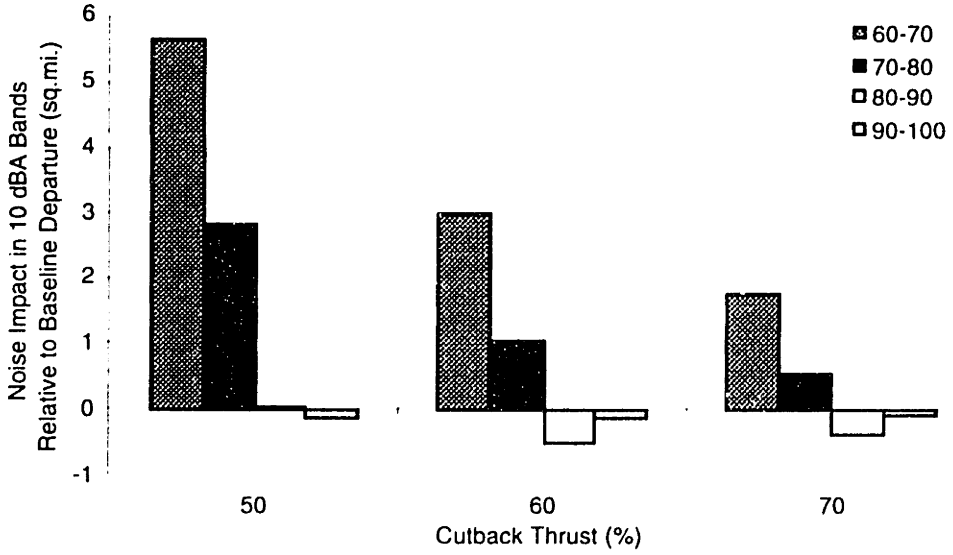

Figure 5-10: Impact of Thrust Cutback Departure vs. Cutback Thrust, in 10 dBA Bands Relative to Baseline Departure

5.1.4.2 Height Climb Thrust Resumed

Figure 5-11 shows the noise footprints of the Thrust Cutback Departure with cutback to 60% thrust at 800 ft. and climb thrust resumed at four different heights above the runway, along with the noise footprint of the Baseline Departure. The figure illustrates that as the height that climb thrust is resumed is increased, the length of the 60 dBA contour increases. The length of the 70 dBA contour increases initially, but then decreases above 2,500 ft. The footprints illustrate how the separation of the 80 dBA contour changes as the height increase.

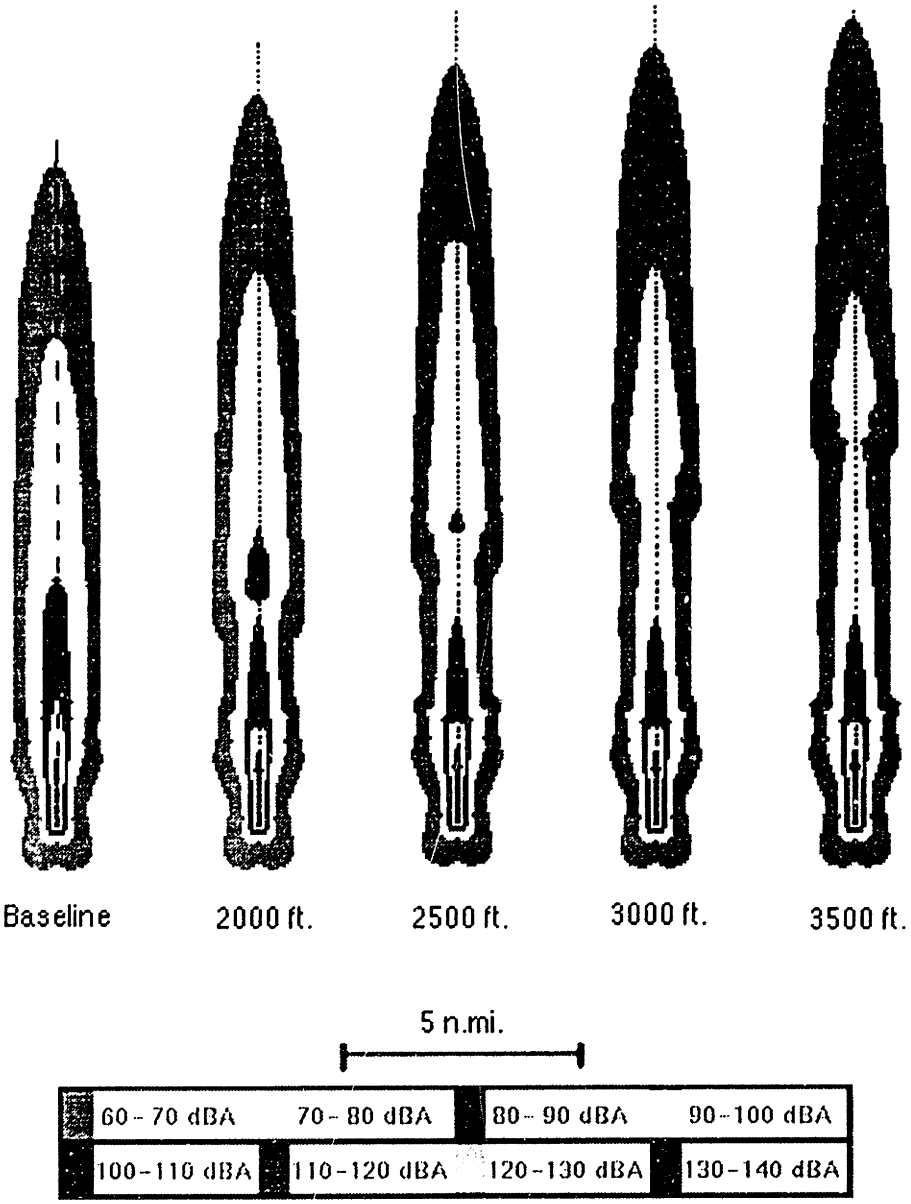

Figure 5-11: Footprints of Thrust Cutback Departure with Climb Thrust Resumed at Four Heights Above the Runway, and Baseline Departure.

Figure 5-12 shows the noise impact of the Thrust Cutback Departure with cutback to 60% thrust at 800 ft. and climb thrust resumed at four different heights above the runway, in 10 dBA bands relative to the Baseline Departure. The figure illustrates that when climb thrust is resumed at 2,000 ft. the area exposed to noise greater than 80 dBA is less than in the Baseline Departure, while the area exposed to noise less than 80 dBA is greater. It also illustrates that most of the reduction in the area exposed to noise greater than 80 dBA is achieved by increasing the height from 2,000 to 2,500 ft. The figure also shows that the area exposed to 70 to 80 dBA noise continues to decrease with increasing height,

while the area exposed to 60 to 70 dBA noise increases when the height is increased from 2,000 to 2,500 ft., then remains constant. Detailed results show that the area exposed to 90 to 100 dBA noise remains constant at 0.154 sq.mi. at all heights. They also show that the area exposed to 80 to 90 dBA noise decreases from 2.247 to 1.598 sq.mi. when the height is increased from 2,000 to 2,500 ft., then decreases to 1.452 sq.mi. when the height is increased to 3,000 ft., and remains constant with further increases in height.

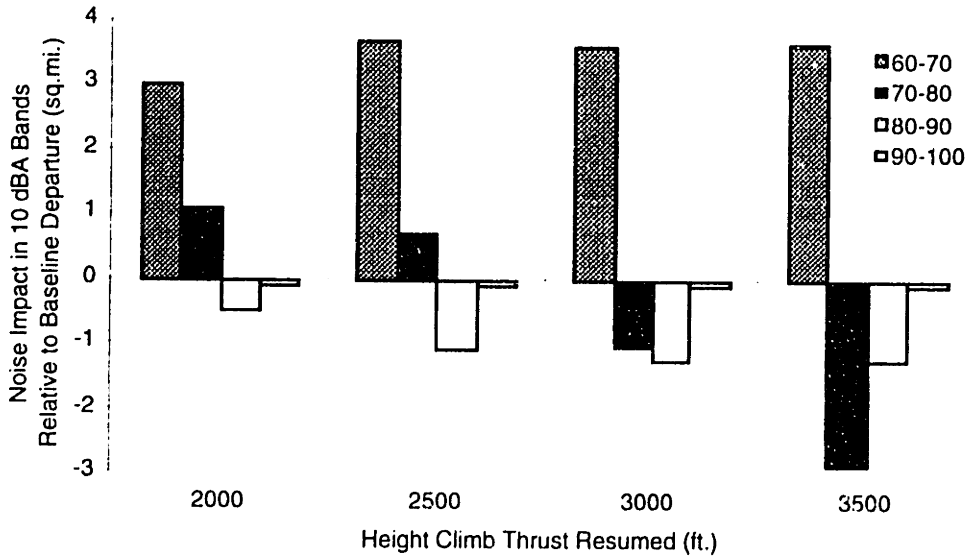

Figure 5-12: Impact of Thrust Cutback Departure vs. Height Climb Thrust Resumed, in 10 dBA Bands Relative to Baseline Departure.

5.1.5 ICAO Noise Abatement Departure

The goal of the ICAO noise abatement departure is to reduce the total area exposed to noise. This is achieved via a steeper than normal climb gradient. Figure 5-13 shows an example profile of the ICAO Noise Abatement Departure. In this example, the thrust is reduced to climb thrust when the aircraft is 1,500 feet above the runway, and the initial climb speed of 170 knots is maintained until the aircraft is 3,000 feet above the runway. At that height, the aircraft accelerates to its enroute climb speed of 250 knots.

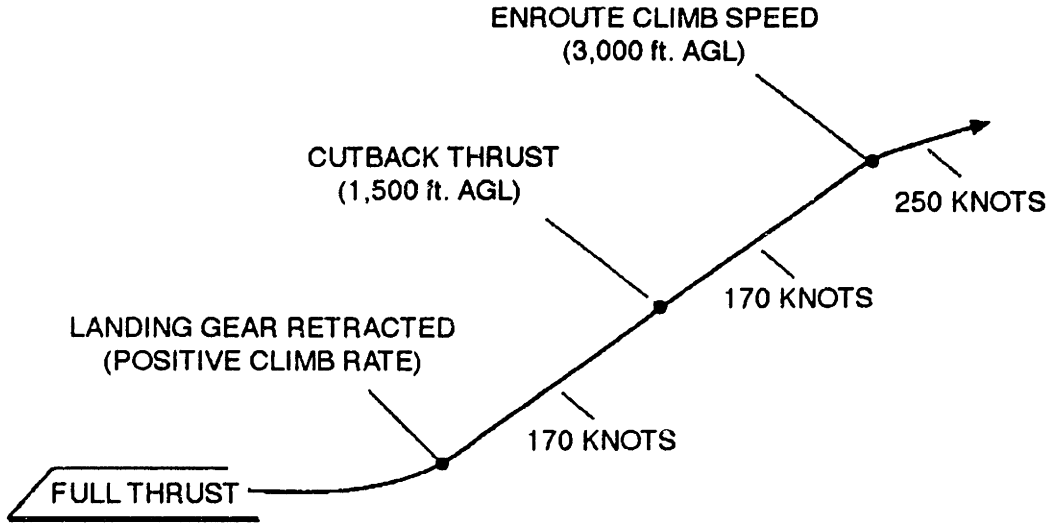

Figure 5-13: ICAO Noise Abatement Departure.

If the height above the runway at which the thrust reduction occurs is fixed, the two parameters that determine the noise impact of the ICAO Noise Abatement Departure are the height above the runway that the aircraft accelerates to the enroute climb speed and the thrust level after the thrust reduction. The effects of changes in these parameters on the noise impact of the ICAO Noise Abatement Departure were investigated, and the results are presented below.

5.1.5.1 Height Aircraft Accelerates to Enroute Climb Speed

Figure 5-14 shows the noise footprints of the ICAO Noise Abatement Departure with climb thrust of 80% and acceleration to an enroute climb speed of 250 knots at five different heights above the runway, along with the noise footprint of the Baseline Departure. Common to all five ICAO footprints is an increase in the width of the footprint near the runway that is representative of the greater height (1,500 ft.) at which the thrust reduction occurs. The figure shows that the length of the 60 dBA contour does not appear to change as the acceleration height is increased. The figure also shows that the length of the 70 dBA decreases significantly above 2,500 ft., but the successive reductions in the length of that contour diminish with increasing height. This indicates that accelerations to the enroute climb speed at greater heights reduces the noise impact in communities that are further away from the airport, but the rate of decrease diminishes with increasing acceleration height.

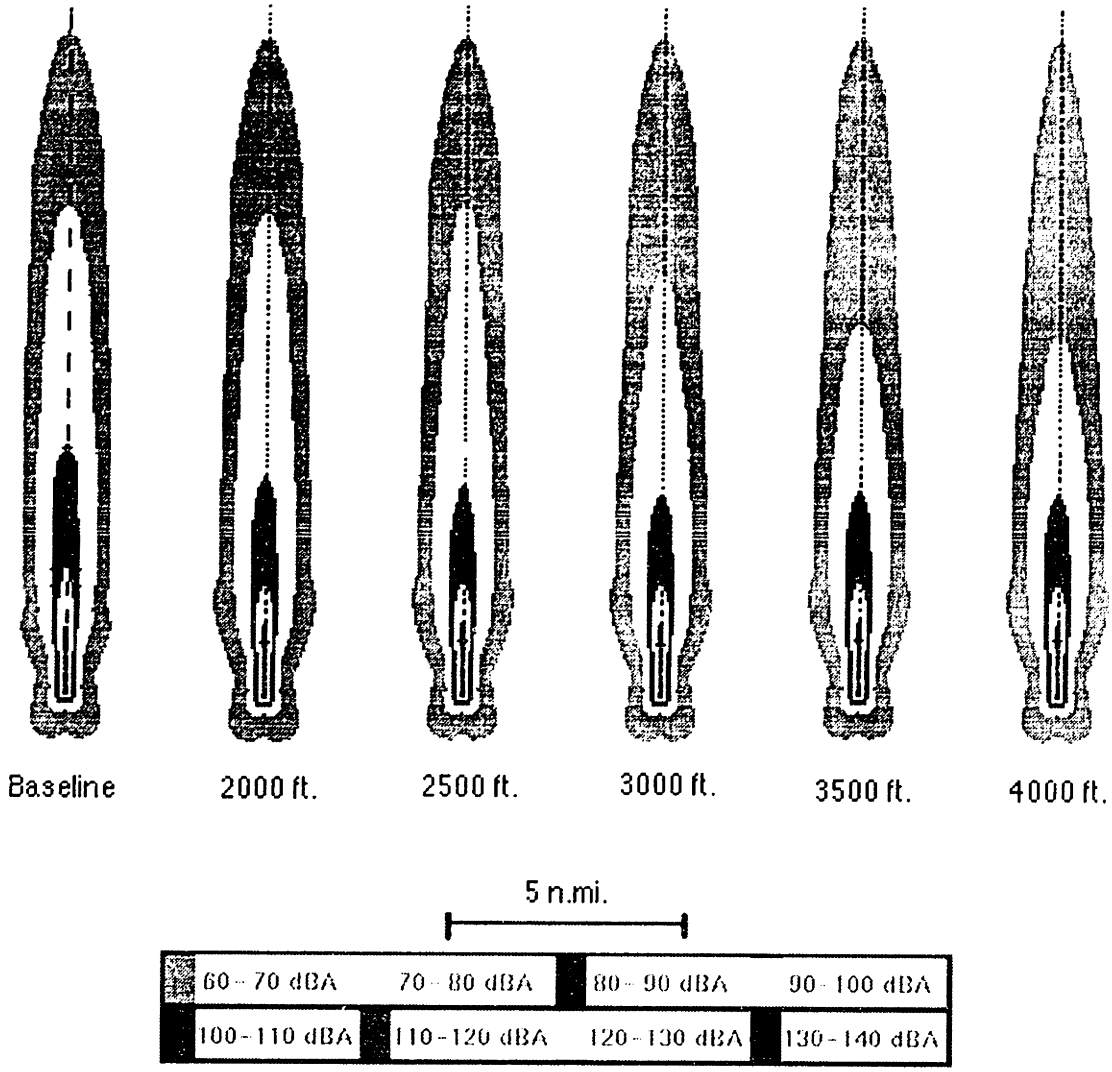

Figure 5-14: Footprints of ICAO Departure With Acceleration to Enroute Climb Speed at Five Different Heights Above Runway, and Baseline Departure.

Figure 5-15 shows the noise impact of the ICAO Noise Abatement Departure when the aircraft accelerates to the enroute climb speed at five different heights, in 10 dBA bands relative to the Baseline Departure. The results clearly indicate that the higher the acceleration to the enroute climb speed occurs, the greater the reduction in the noise impact. They also verify that the 70 dBA contour is most affected by changes in the acceleration altitude, and that the rate of decrease diminishes with increasing altitude. Detailed results show that the area impacted by 90 to 100 dBA noise has a constant value of 0.216 sq.mi. for all the heights studied. They also show that the area exposed to 80 to 90 dBA noise decreases from 2.139 to 1.946 sq.mi. when the height is increased from 2,000 to 2,500 ft., then decreases to 1.900 sq.mi. when the height increases to 3,000 ft., and remains constant with further increases in height.

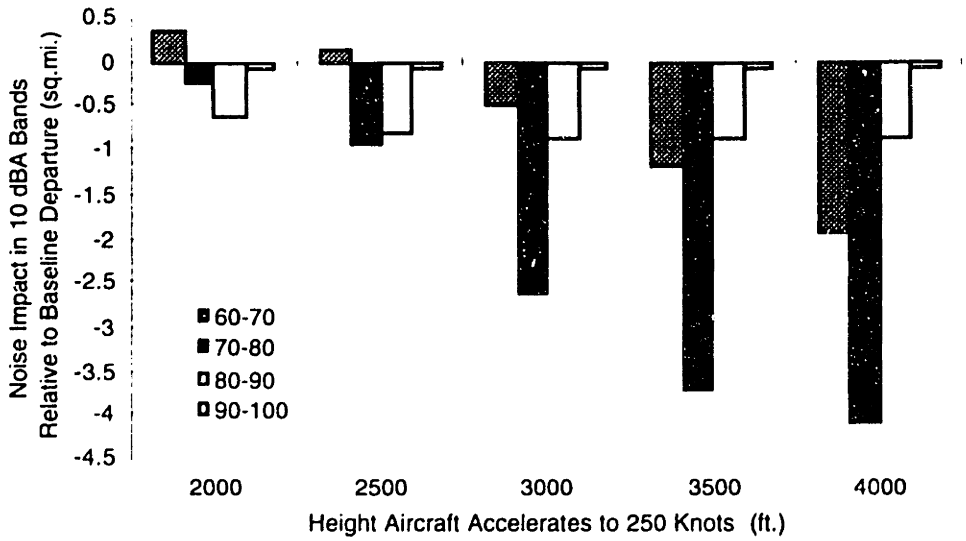

Figure 5-15: Impact of ICAO Departure vs. Height Aircraft Accelerates to Enroute Climb Speed, in 10 dBA Bands Relative to Baseline Departure.

5.1.5.2 Thrust Level

Figure 5-16 shows the noise footprints of the ICAO Noise Abatement Departure at 60, 70, and 80% climb thrust, along with the noise footprint of the Baseline Departure. The increased width of the noise footprint near the runway is again common to all the ICAO departures. As the figure shows, the shape of the 70 dBA contour undergoes much change as the climb thrust is changed. At a climb thrust of 80%, the length and width of this contour are less than in the Baseline Departure. When the climb thrust is decreased from 80 to 70%, the length and width of the 70 dBA contour decrease further. When the climb thrust is decreased to 60% however, the length of the contour increases, while the width of the contour decreases further. This elongation of the contour in the direction of the flight path is due to the difference in climb rate that can be sustained during a climbing acceleration at 60% thrust compared to the corresponding climb rate at 70% thrust.

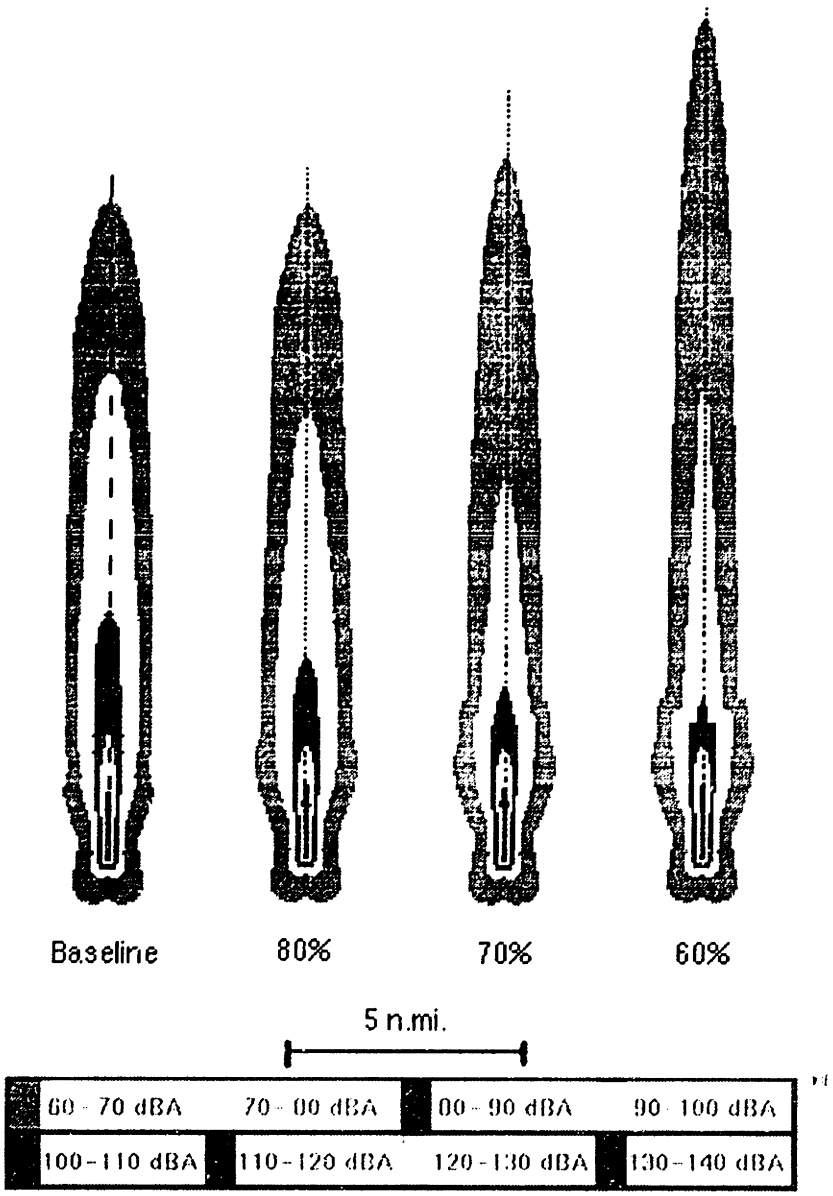

Figure 5-16: Footprints of ICAO Departure at 50, 60, and 70% Climb Thrust, and Baseline Departure.

Figure 5-17 shows the noise impact of the ICAO Noise Abatement Departure at three climb thrust levels, in 10 dBA bands relative to the Baseline Departure. At all three thrust levels, the ICAO Noise Abatement Departure reduces the noise impact in all noise ranges. The lower the thrust, the greater the noise reduction, and the lower the climb rate. Unlike the thrust cutback procedure where the lower thrust segment is transitory, the lower thrust segment of the ICAO Departure continues through a greater altitude range.

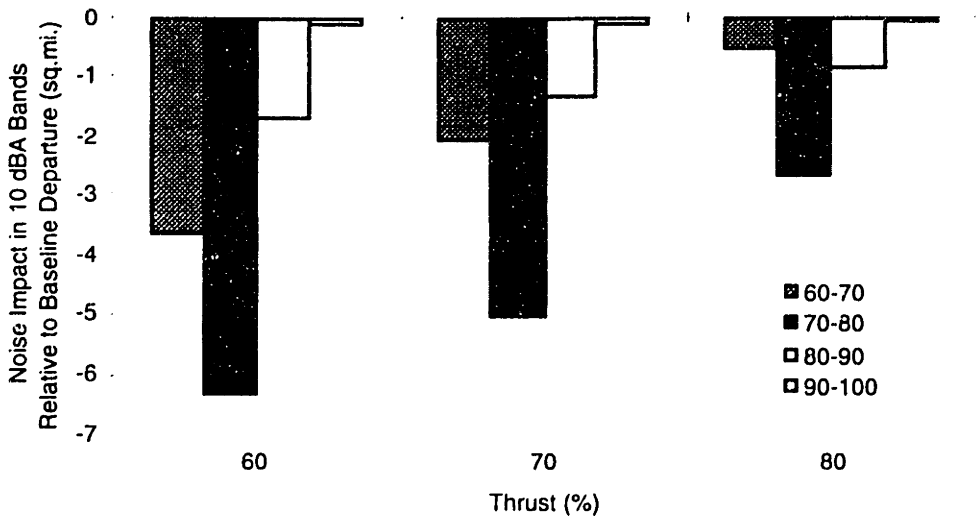

Figure 5-17: Impact of ICAO Departure vs. Climb Thrust Level, in 10 dBA Bands Relative to Baseline Departure.

5.1.6 Comparison of Departures

The results of this generic study illustrate the wide variation in the dimensions of the departure noise footprint as a function of both the type of procedure and the parameters (such as thrust or height) of that procedure. Because of this variation, it is necessary to evaluate the departure procedure at a specific site using a tool such as NOISIM, to determine the procedure that provides the greatest noise reduction for the population distribution and density around that particular airport.

5.2 Generic Study of Lateral Maneuvers

In the lateral domain, noise reductions are achieved by directing aircraft over areas of low noise sensitivity such as rivers or other unpopulated areas. The parameters that determine the effectiveness of these lateral deviations are the width of the noise footprint relative to the width of the low noise sensitivity area, and the lateral navigational precision of the aircraft. This section presents the results of an analysis of the relationship between the lateral navigational precision and the noise impact. Figure 5-18 shows the airport-community geometry used in the study. The airport is located at the beginning of an infinitely long channel of finite width W and zero population density. This channel is sandwiched between two areas of equal non-zero population density. The channel begins

at the departure end of the runway and is centered on the extended runway centerline. The airport is assumed to be sufficiently large that any noise behind the vertical plane defined by the boundary between the airport and the start of the channel, is contained within the airport.

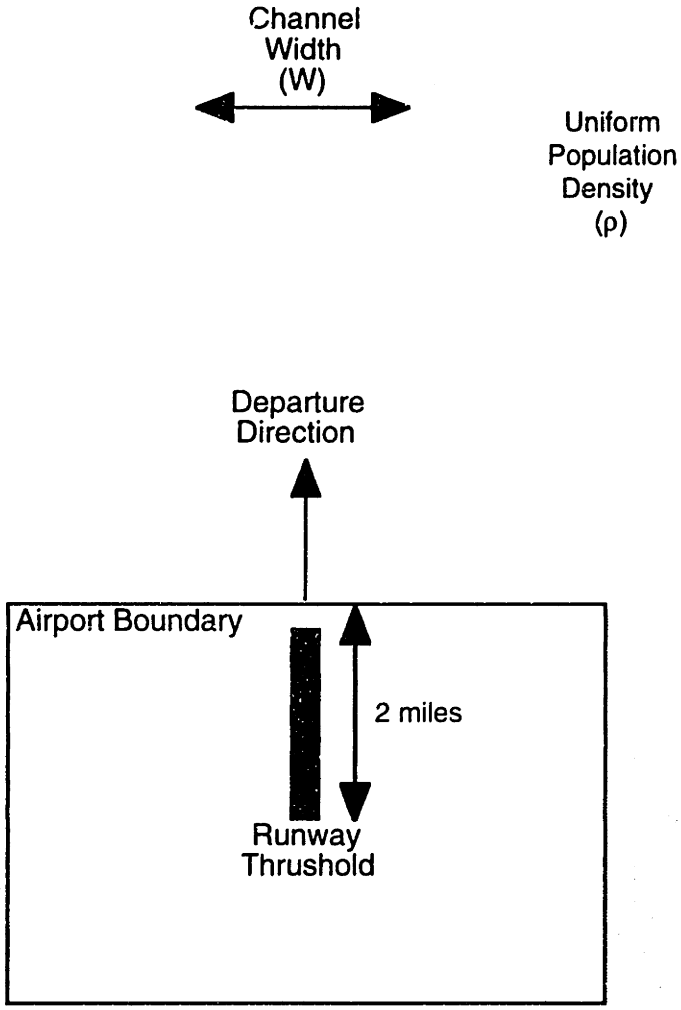

Figure 5-18: Airport-Community Geometry in Lateral Analysis.

The assumed noise abatement departure procedure for this airport requires that aircraft fly along the center of the channel until they are high enough above the runway that any changes in their heading will have no effect on the noise impact above 60 dBA. The

probability density function that describes the deviation from the center of the channel is assumed to have zero mean and a standard deviation equal to the lateral navigational precision of the aircraft.

Figure 5-19 shows the area impacted by noise greater than 60 dBA versus channel width for various levels of lateral navigational precision. As the figure shows, the noise impact in general has a stronger dependence on the width of the channel than the navigational precision. When the width of the channel is comparable to the width of the noise footprint however, as is the case when the channel width is 3,000m, the navigational precision has a greater effect on the noise impact.

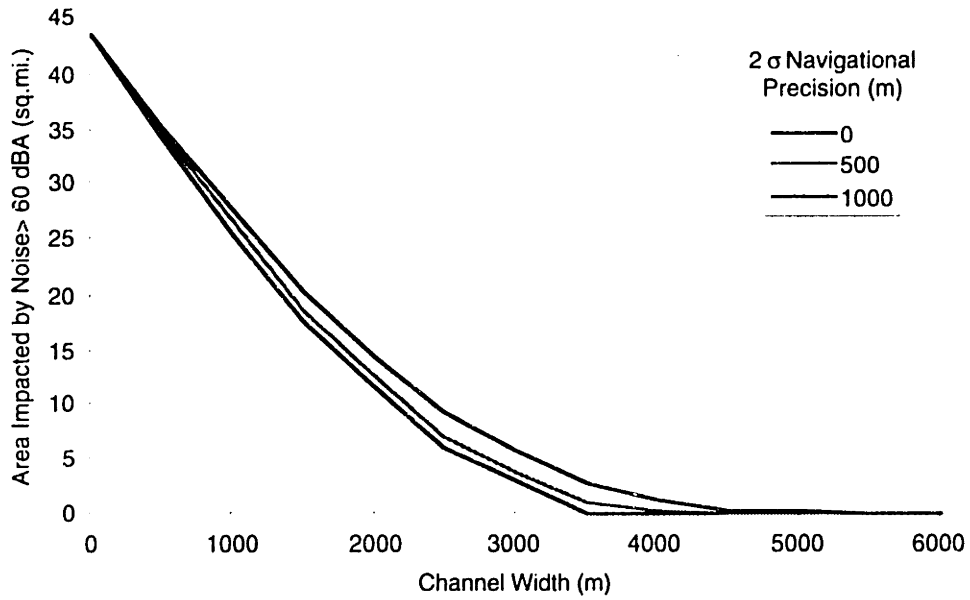

Figure 5-19: Area Impacted by Noise Greater Than 60 dBA vs. Channel Width for Various Levels of Navigational Precision.

Figure 5-20 shows the noise impact of an aircraft that follows the nominal path down the center of a channel that is 3,000 meters wide. The figure illustrates the relative dimensions of the boundaries of the channel and the noise footprints at different noise levels.

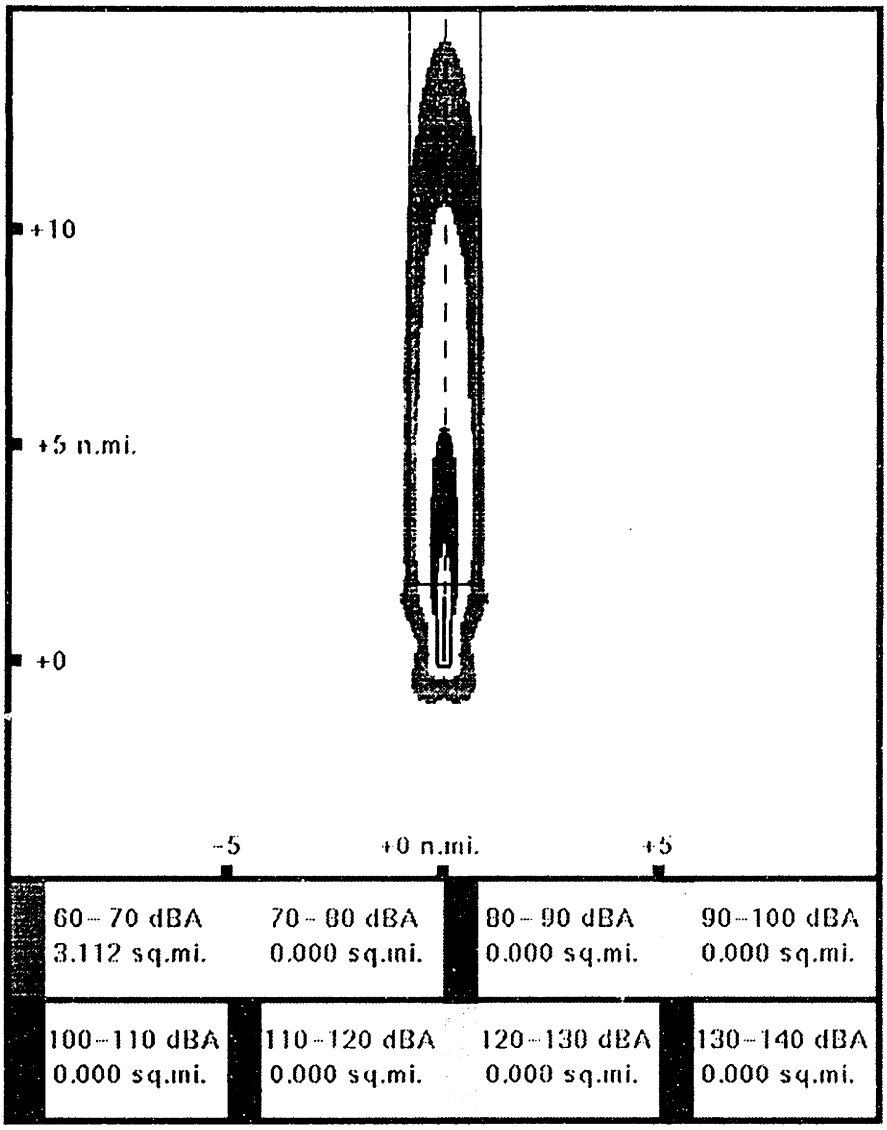

Figure 5-20: Noise Impact for Aircraft Departing Along the Center of a Channel that is 3,000 Feet Wide

Figure 5-21 shows the area impacted by noise greater than 60 dBA versus the lateral navigational precision of an aircraft departing over the 3,000m wide channel. As the figure shows, the navigational precision can have a significant effect on the noise impact. Previous work suggests that an aircraft using GPS position information may have a 2σ navigational precision of less than 500m [Barrows et al., 1996; Huntley, 1993]. For an aircraft with navigational precision of 500m, the area impacted by noise greater than 60 dBA is 3.9 sq.mi., an area that is 20% greater than the 3.112 sq.mi. impacted by the nominal trajectory. For an aircraft using heading guidance with an angular 2σ navigational precision of 7.5°, the area impacted by noise greater than 60 dBA is 7.4 sq.mi. an area that is 138% greater than the area impacted by the nominal trajectory.

These results illustrate the potential noise benefits of improved lateral navigational precision.

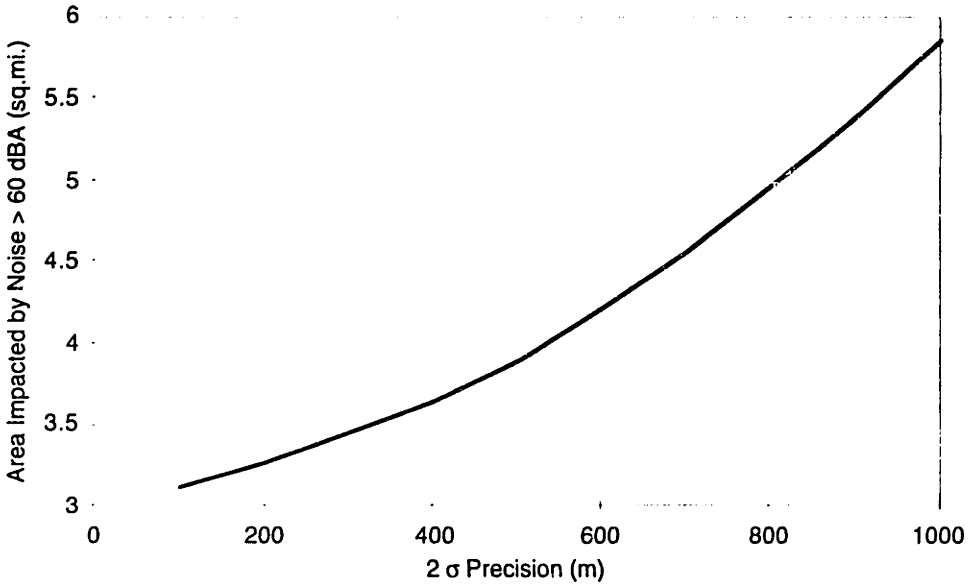

Figure 5-21: Area Impacted by Noise Greater Than 60 dBA vs. Navigational Precision of an Aircraft Departing Along the Center of a Channel that is 3,000 Feet Wide.

5.3 Case Study of Boston Logan Runway 4R

Logan Airport (BOS) is less than 2 miles drive from downtown Boston, and is adjacent to several residential communities in the Boston metropolitan area. The close proximity of these residential areas limit airport operations. One instance where noise restrictions limit aircraft operations is the departure from runway 4R.

5.3.1 Existing Noise Abatement Departure

Jet aircraft departing from runway 4R are required to perform a noise abatement departure designed to reduce the noise impact in these residential communities. In the existing procedure, the pilot maintains the runway heading until the aircraft is 4 nautical miles from the Distance Measurement Equipment (DME) beacon located at the airport. At this point the pilot changes the aircraft's heading to 90 degrees and flies towards the Atlantic Ocean. The noise impact of the existing noise abatement departure is shown in

Figure 5-22. The results shown represent the noise impact of an aircraft that follows the noise abatement procedure precisely.

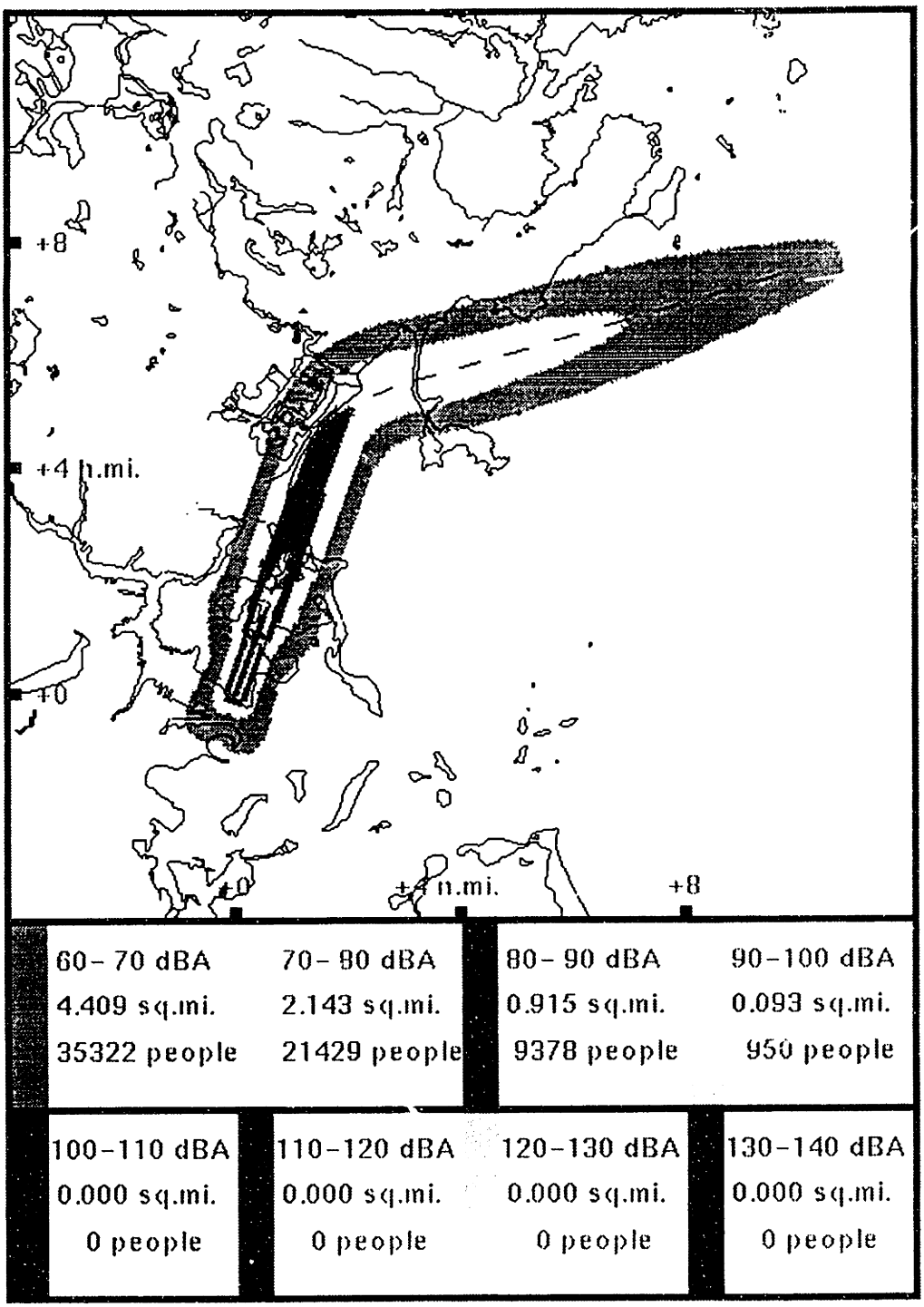

Figure 5-22: Footprint and Impact of Existing Noise Abatement Departure from BOS Runway 4R.

5.3.2 RNAV Enabled Noise Abatement Departure

The results of the generic studies indicate that a thrust cutback would be beneficial to the East Boston community adjacent to the departure end of the runway. Using NOISIM, the noise footprints derived during the generic study of Thrust Cutback Departures were used to determine the noise impact in that community as a function of the height that climb thrust is resumed. This investigation showed that for heights greater than 2,000 ft., the noise reduction in the communities adjacent to the departure end of runway 4R was independent of the height at which climb thrust is resumed, so a height of 2,000 ft. was selected.

Performing a thrust cutback however, increases the dimensions of the noise footprint, especially at locations further away from the runway. If a thrust cutback was combined with the lateral trajectory of the Existing Noise Abatement Departure, the noise reductions achieved during the thrust cutback would be offset by increased noise impact at locations further away from the runway. To compensate for the increase in the dimensions of the footprint, RNAV was to create a lateral trajectory that better matches the area of low noise sensitivity.

Figure 5-27 shows the noise footprint, area impacted, and the number of people impacted during this RNAV Enable Noise Abatement Departure. As the figure shows, the addition of a second turn allows the trajectory to be adjusted to match the area of low noise sensitivity. Thus, using NOISIM, the type of noise abatement procedure and the parameters of that noise abatement procedure may be selected based on the population distribution in the affected communities.

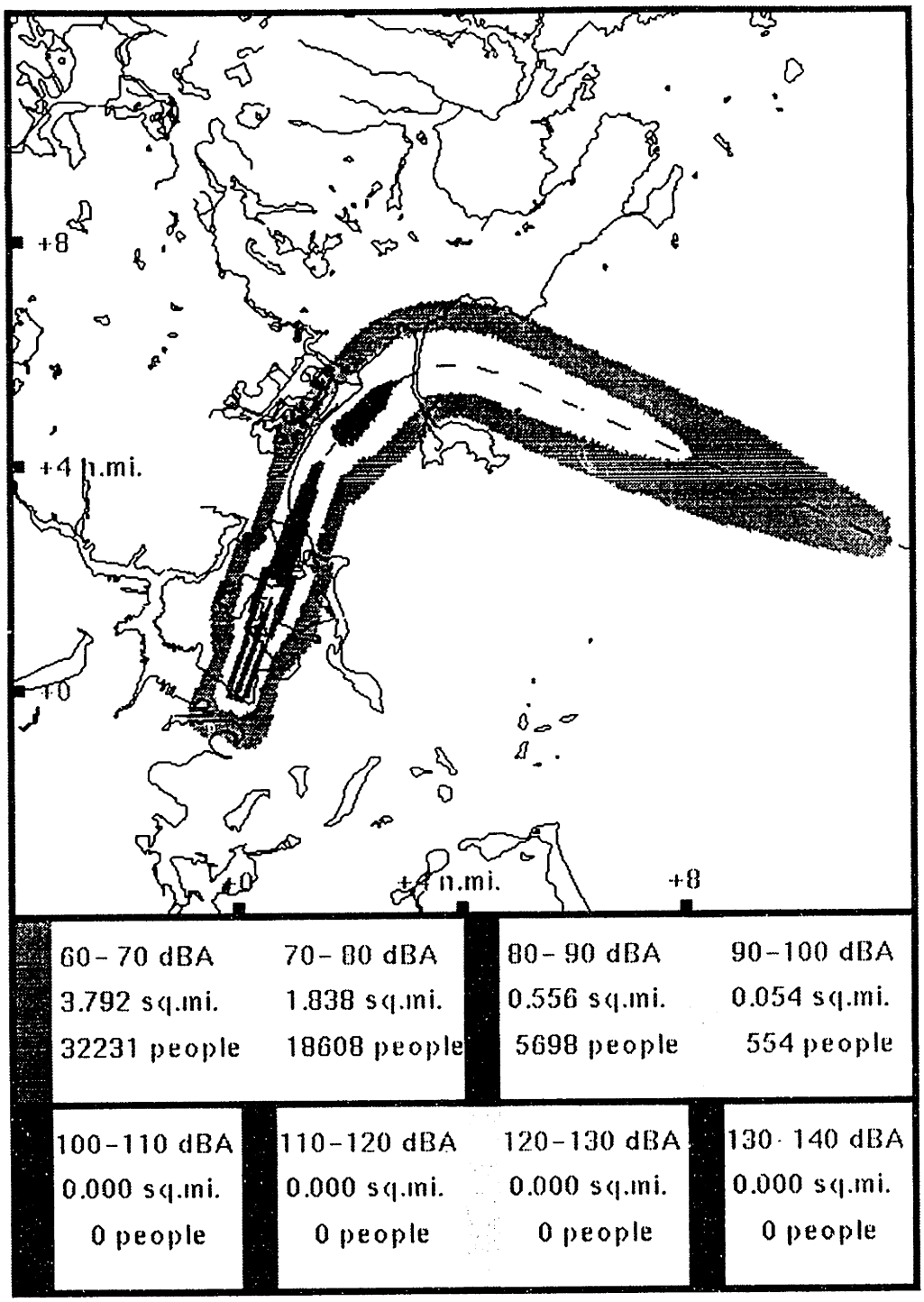

Figure 5-23: Footprint and Impact of RNAV Enabled Noise Abatement Departure from BOS Runway 4R.

5.3.3 Comparison of Departures

Figure 5-24 shows the number of people impacted during both the Existing and the RNAV Enabled Noise Abatement Departures. As the figure shows, the number of people impacted by the RNAV Enabled Noise Abatement Departure is reduced in all noise levels in comparison to the Existing Noise Abatement Departure. In each of the three noise ranges between 60 and 90 dBA approximately 3,000 are relieved from the noise impact of the existing procedure.

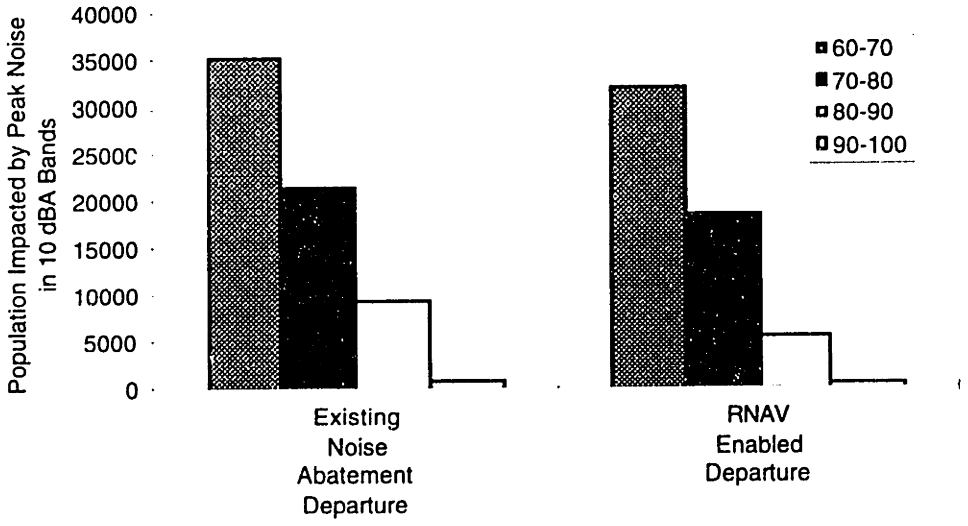

Figure 5-24: Noise Impact of Existing and RNAV Enabled Noise Abatement Departures from BOS Runway 4R, in 10 dBA Bands.

Figure 5-25 shows the total noise impact of the Existing and RNAV Enabled Noise Abatement Departure from runway 4R at Logan Airport. As the figure shows, the number of people impacted by noise greater than 60 dBA is reduced from 67,079 to 57,091, a 15% reduction.

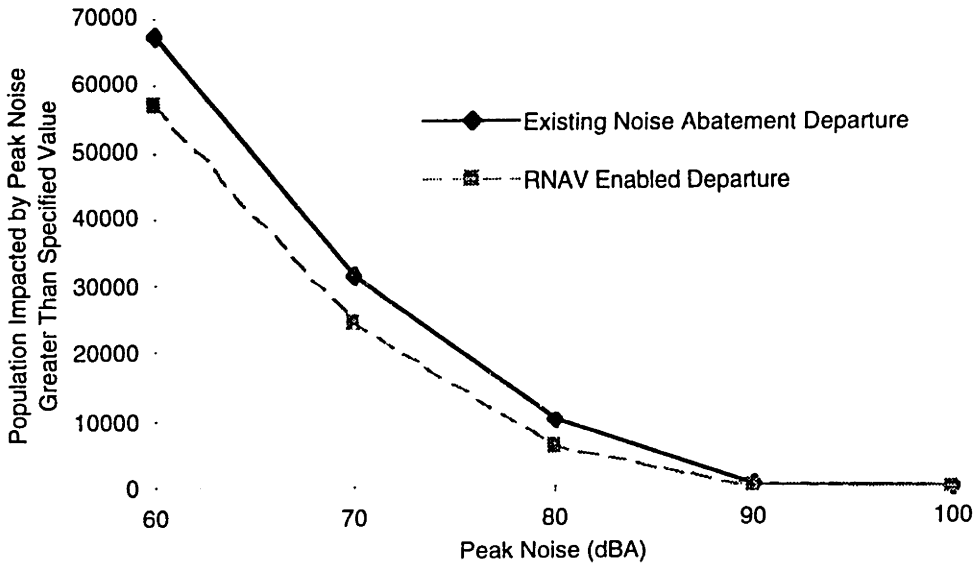

Figure 5-25: Total Noise Impact of Existing and RNAV Enabled Noise Abatement Departures from BOS Runway 4R.

5.3.4 Effect of Lateral Navigational Precision

Figure 5-26 shows a series of measured ground tracks for jet aircraft departing from runway 4R over a two week period beginning on November 17, 1996. As the figure shows, there are significant deviations from the desired track. These deviations are the result of factors such as the accuracy of the heading guidance, the accuracy of the distance measurements, the wind conditions, the time delay in pilot action, and the conformity of pilot action to the desired procedure.

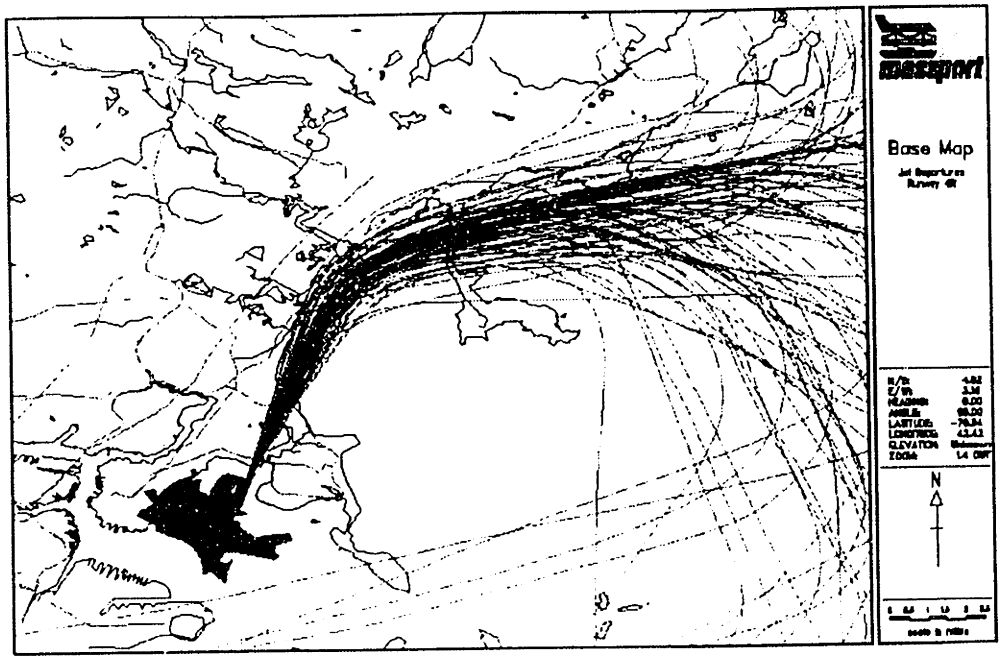

Figure 5-26: Ground Tracks of Aircraft Departing from BOS Runway 4R Over a Two Week Period.
[Reproduced With Permission of Massport]

Because of the lateral deviations in an aircraft's trajectory, it is necessary to investigate the sensitivity of any noise abatement departure to the lateral navigational precision of the aircraft. Figure 5-27 shows the noise impact of the RNAV Enabled Noise Abatement Departure versus lateral navigational precision. As the figure shows, the population impacted by the RNAV enabled departure is increased by approximately 375 people at a navigational precision of 500m (2σ). This increase is small compared to the over 10,000 person reduction from the Existing Noise Abatement Departure. This suggests that the RNAV Enabled Noise Abatement Departure is a robust solution. In addition to demonstrating the level of noise reductions that may be achieved if the aircraft follows the proposed procedure, NOISIM has also been used to determine how robust the noise reduction is to uncertainties in aircraft navigation.

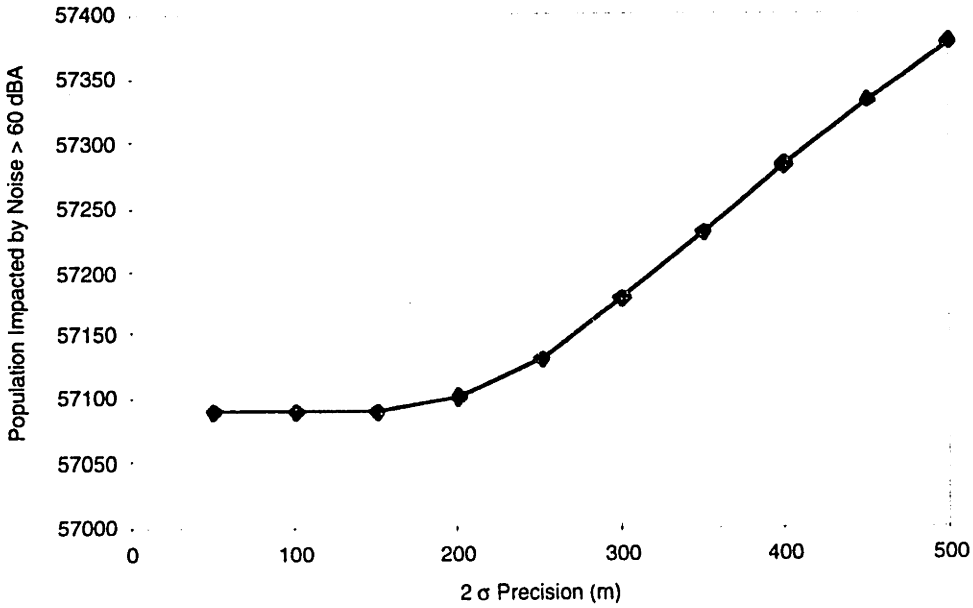

Figure 5-27: Population Impacted by Noise Greater Than 60 dBA vs. Navigational Precision During RNAV Enabled Noise Abatement Departure From BOS Runway 4R

6. Analysis of Missed Approach Procedures

Missed approach procedures are designed to direct aircraft away from airports when the aircraft has a failure that prohibits a normal landing or weather conditions prohibit landings (ceilings and/or visibility below minimums). Missed approach procedures typically involve climbing to a prescribed altitude while turning and flying to a prescribed navigation fix. The climbing turn in the direction of the missed approach fix is initiated when the aircraft has achieved a minimum height such as 500 ft. above the ground. When the aircraft reaches the missed approach fix, it enters a holding pattern until the aircraft can re-enter the approach sequence.

The simplicity of the missed approach procedure is predicated on the assumption that the missed approach is being performed because of a serious aircraft failure. In this scenario, a simple procedure facilitates easy recall and minimal control actions, attributes that are desirable for time critical tasks. In most cases however, it is the weather that precipitates the need for a missed approach. In weather related missed approaches there are no aircraft failures, so all the features of the guidance and control system are available to the flight crew. At the current time, all missed approaches to a specific runway are executed in a similar way regardless of the state of the aircraft. Therefore, although there are two causes of missed approaches, the missed approach procedures is designed to meet the requirements of the most critical case.

The requirement that the aircraft fly directly to the missed approach fix can, in many cases, direct the noise over areas of high population density that would not otherwise be impacted by aircraft operations. This is especially annoying as the low event frequency and high thrust levels of missed approaches magnifies the level of annoyance in these communities.

In weather related missed approaches, RNAV may be used to mitigate the noise impact. The FMS allows pilots to enter and recall specific trajectories that may be selected with a single control action. Storing the noise abatement departure for a runway as the missed approach procedure and using RNAV for lateral guidance enables low noise impact missed approaches. One airport that can benefit significantly from such a strategy is

Washington National Airport. The missed approach procedure for runway 36 is composed of a climbing left turn towards the Georgetown NDB and an altitude of 2,000 ft. The climbing turn is initiated when the aircraft is 500 ft. above the runway elevation. The trajectory of the aircraft takes it over heavily populated residential areas in Arlington, Virginia. The noise impact of this procedure is shown in Figure 6-1. The approach to the runway is a 3° Decelerating Approach. The lower noise impact of this approach over the ILS Approach ensures that the noise impact recorded is due primarily to the missed approach procedure. Figure 6-2 shows the noise impact for a RNAV Enabled Missed Approach procedure that utilizes the track of the noise abatement departure from runway 36.

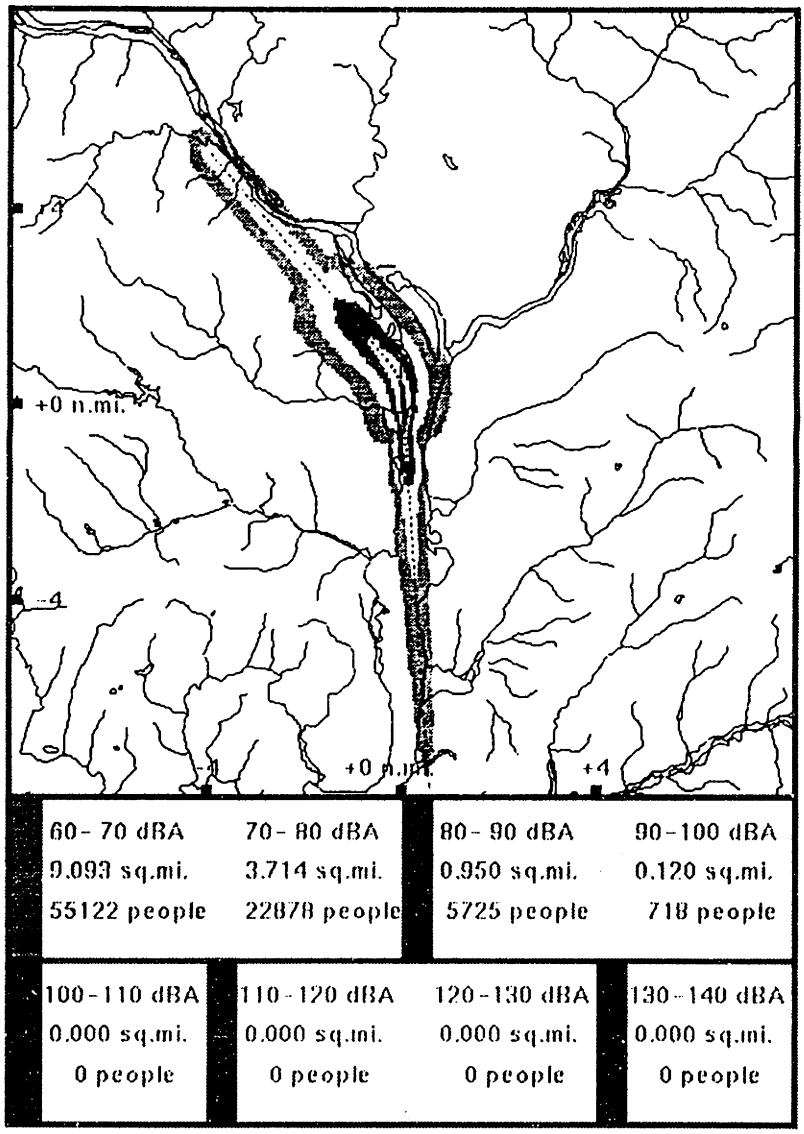

Figure 6-1: Impact of Existing Missed Approach from DCA Runway 36.

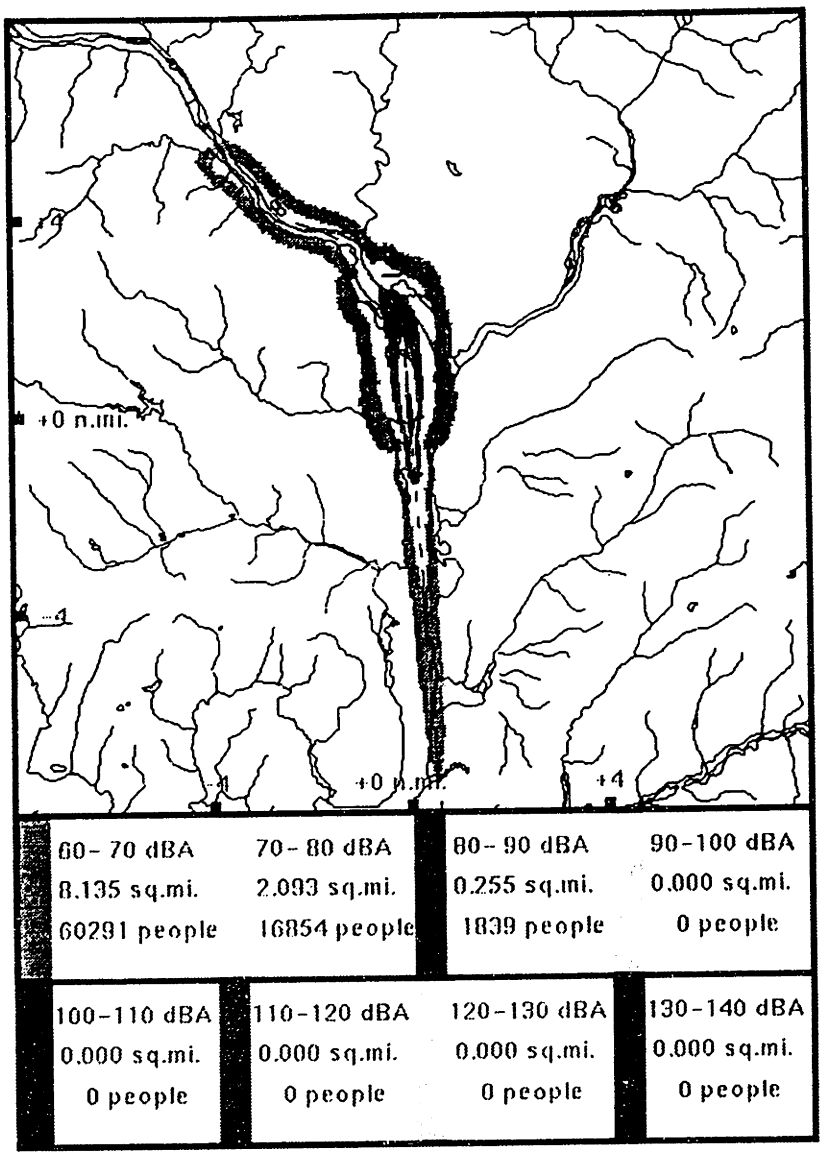

Figure 6-2: Impact of RNAV Enabled Missed Approach from DCA Runway 36.

Figure 6-3 shows the noise impact of the Existing and RNAV Enabled Missed Approaches, in 10 dBA bands. The figure shows that there is a reduction in the number of people impacted by noise between 70 and 100 dBA, and an increase in the number of people impacted by the lower intensity noise between 60 and 70 dBA.

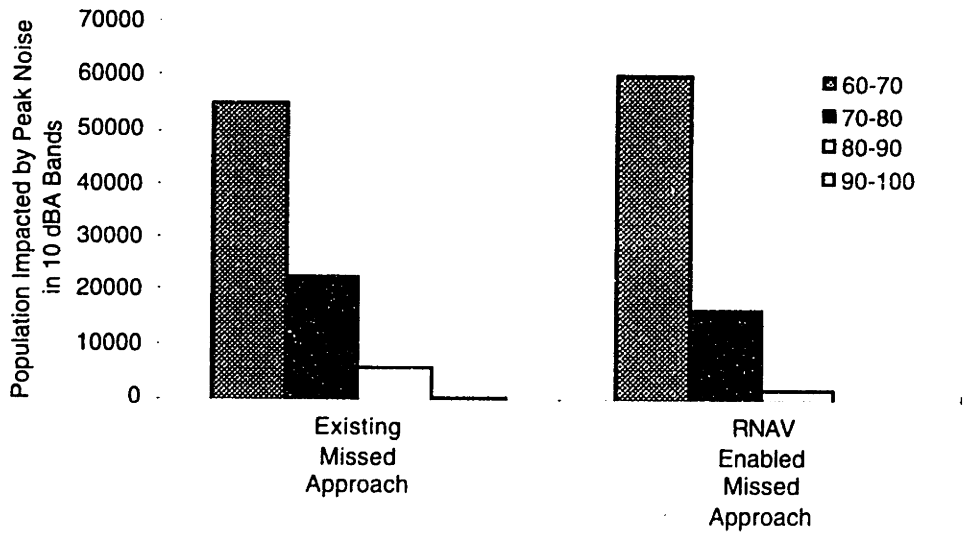

Figure 6-3: Noise Impact of Existing and RNAV Enabled Missed Approaches from DCA Runway 36, in 10 dBA Bands.

Figure 6-4 shows the total noise impact of the existing missed approach and the RNAV enabled missed approach. As the figure shows, when the RNAV enabled missed approach is used in place of the existing missed approach, the number of people impacted by noise greater than 70 dBA noise is reduced from 29,321 to 18,693, a 36% reduction.

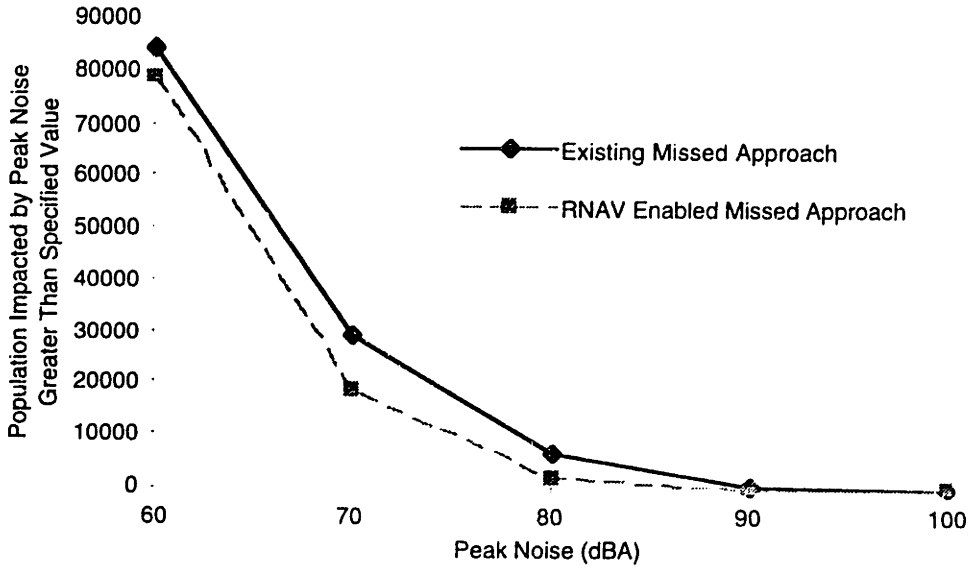

Figure 6-4: Total Impact of Existing and RNAV Enabled Missed Approaches from DCA Runway 36.

7. Summary and Conclusions

7.1 Summary

Advanced flight guidance technologies offer the potential to reduce the impact of aircraft noise on communities surrounding airports by allowing pilots to implement more flexible approach and departure procedures that reduce noise exposure to the most sensitive areas. The International Civil Aviation Organization (ICAO) has recognized the potential benefits of using advanced flight guidance technology to reduce the impact of aircraft noise, and has identified the following tasks:

1. Describe effective existing noise abatement operational procedures and strategies.
2. Evaluate the critical components of aircraft flight procedures that can minimize source noise emissions and community exposure.
3. Identify emerging and future airport systems technologies in the fields of flight management, ATC and airport capacity which could also serve to minimize community noise exposure.
4. Conceive new operating procedures to reduce community noise exposure taking account of the emerging and future technologies identified in 3.

in the development of noise abatement procedures that utilize the capabilities of advanced flight guidance technologies. In this thesis, a system analysis methodology has been presented that incorporates the impact of aircraft noise as a consideration in the design of approach and departure procedures. This methodology utilizes tools developed using the principles of systems analysis.

7.1.1 NOISIM

The primary tool used in the systems analysis is NOISIM. This tool combines a Flight Simulator, a Noise Model, and a Geographic Information System (GIS) to create a unique rapid prototyping environment in which the user can simulate an aircraft's operation in existing and potential guidance and navigation environments, while simultaneously

evaluating the aircraft's noise impact. NOISIM has been designed to incorporate the factors that are critical to the noise performance of flight procedures:

- Aircraft Performance and Trajectory
- Noise Generated by the Aircraft
- Population Distribution and Density
- Flight Safety and Pilot Acceptance
- Guidance and Navigation Requirements
- Local Atmospheric Conditions

Traditionally these factors have been considered either independently or in subsets. NOISIM provides a unique environment in which these factors may be considered simultaneously. This approach to developing noise abatement procedures incorporates the coupled relationships that exist between the factors, thus providing a comprehensive method for developing noise abatement solutions.

7.1.2 Approach

NOISIM was used to perform a generic study of approach procedures. Three procedures were evaluated in the study: the baseline ILS Approach, the Vertically Segmented Approach, and the 3° Decelerating Approach. The Vertically Segmented Approach and the 3° Decelerating Approach are noise abatement procedures. The results of the generic study indicate that both noise abatement procedures provide significant noise reduction in comparison to the ILS Approach, and have comparable noise impact. Pilot acceptance was also evaluated in a Flight Simulator study. Subjective results of that evaluation indicate that the 3° Decelerating Approach is preferred to the Vertically Segmented Approach, and thus provides the best combination of noise reduction and pilot acceptance.

The 3° decelerating approach was evaluated in two case studies that illustrate its effectiveness in two distinctly different circumstances. The approach to runway 22L at Logan Airport was first studied. When the 3° Decelerating Approach was used in place of the existing ILS approach, the number of people impacted by noise greater than 60 dBA was reduced from 26,982 to 20,552, a 24% reduction.

The approach to runway 13L at Kennedy Airport was also studied. When the 3° Decelerating Approach was used in place of the existing ILS Approach, the number of people impacted by noise greater than 60 dBA was reduced from 252,734 to 79,851, a 68% reduction. The noise impact of the 3° Decelerating Approach was found to be comparable to the noise impact of the Canarsie VOR Approach, the existing VMC noise abatement approach. Unlike the Canarsie VOR Approach however, the 3° Decelerating Approach may be used in IMC.

7.1.3 Departure

NOISIM was used to perform a generic study of departure procedures. Five procedures were evaluated in the study. The first, the Baseline Departure, consists of a full thrust takeoff with derated thrust climb. The second, the Derated Thrust Departure, has been developed to address engine maintenance concerns. The third, the Unrestricted Climb Speed Departure, has been proposed as a method of increasing airline efficiency. The fourth and fifth procedures, the Thrust Cutback Departure and ICAO Noise Abatement Departure, are noise abatement procedures.

The results of the generic study indicate that:

- Derated Thrust Departures have little effect on the noise impact at low intensities, but have a significant effect on the impact of higher intensity noise. These procedures impact communities that are adjacent to the airport perimeter as these communities are impacted by changes in the extent of higher intensity noise.

- Implementation of the proposal to remove the indicated airspeed limit in the U.S. of 250 knots below 10,000 ft. will increase the area exposed to noise between 60 and 80 dBA. The increase in the noise impact however, occurs at distances greater than 10 nautical miles from the runway threshold.

- The Thrust Cutback Departure provides noise reduction in communities immediately adjacent to the airport perimeter, but increases the noise impact in communities that are further away from the airport. During the Thrust Cutback Departure, the area impacted by noise between 60 and 80 dBA may be minimized by the choice of cutback thrust. The height above the runway altitude at which the normal climb thrust is resumed had a significant effect on the area impacted

by noise above 70 dBA, but little effect on the area impacted by noise between 60 and 70 dBA.

- The ICAO Noise Abatement Departure provides significant reductions in the total area exposed to aircraft noise. The noise impact of this procedure decreases as the height that the aircraft accelerates to its enroute climb speed is increased, but there are diminishing returns with further increases in height.

The departure from runway 4R at Logan Airport was analyzed in a case study. A noise abatement departure procedure was developed using the results of the parametric studies. In the procedure, a thrust cutback is performed to reduce the noise impact in the residential communities adjacent to the departure end of the runway. The capabilities of RNAV and GPS were used to design a lateral path that directs the aircraft more precisely through an area of low noise sensitivity. The improved lateral precision compensates for the increase in the dimensions of the noise footprint that result from the thrust cutback. When the RNAV Enabled Departure was used in place of the Existing Noise Abatement Departure, the number of people impacted by noise greater than 60 dBA was reduced from 67,079 to 57,091, a 15% reduction.

7.1.4 Missed Approach

Missed approach procedures are designed to direct aircraft away from airports when the aircraft has a failure that prohibits a normal landing or weather conditions that prohibit landings (ceilings and/or visibility below minimums). Although there are two causes of missed approaches, the design of the missed approach procedure is predicated on the assumption that the missed approach is being performed because of a serious aircraft failure. In weather related missed approaches, RNAV may be used to mitigate the noise impact. In a case study of the missed approach to runway 36 at National Airport, it was found that when a RNAV enabled missed approach was used in place of the existing missed approach, the number of people impacted by noise greater than 70 dBA noise was reduced from 29,321 to 18,693, a 36% reduction.

7.2 Conclusions

- NOISIM has proven to be a unique and effective tool for developing and evaluating noise abatement procedures. Its combined features enable accurate

simulation of an aircraft's trajectory and thrust profile, evaluation of operational issues, and determination of the aircraft's noise impact.

- The results of the generic and case studies indicate that significant noise reductions may be achieved through approach, departure, and missed approach procedures that utilize advanced flight guidance technologies. The results also show that the level of noise reduction that may be achieved is heavily dependent on the details of the aircraft's trajectory and thrust history, as well as the population distribution and density in the communities around the airport. This verifies the need for a tool such as NOISIM which may be used to evaluate specific procedures at specific locations.

- In combination, RNAV and GPS appear to provide the accuracy and flexibility required to implement flight procedures that may be adjusted for noise considerations. Implementation of RNAV enabled procedures using NOISIM suggests that implementation of these procedures in the cockpit is feasable.

7.3 Recommendations

- Cockpit implementation of noise abatement procedures such as the 3° Decelerating Approach is now possible with the capabilities of advanced flight guidance technology. Implementation of such procedures however, must be made within the context of the air traffic control structure in which the aircraft must operate. At the present time, air traffic controllers utilize many of the features of the ILS Approach such as the straight approach at constant speed to sequence aircraft for landing. During a 3° Decelerating Approach however, the ability of a controller to predict the future position of an aircraft may be diminished. A sequencing methodology must be developed to account for the 3° Decelerating Approach.

- Recent advances in air traffic control decision aiding technology such as the Center TRACON Automation System (CTAS) have greatly improved the ability to predict the future position of aircraft. Using a system such as CTAS to aid in the sequencing of aircraft, should be investigated.

- The aircraft simulated in NOISIM is a 737-200 with JT8D engines. The flight and noise characteristics of this aircraft-engine combination cannot be used to

accurately represent the characteristics of other aircraft-engine combinations, thus NOISIM needs to be expanded to include a wider variety of aircraft and engine types.

- NOISIM provides a unique rapid prototyping environment to develop and evaluate single event noise abatement procedures. Many people, including airport planners, utilize the extended or average noise impact to determine the appropriate runway utilization. The noise simulation component of NOISIM needs to be expanded to include averaging so that once a procedure is developed, appropriate runway utilization may be determined.

Bibliography

[Abbot, 1989] Abbot, T. S., *Task-Oriented Display Design: Concept and Example*, SAE-892230, Presented at the SAE Aerospace Technology Conference, Anaheim, California, September 25-28, 1989.

[Barrows et al., 1996] Barrows, A. K., Enge, P., Parkinson, B. W., and Powell, J. D., *Evaluation of a Perspective-View Cockpit Display for General Aviation Using GPS*, Navigation, Journal of the Institute of Navigation, Vol. 43, No. 1, Spring 1996, pp. 55-69.

[Bose, 1990] Bose, K. W., *Aviation Electronics*, IAP, 1990.

[Clarke and Hansman, 1995] Clarke, J.-P., and Hansman, R. J., *Parametric Study of the Noise Impact of Approach and Departure Maneuvers Using Advanced Flight Guidance Techniques*, AIAA-95-0835, Presented at the 33rd Aerospace Sciences Meeting, Reno, Nevada, January 7-12, 1995.

[Demosthenes, 1992] Demosthenes, T. A., *Situation versus Command Symbology for Hybrid Landing Systems Applications*, SAE-921967.

[Denery et al., 1973] Denery, D. G., Bourquin, K. R., White, K. C., and Drinkwater III, F. J., *Evaluation of Three-Dimensional Area Navigation for Jet Transport Noise Abatement*, Journal of Aircraft, Vol. 10, No. 4, April 1973, pp. 226-231.

[Denery et al., 1975] Denery, D. G., White, K. C., and Drinkwater III, F. J., *Status and Benefits of Instrumented Two Segment Approach, August 1974*, Journal of Aircraft, Vol. 12, No. 10, October 1975, pp. 791-798.

[Epstein, 1993] Epstein, A. H., *16.54 Classnotes*, MIT, 1993.

[FAA, 1969] Anon., "Noise Standards: Aircraft Type Certification," *Federal Aviation Regulations Part 36, 34 FR 18364*, November 18, 1969. Amended (36-1), 34 FR 18815, November 25, 1969.

[FAA, 1976] Anon., *United States Standard for Terminal Instrument Procedures (TERPS)*, FAA Handbook 8260.3B, July 7, 1976.

[FAA, 1994a] Anon., *Federal Aviation Regulations*, FAA, 1994.

[FAA, 1994b] Anon., *Airmans Information Manual*, FAA, 1994.

[Fishbein, 1995] Fishbein, S. B., *Flight Management Systems*, Praeger, 1995.

[Flythe, 1992] Flythe, M. C., *Integrated Noise Model - Version 3: User's Guide - Revision 1*, DOT/FAA/EE Report No. 92/02, June, 1992.

[Garbell, 1990] Garbell, M. A., *The Effect of Noise Abatement Profiles on Noise Emissions and Human Annoyance Underneath a Subsequent Climb Path*, Presented at the FAA/NASA En Route Noise Symposium, 1990.

[Hansman et. al., 1992] R. J. Hansman, C. R. Wanke, M. Mykityshyn, E. Hahn, and A. H. Midkiff, *Hazard Alerting and Situational Awareness in Advanced Air Transport Cockpits*, Presented at the 18th International Council for the Aeronautical Sciences, Beijing, China, September 1992.

[Heidmann, 1975] Heidmann, M. F., *Interim Prediction Method for Fan and Compressor Source Noise*, NASA TM X-71763, 1975.

[Helfrick, 1984] Helfrick, A. D., *Modern Aviation Electronics*, Prentice-Hall, 1984.

[Hill and Peterson, 1992] Hill, P. G., and Peterson, C. R., *Mechanics and Thermodynamics of Propulsion*, Addison-Wesley, 1992.

[Huntley, 1993] Huntley, M. S., *Flight Technical Error from 93 Category B Approaches Using Non Differential GPS for Guidance*, GPS/VOR Overlay Project Data Report, Volpe National Transportation Systems Center, 1993.

[ICAO, 1993] Anon., *Attachment C to the Report on Agenda Item 7, Terms of Reference of Working Group 2, Aerodromes and Operations - Noise and Emissions*, ICAO, 1993.

[Jacobs, 1987] Jacobs, H. G., *Flight management procedures for noise-minimal landing trajectories with consideration of temperature and wind gradients*, Presented at the 10th Triennial World Congress of the International Federation of Automatic Control, Munich, 27-31 July 1987.

[Kelly and Davis, 1994] Kelly, R. J., and Davis, J. M., *Required Navigational Performance for Precision Approach and Landing with GNSS Applications*, Navigation, Journal of the Institute of Navigation, Vol. 38, No. 1, Spring 1994, pp. 1-30.

[Kendal, 1987] Kendal, B., *Manual of Avionics*, BSP Professional Books, 1987.

[Kerrebrock, 1992] Kerrebrock, J. L., *Aircraft Engines and Gas Turbines*, MIT Press, 1992.

[Logsdon, 1992] Logsdon, T., *The NAVSTAR Global Positioning System*, Van Nostrand Reinhold, 1992.

[Mattingly, 1996] Mattingly, J. D., *Elements of Gas Turbine Propulsion*, MacGraw Hill, 1996.

[Middleton, 1989] Middleton, D. H., *Avionic Systems*, Longman Scientific and Technical, 1989.

[Midkiff, 1993] Midkiff, A. H., *Benefit Analysis of Additional Incremental Teakeoff Power Derating in MD-80 and DC-10 Fleets*, American Airlines, 1993.

[Pierce, 1989] Pierce, A. D., *Acoustics: An Introduction to its Physical Principles and Applications*, Acoustical Society of America, 1989.

[Pratt and Whitney, 1974] *The Aircraft Gas Turbine Engine and Its Operation*, Pratt and Whitney Operating Instructions 200, May, 1974.

[Romrell et al., 1996] Romrell, G., Johnson, G., Brown, R., and Kaufman, D., *DGPS Category IIIB Feasibility Demonstration Landing System With Flight Test Results*, Navigation, Journal of the Institute of Navigation, Vol. 43, No. 2, Summer 1996, pp. 131-147.

[RTCA, 1995] RTCA Task Force 3, *Incremental Packages for Introducing Successive Stages of Transition to Free Flight (Near-Term)*, Final Report of RTCA Task Force 3: Free Flight Implementation, RTCA, November 1995.

[Ruijgrok, 1993] Ruijgrok, G. J. J., *Elements of Aviation Acoustics*, Delft University Press, 1993.

[SAE, 1986] SAE Committee A-21 on Aircraft Noise, *Procedure for the Calculation of Airplane Noise in the Vicinity of Airports*, SAE AIR 1845, March, 1986.

[Shepherd, 1994] Shepherd, K. P., *Personal Conversation*, September, 1993.

[Smith, 1989] Smith, M. J. T., *Aircraft Noise*, Cambridge University Press, 1989.

[Snyder, 1987] Snyder, J. P., *Map Projections - A Working Manual*, U.S. Geological Survey Professional Paper 1395, United States Government Printing Office, Washington, 1987.

[Sperry, 1978] Sperry, W. C., *Aircraft and Airport Noise*, Noise Control Handbook of Principles and Practices, Van Nostrand Reinhold, 1978.

[Stone and Montegani, 1980] Stone, J.R., and Montegani, F.J., *An Improved Prediction Method for the Noise Generated in Flight by Circular Jets*, NASA TM-81470, 1980.

[Timmerman, 1993] Timmerman, N. S., *Features of Massport's New Noise Monitoring System*, Presented at NOISE-CON 93, Williamsburg, Virginia, May 1993.

[USGS, 1989] Office of Technical Management, *Data Users Guide 2: Digital Line Graphs From 1:100,000-Scale Maps*, U. S. Geological Survey, 1989.

[USGS, 1990] Office of Technical Management, *Data Users Guide 4: Land Use and Land Cover Digital Data From 1:250,000 and 1:100,000-Scale Maps*, U. S. Geological Survey, 1990.

[van Grass et al., 1994] van Grass, F., Diggle, D. W., and Hueschen, R. W., *Interferometric GPS Flight Reference/Autoland System: Flight Test Results*, Navigation, Journal of the Institute of Navigation, Vol. 38, No. 1, Spring 1994, pp. 57-81.

[Wickens and Carswell, 1995] Wickens, C. D., and Carswell, C. M., *The Proximity Compatibility Principle: Its Physiological Foundation and Relevance to Display Design*, Human Factors, Vol. 37, No. 3, September 1995, pp. 473-494.

[Zorumski, 1982] Zorumski, W. E., *Aircraft Noise Prediction Program Theoretical Manual*, NASA TM-83199, 1982.

A. Existing Guidance and Navigation Technology

This appendix gives background information on the navigational precision of aircraft using existing guidance and navigation technology during approach and departure.

The guidance and navigational requirements for all standard instrument approach and departure procedures are defined in the United States Standard for Terminal Instrument Procedures (TERPS) published jointly by the Federal Aviation Administration (FAA) and the Armed Services [FAA, 1976]. The TERPS specifies the guidance and navigation systems that may be used during a flight procedure, and the obstacle clearway (the region around the nominal trajectory that must be free of objects). If it is assumed that an aircraft has a 99.9% (4σ) probability of staying within the obstacle clearway, then the dimensions of the obstacle clearway are twice the 2σ navigational precision of the aircraft.

A.1 Approach Precision

During standard instrument approaches, an aircraft may utilize two different guidance and navigation systems:

1. Non-Directional Beacon (NDB).
2. Instrument Landing System (ILS).

A.1.1 NDB Guidance

The NDB approach is a non-precision approach, where the final phases of the approach is completed visually. Vertical guidance is provided by altimeter readings and lateral guidance is provided by the NDB. The NDB is a radio transmitter, operating in the 200 to 500 kHz range, identifying a geographical location which may be located by airborne equipment. Figure A-1 shows the obstacle clearway for an NDB approach. As the figure shows, the width of the obstacle clearway increases with the distance from the NDB. The 2σ navigational precision is ± 0.625 n.mi. at the NDB beacon and ± 1.25 n.mi. at a distance of 15 n.mi. from the beacon.

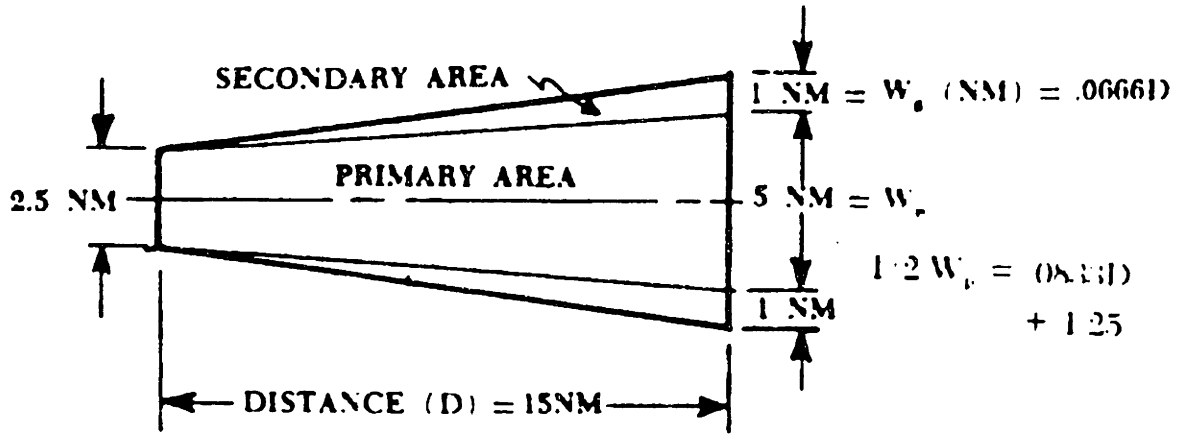

Figure A-1: NDB Clearway Trapezoid [FAA, 1976].

A.1.2 ILS Guidance

The obstacle clearway for the ILS approach is also a trapezoid, but its dimensions are much smaller than the NDB clearway trapezoid, and unlike the NDB trapezoid which begins at the NDB facility, the ILS trapezoid begins at the approach end of the runway. The small end of the trapezoid is 1000 ft. (±500 ft.) and the width at any point along the final approach course is given by

$$0.5\,W = 500 + 0.15\,D \quad ft., \tag{A-1}$$

where D is the distance from the approach end of the runway. Thus, the navigational precision is given by

$$2\sigma = \pm 0.5\,(500 + 0.15\,D) \quad ft. \tag{A-2}$$

A.2 Departure Guidance

During standard instrument departures, an aircraft may utilize three different guidance and navigation systems:

1. Heading.
2. Air Traffic Control (ATC) Radar Vectors.
3. Ground Navigational Facilities e.g. VHF Omni-Range (VOR).

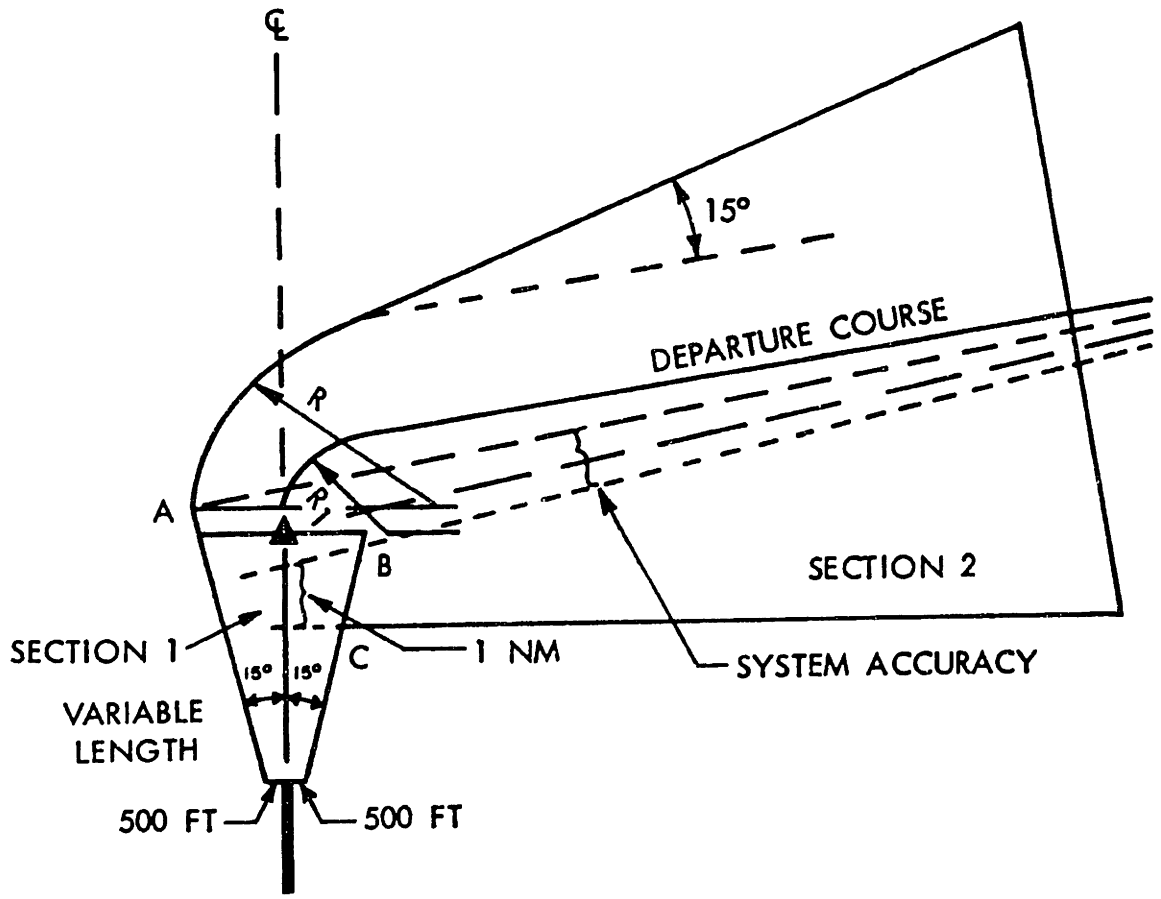

Figure A-3: Plan View of Obstacle Clearway for Heading Guidance Departure With Turn [FAA, 1976].

A.2.2 ATC Radar Vectors

Air Traffic Control Radar Vectors are used for guidance is cases where heading guidance alone is insufficient, and improvements can be achieved through radar monitoring and periodic heading corrections. Radar surveillance allows the controller to monitor the progress of the aircraft and make corrections to account for the effect of system errors and wind. The dimensions of the obstacle clearway depends on distance between the aircraft and the radar monitoring facility. The width of the obstacle clearway if given by

$$W = 1 + 0.1D, \tag{A-3}$$

where D is the distance between the aircraft and the radar monitoring facility. Thus, the navigational precision is given by

$$2\sigma = \pm 0.25\,(1 + 0.1D). \tag{A-4}$$

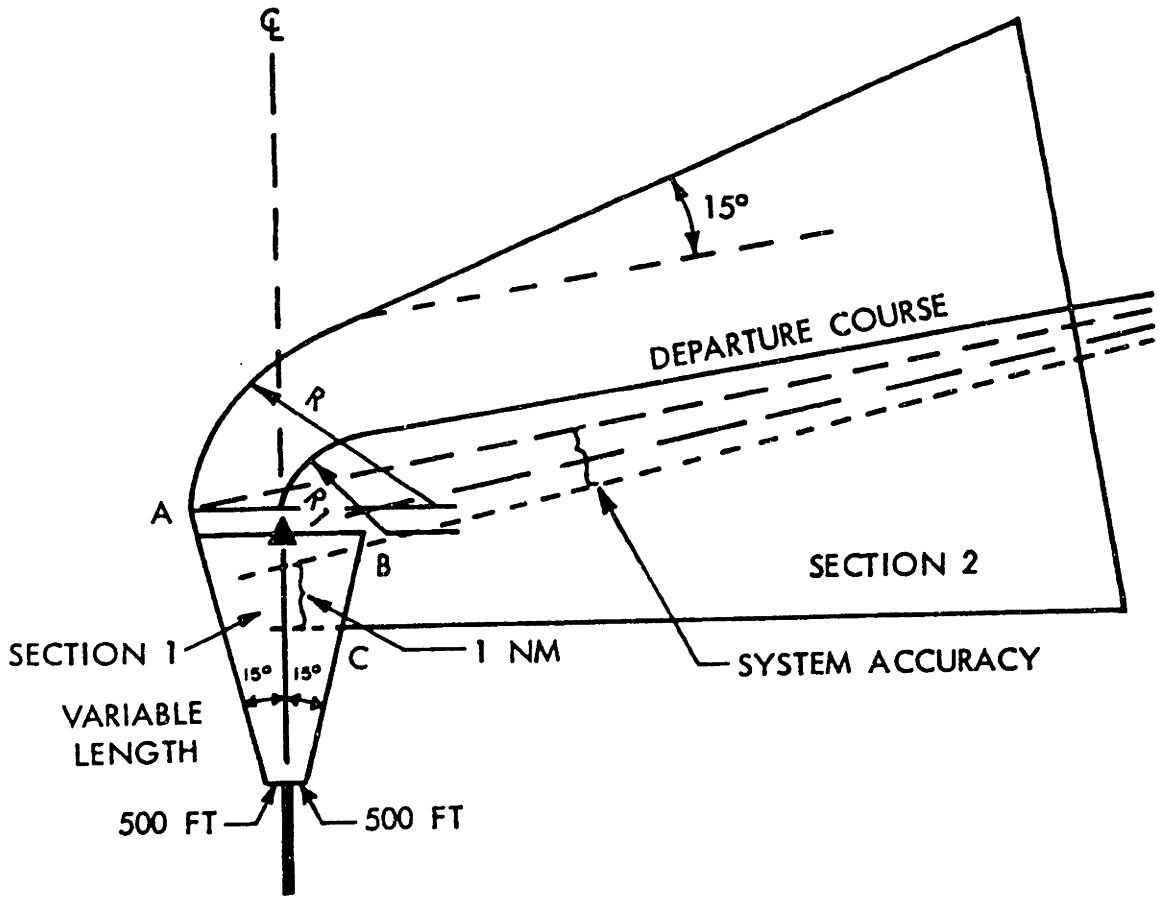

Figure A-3: Plan View of Obstacle Clearway for Heading Guidance Departure With Turn [FAA, 1976].

A.2.2 ATC Radar Vectors

Air Traffic Control Radar Vectors are used for guidance is cases where heading guidance alone is insufficient, and improvements can be achieved through radar monitoring and periodic heading corrections. Radar surveillance allows the controller to monitor the progress of the aircraft and make corrections to account for the effect of system errors and wind. The dimensions of the obstacle clearway depends on distance between the aircraft and the radar monitoring facility. The width of the obstacle clearway if given by

$$W = 1 + 0.1D, \tag{A-3}$$

where D is the distance between the aircraft and the radar monitoring facility. Thus, the navigational precision is given by

$$2\sigma = \pm 0.25\,(1 + 0.1D). \tag{A-4}$$

A.2.3 VOR Guidance

The VHF Omni-Range (VOR) is a ground beacon that aircraft use to determine their position. The VOR measures the aircraft's bearing relative to the location of the VOR. Two or more VOR measurements are used to determine the aircraft's position. Often times the VOR is combined with DME so that aircraft can determine their position using distance and bearing information from a single VOR.

Figure A-4 shows the obstacle clearway for a departure using VOR guidance. As the figure shows the dimensions of the obstacle clearway depend on the location of the VOR and the distance of the aircraft from the VOR. The clearway diverges or converges depending on the direction of flight. If the aircraft is flying towards the VOR, the clearway converges. If the aircraft is flying away from the VOR, the clearway diverges. The angle of divergence is 8° (±4°), so the expected 2σ lateral navigational precision for VOR guidance is ±2°.

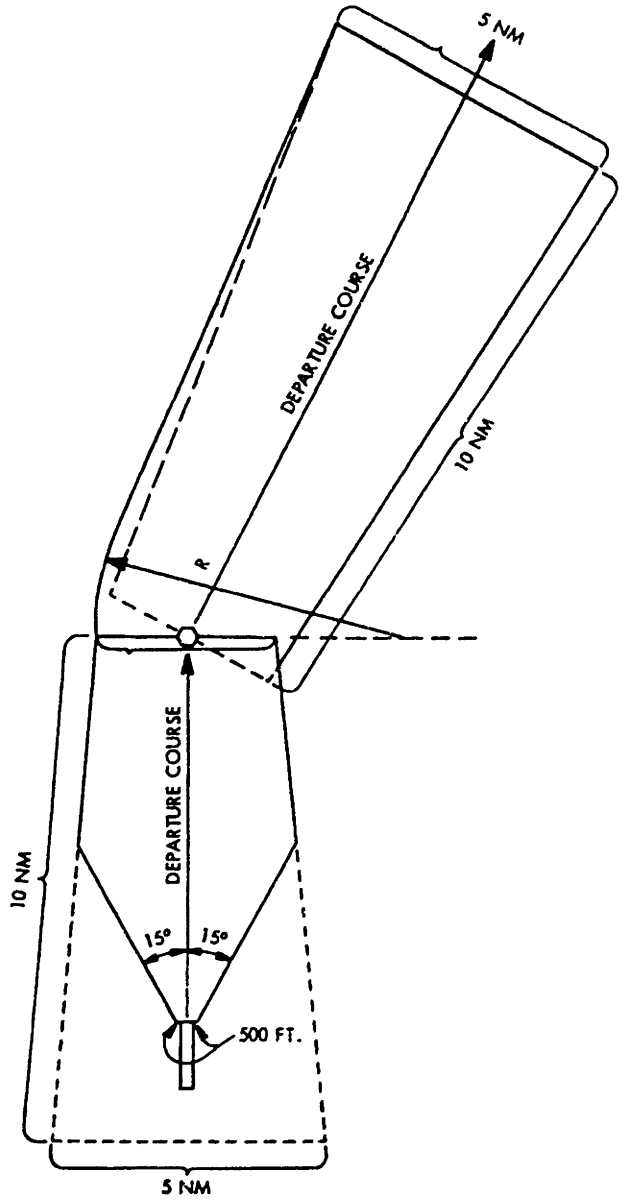

Figure A-4: VOR Obstacle Clearway [FAA, 1975].

B. Advanced Flight Guidance Technology

This appendix gives background information on Area Navigation (RNAV), and describes how the capabilities of the Flight Management System (FMS) and the Global Positioning System (GPS) may be used within the RNAV structure.

B.1 Area Navigation

Area Navigation (RNAV) is the structure used by aircraft to fly precise trajectories. The basis of this structure is the waypoint, or a point characterized by its location (latitude, longitude) and target values for certain aircraft states (altitude, speed). Trajectories are defined by a series of these waypoints joined by straight-line segments. The RNAV structure is divided into two orthogonal and independent domains: Lateral and Vertical.

B.1.1 Lateral Domain

In the lateral domain, the ground track of the aircraft is specified by the latitude and longitude of the waypoints that make up the trajectory. In plan view, an aircraft will fly from waypoint to waypoint along the straight line segments that join them.

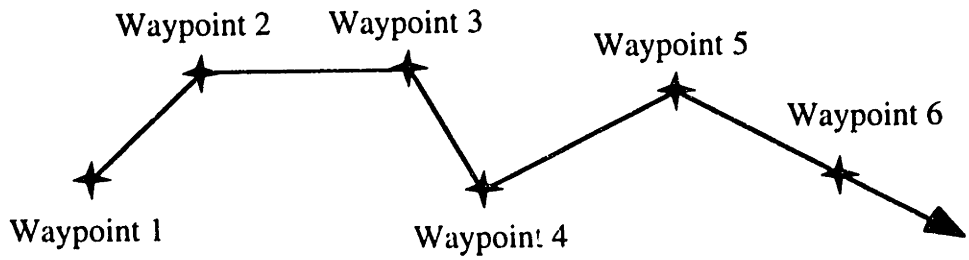

Figure B-1: Plan view of a RNAV trajectory

When the aircraft nears its current target waypoint, it anticipates the transition between segments and deviate from the straight lines between the waypoint to form a transition fillet between segments.

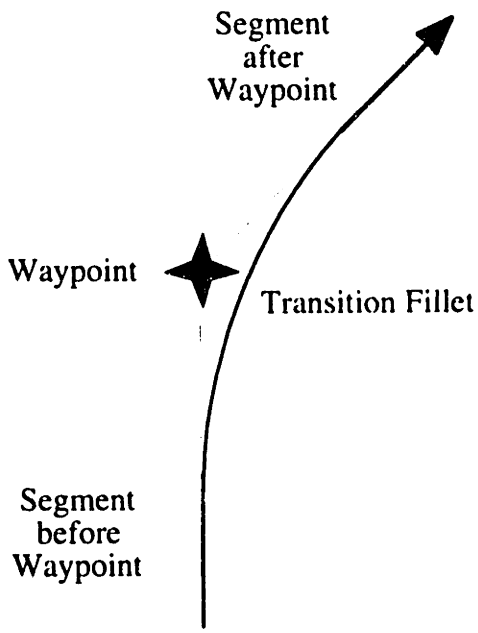

Figure B-2: Lateral transition fillet between two segments in a RNAV trajectory.

The exact nature of the lateral transition fillet depends on the internal logic of the Flight Management System that is being used to perform the procedure. Details of that internal logic is proprietary and is not standardized. Therefore, some margin has to be incorporated into the design of the transitions between segments to account for the variation in FMS logic.

B.1.2 Vertical Domain

In the vertical domain, the flight path angle and speed of the aircraft are specified by the target altitude and target speed at each waypoint. When a waypoint has a target altitude, the aircraft must climb or descent to that altitude before reaching that waypoint. If a waypoint has no target altitude, the aircraft maintains its current altitude during the segment after that waypoint, and in all subsequent segments until it reaches a waypoint with a target altitude. Figure B-3 shows part of the profile view of a trajectory with two successive waypoints that have different target altitudes. The altitude at the second waypoint is higher than the first, so the aircraft must climb to the second altitude before it reaches the second waypoint. Because jet aircraft have better performance at higher altitudes, the aircraft starts its climb immediately after passing the first waypoint. The converse is true in a descent. The

aircraft maintains the higher altitude until the last possible moment that the aircraft can descend and still reach the target altitude.

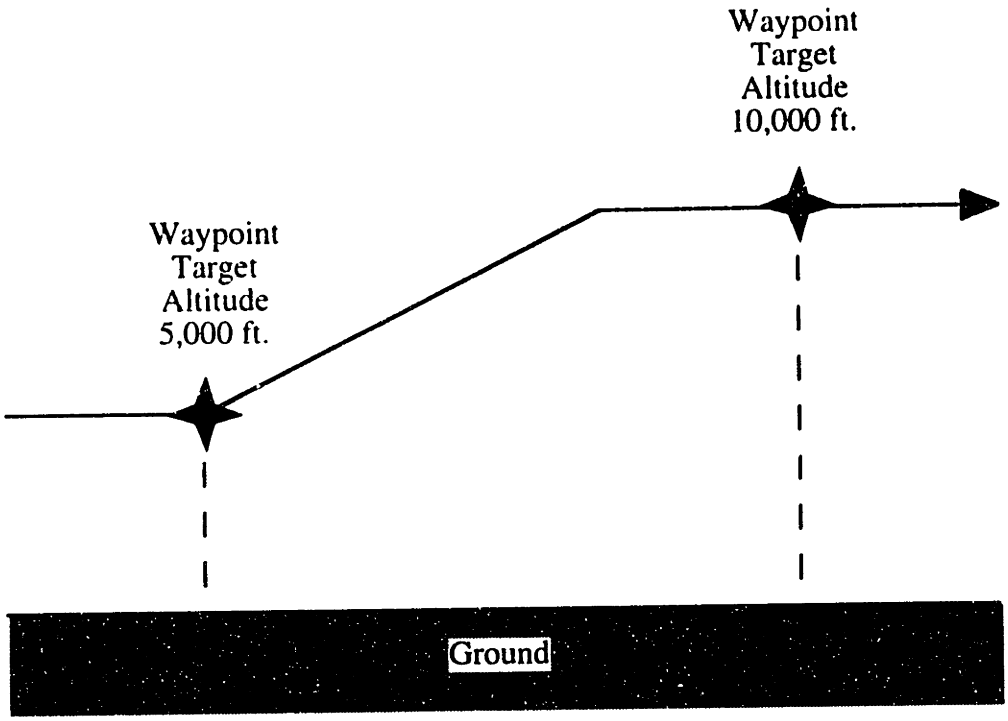

Figure B-3: Part of the profile view of a trajectory with two successive waypoints that have different target altitudes.

Similarly, if a waypoint has a speed restriction, the aircraft must accelerate or decelerate to that speed before reaching that waypoint. The performance of jet aircraft improves with increased speed. If the target speed in greater than the current speed, the aircraft begins to accelerate as soon as it has passed the previous waypoint. Conversely, if the target speed is less than the current speed, the aircraft will wait until the last possible moment to decelerate and still reach the target speed.

B.2 Flight Management System

The Flight Management System (FMS) manages the aircraft's control functions in flight. The FMS has many modes of operation in both the vertical and lateral domains, but the functions that these modes perform may be categorized by the role that the FMS plays.

B.2.1 Roles

Within each domain, the FMS functions in two distinct roles: (1) Supervisor-Executor, (2) Executor.

B.2.1.1 Supervisor-Executor

In this role, the FMS serves as the supervisor and as the executor for all the control functions within a domain. As a supervisor, the FMS uses the information supplied in the pre-programmed trajectory to determine the appropriate target values for all the relevant aircraft states, and the time that these values should be changed. As an executor, the FMS executes the control inputs required to achieve the target values. Once the pilot enters information describing the intended path of the aircraft and engages the FMS, the FMS monitors the progress of the aircraft relative to the desired path and performs the necessary actions required to follow that path. For example, if we examine the trajectory shown in Figure B-1, we see that the aircraft must make several heading changes to follow the trajectory. Assuming that the pilot has correctly entered the trajectory into the FMS and engaged the FMS in the LNAV mode, the FMS will determine what heading change is required to stay on the path and when to initiate each heading change. This is the supervisory role. It will also implement all the control actions needed to accomplish the heading change. This is the executor role.

B.2.1.2 Executor

In this role, the FMS serves as the executor for all control functions within a domain. Here, the pilot retains the job of monitoring the aircraft's progress relative to the desired path and making sure that the aircraft stays on that path. The pilot determines the target values for each aircraft state, and the time that these values are to be changed. When the pilot has decided that it is time to change an aircraft state, he/she enters new target values into the FMS. As the executor, the FMS implements the required control inputs.

B.2.2 Lateral Modes

The lateral mode specifies the role of the FMS in the lateral domain. The lateral modes are independent of the vertical modes.

B.2.2.1 Lateral Navigation Mode

In the Lateral Navigation (LNAV) Mode, the FMS serves in a supervisor-executor role within the lateral domain of the RNAV structure. When this mode is selected, the aircraft follows the straight line segments and transition fillets that are defined by the waypoints that make up the trajectory.

B.2.2.2 Heading Select Mode

In the Heading Select (HDG SEL) Mode, the FMS executes the control actions required to achieve the selected heading. Thus, the FMS serves an executor role.

B.2.3 Vertical Modes

The vertical mode specifies the role of the FMS in the vertical domain. It also specifies how the FMS will play that role. For example, if the pilot wants the FMS to function in an executor role and move the aircraft to a new altitude, he/she has two ways to achieve that altitude change. The pilot can select either the vertical speed during the altitude change or the thrust to be used during the altitude change. If the pilot selects the vertical speed during the altitude change, the FMS implements whatever thrust and pitch control actions are necessary to attain and maintain the selected vertical speed. If the pilot selects the thrust to be used during the altitude change, the FMS implements whatever pitch control actions are necessary to maintain the selected airspeed. In both modes, the FMS acts as an executor, but it has different ways of executing its assigned task. Details of the vertical modes of the FMS are described below.

B.2.3.1 Vertical Navigation Mode

In the Vertical Navigation (VNAV) Mode, the FMS serves in a supervisor-executor role within the vertical domain of the RNAV structure. This mode cannot be engaged without the LNAV mode, as the target states used to define the vertical path have no meaning outside the RNAV structure. When this mode is selected, the aircraft follows the RNAV path and the FMS modifies the aircraft states at the appropriate times to meet the target altitude and speeds at each waypoint.

B.2.3.2 Altitude Hold Mode

In the Altitude Hold (ALT HOLD) Mode, the target altitude of the aircraft is selected by the pilot and the FMS implements whatever control actions are required to maintain that altitude. This mode is the default vertical mode. If an aircraft is in another vertical mode and it reaches the target altitude entered into the FMS, that vertical mode will transition to ALT HOLD.

B.2.3.3 Flight Level Change Mode

In the Flight Level Change (FLCH) Mode, the aircraft will climb or descend at fixed thrust and fixed airspeed. If the aircraft is climbing, maximum climb thrust is used. If the aircraft is descending, idle thrust is used. In either case, the airspeed of the aircraft is maintained by varying the pitch of the aircraft. This mode is characterized as a "speed on pitch" mode, since the thrust is constant and the airspeed is maintained by varying the pitch.

B.2.3.4 Vertical Speed Mode

In the Vertical Speed (V/S) Mode, the aircraft will climb or descend at the selected vertical speed. The pitch and the thrust of the aircraft are both varied, but the selected airspeed is maintained. If the airspeed and the vertical speed cannot be maintained at the same time, the vertical speed is maintained in preference to the airspeed. This mode is characterized as a "speed on thrust" mode, since the vertical speed and airspeed are maintain by primarily varying the thrust.

B.3 Global Positioning System

The Global Positioning System (GPS) is a satellite based navigation system that provides accurate estimates of time and position (in three dimensions) at any point on the earth's surface or in the earth's atmosphere. As currently implemented, the GPS satellite constellation consists of 24 satellites in 6 equally spaced orbits, inclined at 55° to the Equator (Figure B-4). The radius of each orbit is 20,200 km (10,898 nautical miles) and the period of each orbit is 12 hours. The satellites are arranged so that a minimum of 5 satellites are in view at all times from any location in the world.

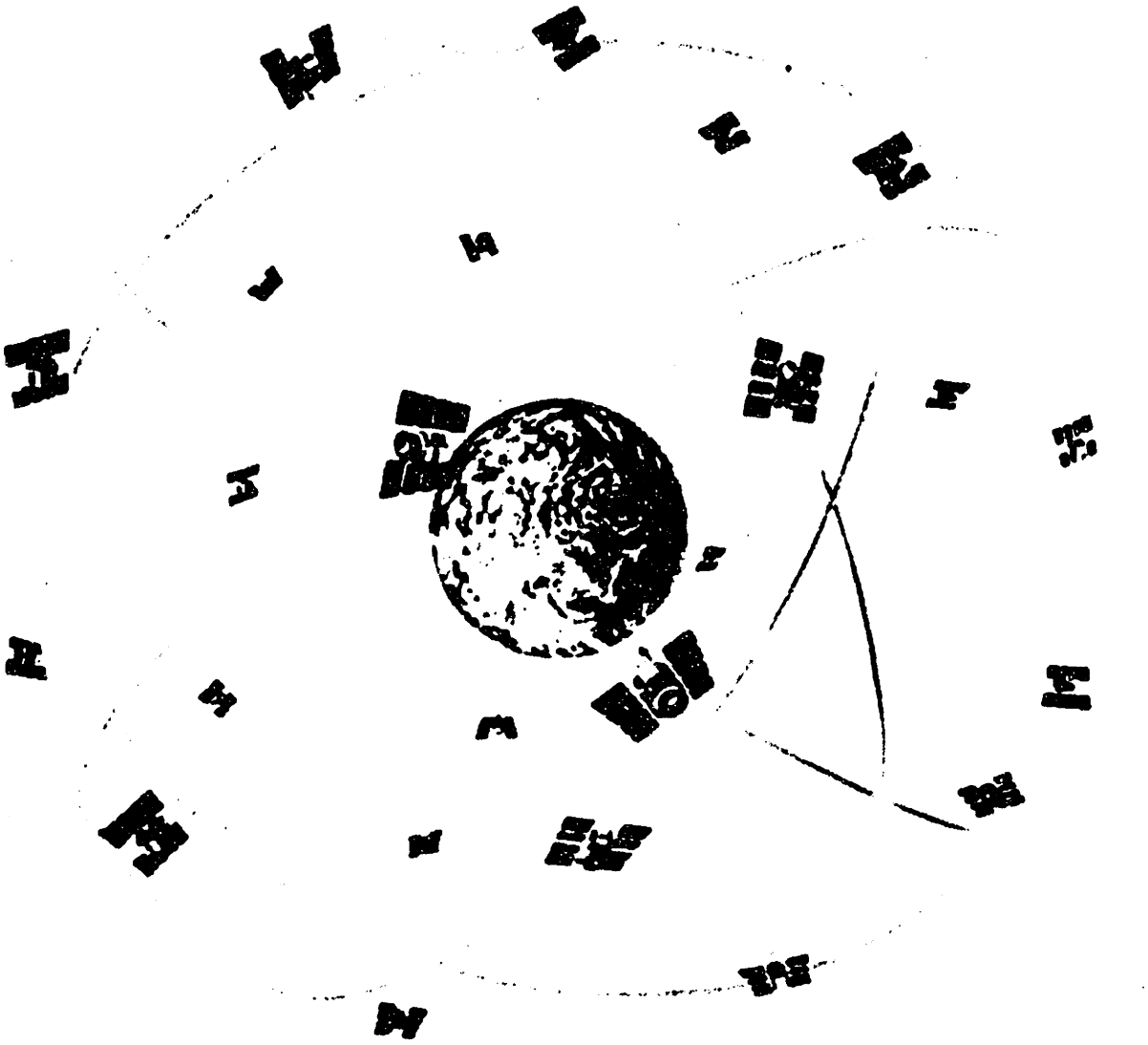

Figure B-4: The GPS Constellation [Logsdon, 1994].

Each satellite broadcasts on two frequencies in the L-band: (1) the L1 signal at 1575.42 MHz and (2) the L2 signal at 1227.6 MHz. Two modulations are added to the carrier signals. The first modulation is called the Precise (P) code and is intended for military and survey applications. The second modulation is called the Coarse-Acquisition (C/A) code and is intended for general use. Only the C/A code is available for public use. Both the P and C/A codes are pre-determined pseudo-random digital signals. The P code is clocked at 10.23 MHz and repeats itself after 7 days. The C/A code (1,023 bits long) is clocked at 1.023 MHz and repeats itself after 1 millisecond.

Each GPS satellite has an internal atomic clock of 10.23 MHz nominal frequency. All frequencies within the satellite are derived from and synchronized to this 10.23 MHz

frequency standard. Although these clocks gain or loose only one second in 36,000 years, correction factors for the each satellite's clock are uplinked daily from the Master Control Station (MCS) using a more accurate cesium clock. In addition to the P and C/A code modulated carrier signals, each GPS satellite also transmits a 50 bit per second (bps) data stream with information about the status of the satellite, the ephemeris data for the satellite, the parameters required to compute the correction for the satellite clock, the time synchronization information required to decode the modulations, and the corrections for atmospheric delays. Atmospheric refraction depends on the signal frequency. Since the GPS satellite broadcasts on two frequencies, the effects of atmospheric refraction may be determined.

The signals broadcast by the GPS satellites are intercepted by a GPS receiver. The GPS receiver has its own internal clock, but this clock will have some time bias relative to the clocks on the GPS satellites. The GPS receiver uses the range estimates from four or more satellites to determine the receiver position and the receiver clock bias.

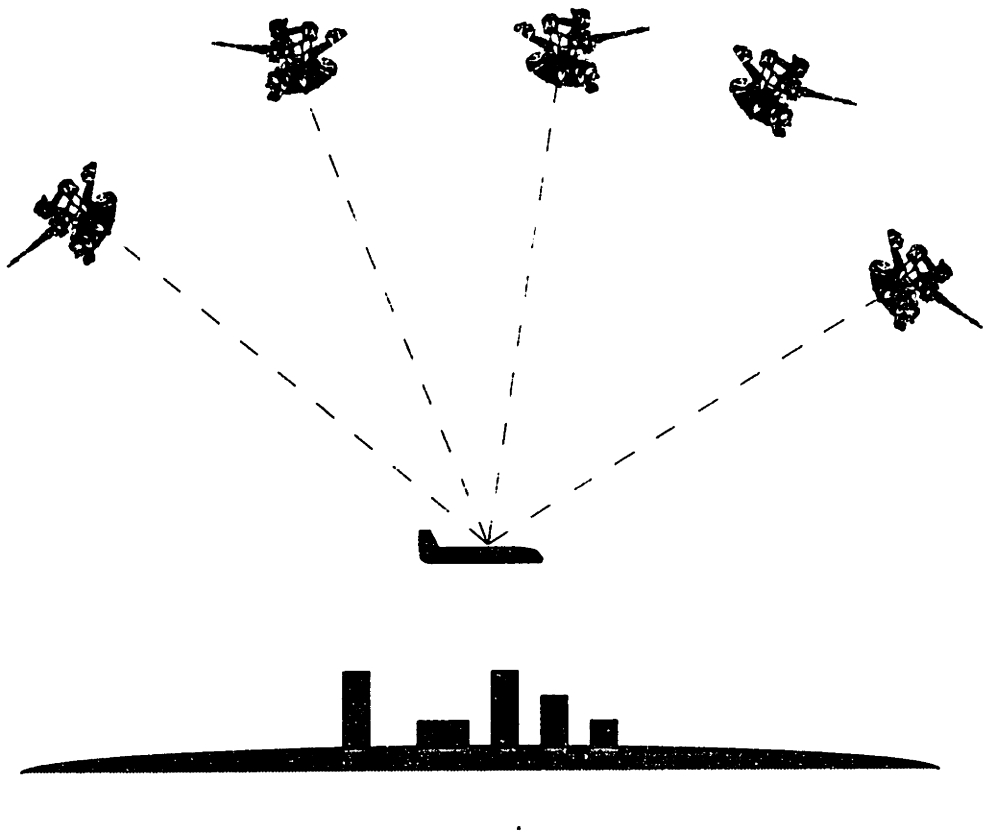

Figure B-5: Aircraft in flight with 5 GPS satellites in view.

The accuracy of the calculation in a particular direction depends of the geometry of the satellites relative to the receivers location. For example, if all the satellites that the receiver uses to calculate its position are directly overhead, the position estimate in the vertical direction will be very good while the position estimate in the lateral direction will be poor. If the satellites are all along the horizon, the position estimate in the lateral direction will be good while the position estimate in the vertical direction will be poor. GPS has been designed to provide a 2σ (95%) accuracy of 100m.

Some methods to augment the accuracy of the system have been implemented. They involve placing a receiver at a known location to determine a correction factor to account for the degradation of the GPS signals. This technique is called differential GPS or DGPS. The correction factor is used by other receivers in that area to improve the accuracy of their calculations (Figure B-6).

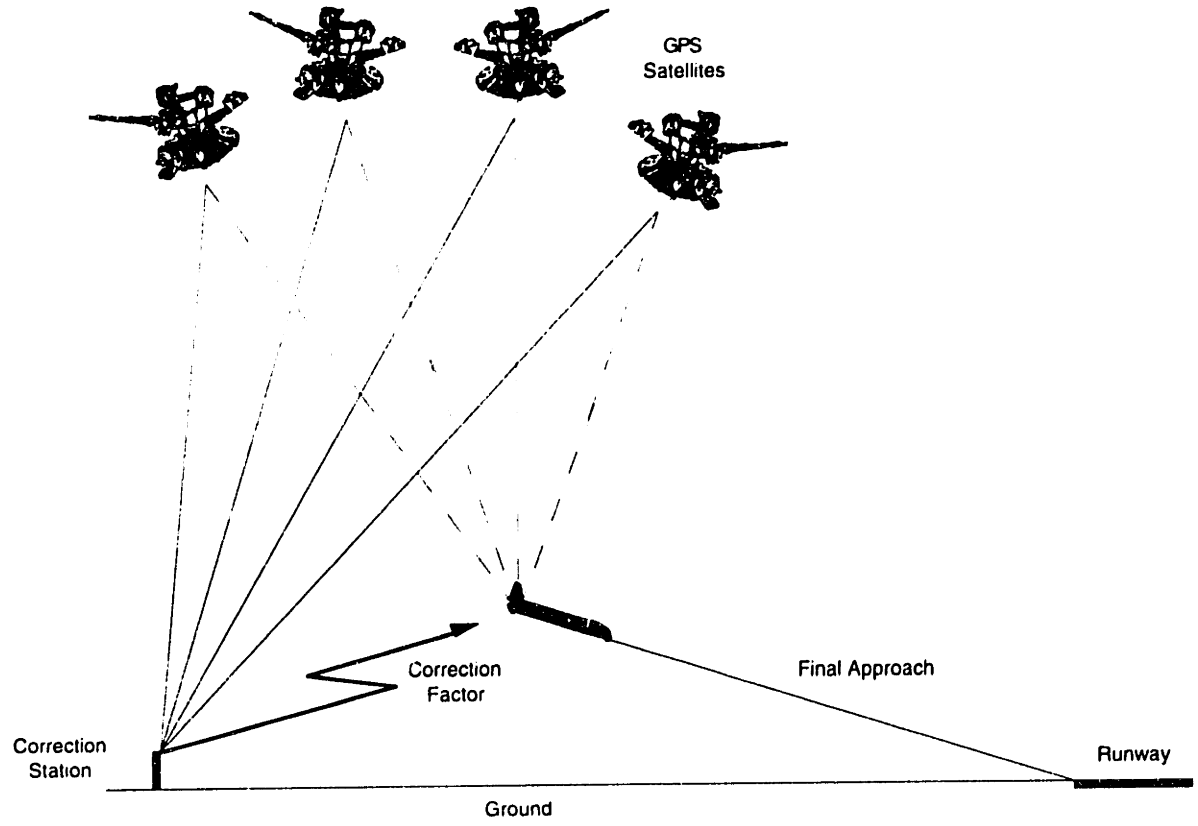

Figure B-6: Differential Correction of GPS Signal

Since the fidelity of the correction factor depends on the similarity of the atmospheric conditions faced by signals reaching the correction station compared to signals reaching the receiver, the usefulness of the correction factor depends on the distance to the correction

station. This augmentation system has been proposed in two levels. The first level is the Wide Area Augmentation System (WAAS), a course grid of correction stations about 200 km apart, which provides 5m. Airports that desire higher accuracy may implement a second level or Local Area Augmentation System (LAAS). At this level, a correction station is placed very near the airport to improve the fidelity of the correction factor. LAAS provides 1m accuracy.

C. NOISIM

This appendix presents details of NOISIM that were not presented in the main body of the thesis.

The platform is a Silicon Graphics Indigo R10000 Maximum Impact Graphical Workstation. Analog/Digital Conversion is performed by an Intel 80386 based machine.

C.1 Flight Simulator

C.1.1 Aerodynamics

The aircraft model used in this simulation has been developed at the MIT Aeronautical Systems Laboratory using performance data from the Boeing 737 which served as the NASA Advanced Transport Operations (ATOPS) Aircraft [Hansman et al., 1993].

C.1.1.1 Aerodynamic Coefficients

In the aerodynamic model, the aircraft is assumed to be a point mass. The aerodynamic coefficients of the aircraft are determined from flight test data. The coefficient of lift and drag are provided for the aircraft in a "clean" configuration and in a combination of configurations where the movable devices such as flaps and landing gear are extended. In instances where a particular configuration lies between known configurations, the lift and drag coefficients are interpolated from the values for the different configurations that bound it. Although the pitching moments during the extension and retraction of these devices cannot be fully modeled by the point mass model, the changes in the lift and drag that occur are translated into a new pitch attitude in each iteration, thus giving a "false" pitching moment.

C.1.1.2 Attitude Control

Changes to the pitch and bank attitude of the aircraft are made through a rate based sidestick controller. The aircraft is assumed to have a yaw damper that removes any sideslip. In this "Control Wheel Steering" scheme, the commanded bank rate is proportional to the square of the normalized sidestick deflection. A full deflection of the sidestick to the left or right will command the maximum allowable bank rate in the direction that the stick is deflected. If the sidestick is deflected to half of its maximum deflection then the commanded bank rate will be one quarter of the maximum allowable bank rate. If the sidestick is in the center or neutral position, the bank rate will be zero and the aircraft will maintain whatever bank attitude it had when the sidestick returned to the neutral position.

The pitch rate is also commanded via the sidestick. When the sidestick is deflected forward or aft of the neutral position, the commanded pitch rate is proportional to the square of the normalized sidestick deflection. One of the notable feature of this control scheme is that if the sidestick is in the neutral position in a non-zero bank attitude, the pitch rate is compensated to maintain the same climb rate the aircraft had when the sidestick returned to the neutral position. Thus, in a climbing or descending turn, the pitch and bank will remain unchanged without having to apply any aft pressure on the sidestick.

C.1.2 Flight Management System

The Flight Management System (FMS) is a software emulation of the FMS system used in many advanced commercial aircraft. The Mode Control Panel (MCP) is flight hardware from a Boeing 737-300. The Control Display Unit (CDU) is a replica of the CDU found in the cockpit of the 747-400.

C.1.2.1 Mode Control Panel

The Mode Control Panel (MCP) is used by the pilot to set the mode of the FMS. In the vertical domain, the pilot may select one of four (4) modes: VNAV, Altitude Hold, Altitude Change, and Vertical Speed. In the lateral domain, the pilot may select one of two (2) modes: LNAV and Heading. The role that the FMS plays in a domain is not dependent on the role in plays in the other. For example, the FMS can function in a supervisory role in the lateral domain (LNAV mode) while functioning as an executor in the vertical domain (Altitude Change Mode).

C.1.2.2 Control Display Unit

Information for programmed trajectories are input in the Control Display Unit (CDU). The CDU is located in front of the throttle levers on the center console, and has an alphanumeric keypad and several function keys (Figure C-1). These keys are used to input, delete, or modify the parameters which define the trajectory. The information is stored in several groups or pages. Only one page may be accessed at a given time, but the user may switch between pages. As outlined previously, a trajectory is defined by a series of waypoints joined by straight line segments. Each waypoint has an identification code. When the user enters this code, the latitude and longitude of the waypoint is retrieved from a database. The waypoints in a trajectory are displayed on the CDU as row entries. Each row contains the name of the waypoint and the altitude and speed restriction that the aircraft must meet at that waypoint. The first row contains information about the first waypoint, and the successive rows contain the waypoints in the order they occur in the trajectory. Once a trajectory has been entered into the CDU and the relevant FMS modes have been selected, the commands to the autopilot and autothrottles are determined by the FMS.

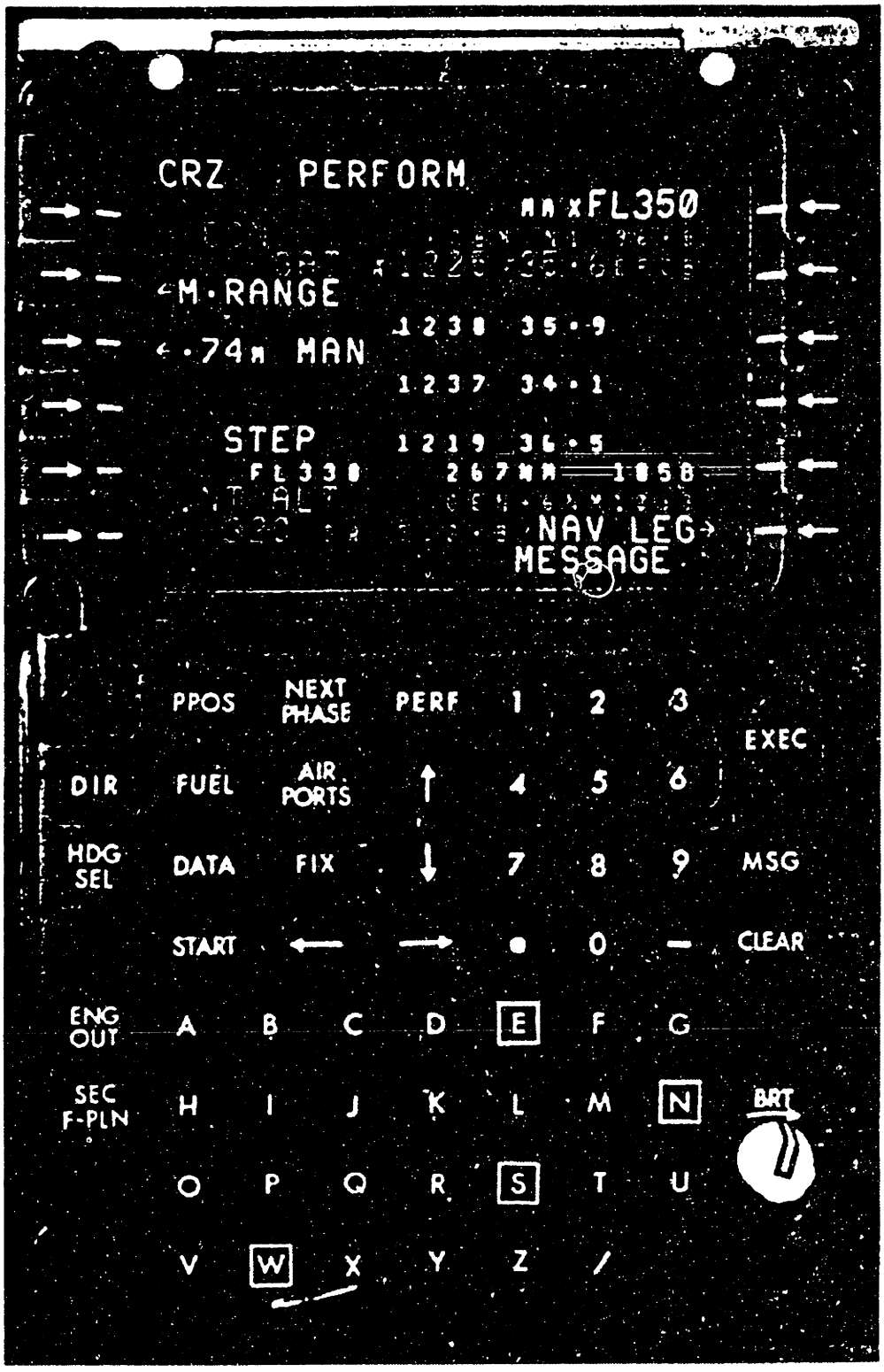

Figure C-1: Control Display Unit.

C.1.2.3 Electronic Horizontal Situation Indicator

The Electronic Horizontal Situation Indicator (EHSI) depicts a plan view of the area around the aircraft, detailing the aircraft's route, navigation aids, and airport features such as runways. Figure C-2 shows the EHSI of an aircraft following a programmed trajectory. The map is oriented so that the aircraft (represented by a triangle) is at the bottom of the screen and the current aircraft heading is depicted by solid line that forms the longitudinal axis of the screen. The programmed trajectory is shown by the solid line that runs from the aircraft's position at waypoint WPT01 to the waypoint SEY, then to the waypoint LAFAY, and then to the waypoint PVD. The heading that is entered into the MCP is depicted by a dashed line immediately to the right of the current heading. When the aircraft is in LNAV mode, as it is in the figure, the FMS sets the selected heading equal to the heading of the current segment of the programmed trajectory. The small divergence of the current heading and the selected heading in the figure represents the integer limitations of the selected heading. When the aircraft is in the heading mode, the FMS will maneuver the aircraft so that the current heading and the dashed line are aligned.

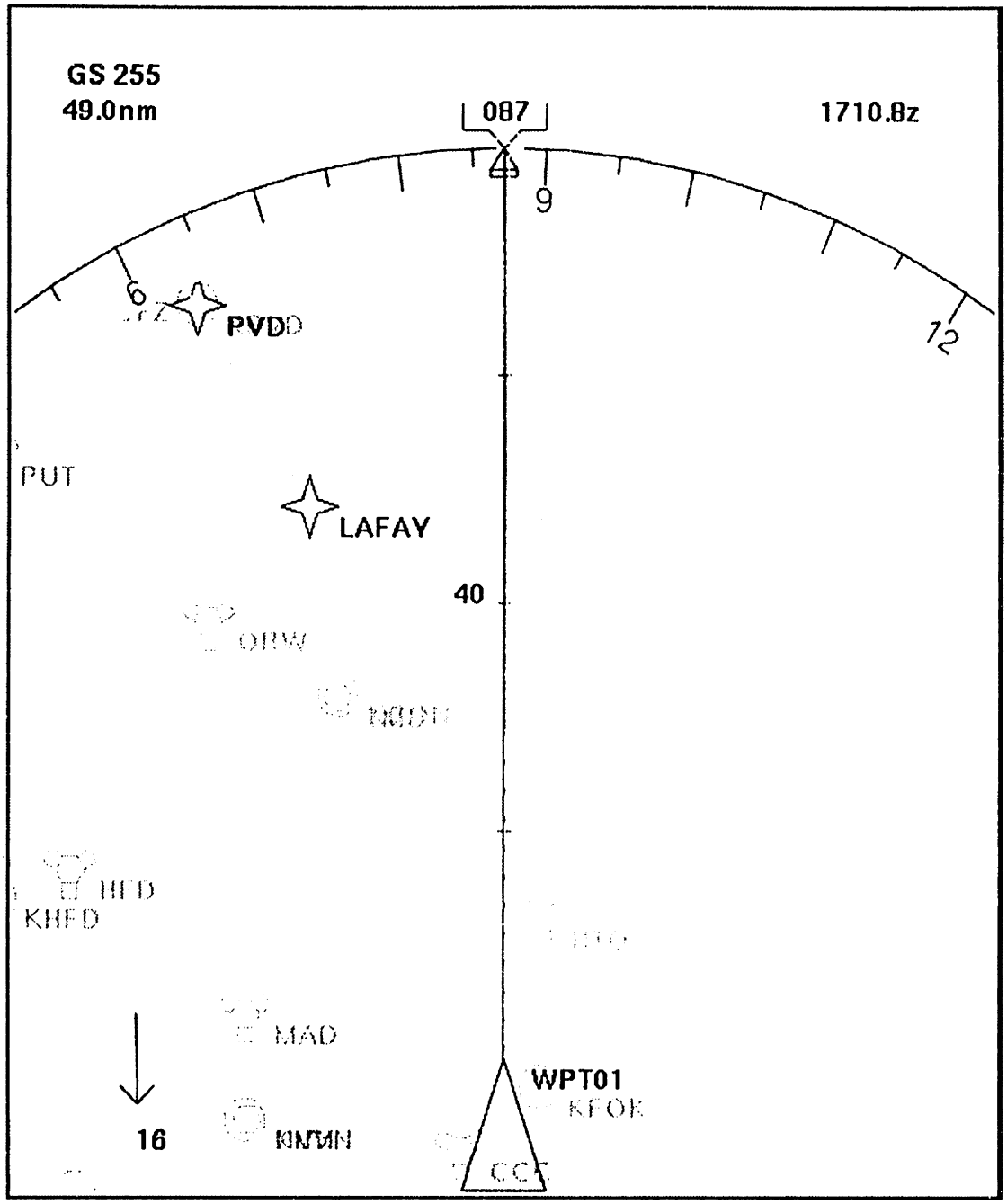

Figure C-2: EHSI depicting a pre-programmed trajectory.

C.1.3 Engines

The engine modeled in the simulator is the Pratt and Whitney JT8D-7, the engine used on this aircraft. This engine is a two spool turbofan engine with mixed exhaust flows. A schematic of the engine is shown in Figure C-3. The points between the different engine components have been labeled with station numbers. The total pressure and temperature at

each station are given for the engine operating at its maximum static thrust of 14,000 lbf. In the figure, the outer spool connects the high pressure compressor (station 2.5 - station 3) to the high pressure turbine (station 4 - station 4.5). The inner spool connects the fan (station 2 - station 2.3) and the low pressure compressor (station 2 - station 2.5) to the low pressure turbine (station 4.5 - station 5).

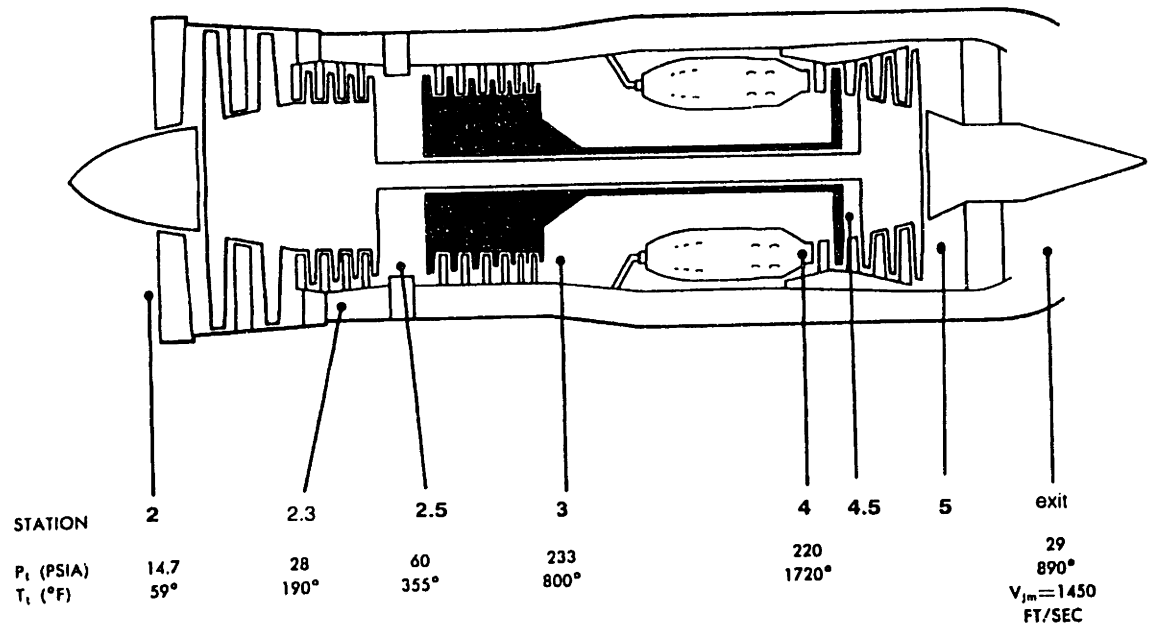

Figure C-3: Schematic of Pratt and Whitney JT8D Turbofan Engine [Pratt and Whtitney, 1974].

The total pressure and temperature at each station varies appreciably throughout the entire operating range of the engine. To determine these values at different engine conditions usually requires an extensive iterative engine analysis. This analysis is a computationally intensive process. To reduce computational time, this model uses a semi-iterative scheme to determine conditions at each station in the engine. Information about the engine such as the relationship between the pressure ratio and the corrected mass flow through the fan and compressors in steady state conditions (operating line), and the corrected mass and fuel flows as a function of compressor rotational speed are used to reduce the number of iterations required to solve for the engine operating conditions. Below is a detailed explanation of the relationships that are assumed, and the expressions used to derive the relevant parameters. In all cases, the sub-subscript *R* denotes the corresponding value at maximum thrust.

C.1.3.1 Fan

The fan stage of the JT8D is a dual rotor-stator pair preceded by inlet guide vanes. The fan accelerates that portion of the air flow that will bypass the core of the engine. This flow is mixed with the exhaust from the engine core before both flows leave through a single engine exit nozzle. At maximum static thrust of 14,000 lbf (? N) this engine has a bypass ratio of 1.1. The fan is assumed to have a constant polytropic efficiency η_{FAN}, so the temperature ratio is expressed in terms of the pressure ratio by the expression [Hill and Peterson, 1992]

$$\tau_{FAN} = \pi_{FAN}^{\frac{\gamma_n}{\gamma - 1}},$$

where γ is the ratio of specific heats. The corrected rotational speed of the outer spool is derived from the temperature ratio across the fan using the relationship [Mattingly, 1996]

$$N_{FAN} = \sqrt{\frac{\tau_{FAN} - 1}{\tau_{FAN_R} - 1}} \cdot N_{FAN_R}$$

where N_{FAN} is the corrected rotational speed.

C.1.3.2 Compressor

The compressor is a dual stage compressor attached to separate shafts or spools. At maximum static thrust, the total pressure ratio across both compressors is 16.1:1. The pressure ratio across the low pressure compressor is 4.1:1 and the pressure ratio across the high pressure compressor is also 4.1:1.

The low pressure compressor is attached to the same shaft as the fan, so the corrected rotational speed of the low pressure compressor N_{LPC} is equal to the corrected rotational speed of the fan. The low pressure compressor is assumed to have a constant adiabatic efficiency.

The compressor map relates the following four parameters to each other: (1) the rotational speed, (2) the corrected mass flow, (3) the pressure ratio, and (4) the adiabatic efficiency. Figure C-4 shows the non-dimensionalized map used in the engine model [Epstein, 1994].

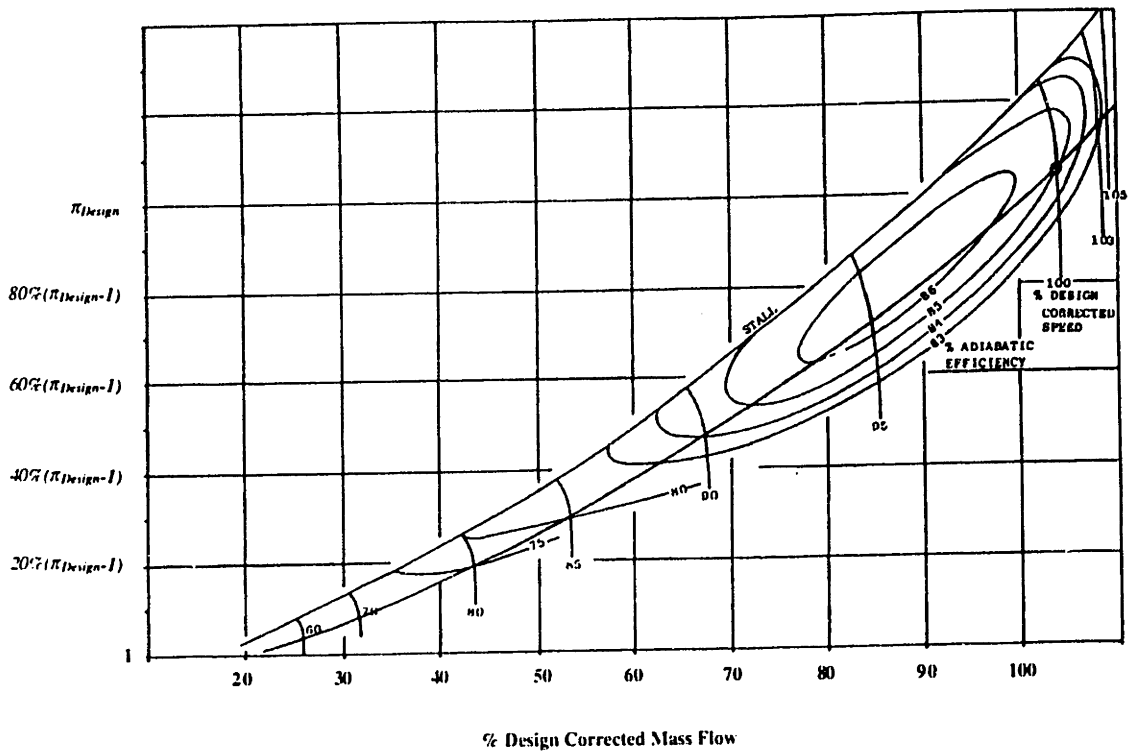

Figure C-4: Non-Dimensional Fan or Compressor Map [Epstein, 1993].

In the figure, there are two monotonically increasing lines. The upper of these two lines is the stall line, or the line that defines the maximum pressure rise for a given mass flow. The lower of these two lines is the operating line, or the line on which the compressor operates in steady state conditions. For the purposes of this simulation, the high pressure compressor is assumed to always be in steady state operation. This means that the corrected mass flow, pressure ratio, and adiabatic efficiency may all be derived from the corrected rotational speed.

The relationship between the rotational speed and the mass flow is given by

$$\dot{m}_{HPC} = \dot{m}_{HPC_R} \cdot \left(\frac{N_{HPC}}{N_{HPC_R}} \right)^{k_{\dot{m}_{HPC}}}, \tag{C-1}$$

where $\dot{m}_{HPC}$ is the corrected mass flow, N_{HPC} is the corrected rotations speed, and $k_{\dot{m}_{HPC}}$ is a constant.

The relationship between the pressure ratio and the mass flow shown in Figure C-4 is modeled by the quadratic expression

$$\pi_{HPC} = 1 + \left(\pi_{HPC_R} - 1\right) \times \left(C_{HPC_1} \left(\frac{\dot{m}_{HPC}}{\dot{m}_{HPC_R}} \right) + C_{HPC_2} \left(\frac{\dot{m}_{HPC}}{\dot{m}_{HPC_R}} \right)^2 \right), \tag{C-2}$$

where π_{HPC} is the pressure ratio, $\dot{m}_{HPC}$ is the corrected mass flow, and C_{HPC_1} and C_{HPC_2} are constants.

The adiabatic efficiency is also determined from the non-dimensional map shown in Figure C-4. Along the operating line, the adiabatic efficiency is only a function of the rotational speed. The relationship between the efficiency and rotational speed has been modeled in two parts. When the rotational speed is less than 80% of the design speed, the efficiency is modeled by the expression

$$\eta = \eta_0 + \left(\eta_{80} - \eta_0\right) \cdot e^{(N-80\%)} \tag{C-3}$$

where η_0 is the efficiency that is asymptotically approached at low rotational speeds, and η_{80} is the efficiency at 80% of design speed. When the rotational speed is greater than 80% of the design speed, the efficiency is modeled by the expression

$$\eta = C_{\eta 0} + C_{\eta 1}\eta + C_{\eta 2}\eta^2 + C_{\eta 3}\eta^3, \tag{C-4}$$

where $C_{\eta 0}$, $C_{\eta 1}$, $C_{\eta 2}$, and $C_{\eta 3}$ are constants.

The corrected fuel flow rate is assumed to be a function of the corrected rotational speed of the high pressure compressor only. The value of the corrected fuel flow is modeled by the expression

$$\dot{m}_{fuel} = \dot{m}_{fuel_R} \cdot \left(\frac{N_{HPC}}{N_{HPC_R}} \right)^{k_{fuel}},$$

where $\dot{m}_{fuel}$ is the corrected fuel flow and k_{fuel} is a constant.

C.1.3.3 Combustor

The pressure drop across a combustor is a function of the speed of the air that mixes with the fuel. Because combustion cannot occur with too much or too little air, or when the air

is moving too fast, the air that is to be mixed with the fuel is separated from the main flow and slowed so that it can support combustion. In this engine model, the combustion is assumed to occur at a fixed Mach number regardless of thrust or aircraft speed. Therefore, the pressure drop will be constant. The pressure ratio used in the model is 0.95, which is a typical value for modern turbojet and turbofan engines.

The temperature rise across the combustor is proportional to the fuel-air ratio f. The combustor exit temperature is given by [Hill and Peterson, 1992]

$$T_4 = T_3 + \frac{f\ \dot{m}\ Q_R}{C_p}, \tag{C-5}$$

where Q_R is the energy density of the fuel and C_p is the heat coefficient at constant pressure.

The combustor outlet (turbine inlet) is assumed to be choked throughout the range of operation. The mass flow parameter at this station is assumed to be constant and equal to its value at the reference conditions. Thus for a constant area, the combustor outlet temperature, pressure, and actual mass flow are related through the relationship [Mattingly, 1996].

$$\frac{(1+f)\ \dot{m}\ \sqrt{T_4}}{P_4} = MFP_R = \frac{(1+f_R)\ \dot{m}_R\ \sqrt{T_{4_R}}}{P_{4_R}}.$$

C.1.3.4 Turbines

The temperature difference across the turbines depend on the work done to the flow entering the engine by the fan and compressors. The high pressure turbine is connected to the high pressure compressor via the outer engine spool or power shaft. The temperature difference across the high pressure turbine is therefore related to the temperature difference across the high pressure compressor via the power conservation equation [Hill and Peterson, 1992]

$$f\ \dot{m}\ C_p(T_4 - T_{4.5}) = \dot{m}\ C_p(T_3 - T_{2.5}). \tag{C-6}$$

The low pressure turbine is connected to the low pressure compressor and the fan, via the inner engine spool or power shaft. The temperature difference across the low pressure

turbine is related to the temperature difference across the low pressure compressor and the temperature difference across the fan by the power conservation relationship [Hill and Peterson, 1992]

$$f\dot{m}C_p(T_{4.5}-T_5)=\dot{m}C_p(T_{2.5}-T_2)+\alpha\dot{m}C_p(T_{2.3}-T_2). \tag{C-7}$$

Equations C-6 and C-7 are commonly referred to as the matched working conditions of the engine. As discussed in the section on the fan and compressors, the turbine is assumed to be choked throughout its operating range. In addition to restricting the operation of the fan and compressors, this condition restricts the relationship between the temperature and pressure changes in the turbine. A choked turbine will typically have a constant polytropic efficiency η_p, so the temperature and pressure ratio are related by

$$\tau=\pi^{\gamma/\eta_p}. \tag{C-8}$$

In this simulation, both turbines are assumed to have the same constant polytropic efficiency.

C.1.3.5 Mixed Flow Exit Nozzle

To minimize pressure losses and prevent back flow in a mixed flow exit nozzle, the exit pressure of the fan and the exit pressure of the core are approximately equal [Kerrebrock, 1992]. Thus, the fan pressure ratio is approximately equal to the engine pressure ratio (EPR).

C.1.3.6 Iteration Scheme

The iteration scheme used to determine engine conditions is outlined below.

1. Iterate EPR from lower limit to upper limit.
2. Set π_{FAN} equal to EPR.
3. Calculate τ_{FAN}, N_{FAN}, $P_{2.3}$ and $T_{2.3}$.
4. Set N_{LPC} equal to N_{FAN}.
5. Calculate τ_{LPC} and π_{LPC}, $P_{2.5}$ and $T_{2.5}$.

6. Iterate N_{HPC} from upper limit to lower limit.

7. Calculate $\dot{m}_{HPC}$, π_{HPC}, η_{HPC}, τ_{HPC}, $\dot{m}_{fuel}$, P_3 and T_3.

8. Calculate f, P_4, T_4, and MFP.

9. If $MFP > MFP_R$, return to 6, otherwise continue.

10. Calculate $T_{4.5}$.

11. Calculate T_5.

12. Calculate exhaust velocity and thrust.

13. If thrust > required thrust, return to 1, otherwise end.

C.2 Noise Model

C.2.1 Source Intensity

The noise generated by the aircraft is determined using the relationships developed in the NASA Aircraft Noise Prediction Program (ANOPP) [Zorumski, 1982]. Both the fan and jet noise are modeled in one-third octave bands (tertsbands) and in one degree increments from the longitudinal axis of the aircraft. The source model has been augmented with other propagation and human response models that account for the effects of atmospheric attenuation, excess ground attenuation, and the varying response of the human ear to noise at different frequencies.

C.2.1.1 Fan Noise

Fan noise is generated by several interactions between the rotor, stator, inlet guide vanes, and fan housing. In the empirical model used, each of the fan noise components are given by an expression of the form

$$p_{fan}^2 = \frac{A_{fan}^2 \Pi}{4\pi r^2} \frac{D(\theta)\, S(\eta)}{\left(1 - M_\infty \cos\theta\right)^4}, \tag{C-9}$$

where A_{fan} is the cross-sectional area of the fan, Π is the acoustic power function, r is the distance of the observer from the engine, D is the directivity function, S is the spectral

function, and $(1 - M_\infty \cos\theta)^4$ is the Doppler factor, that accounts for the effects of forward velocity [Heidmann, 1975; Zorumski, 1982].

C.2.1.2 Jet Noise

Jet noise is generated by the mixing of exhaust gases and shock-turbulence interaction. The expressions for both mixing and shock noise are complex functions of velocity, angle, relative density of the exhaust, relative temperature of the exhaust, and non-dimensionalized frequency. The details of the jet noise model may be found in the ANOPP Theoretical Manual [Zorumski, 1982].

C.2.2 Propagation and Attenuation

C.2.2.1 Atmospheric Attenuation

The attenuation of noise in the atmosphere is a function of frequency, temperature, humidity, and the distance the noise travels through the atmosphere. The atmospheric attenuation coefficient in decibels per 100 m is given by the relationship [Ruijgrok, 1993]

$$\alpha = 10^{\left[2.05\log\left(f_0/1000\right)+1.1394\times10^{-3}T-1.916984\right]} + \eta \times 10^{\left[\log\left(f_0\right)+8.42994\times10^{-3}T-2.755624\right]}, \qquad \text{(C-10)}$$

where η is given by

$$\eta = 4.1763\times10^{-5} + 1.2036\,\delta - 0.94116\,\delta^2 + 7.2373\,\delta^3 - 11.684\,\delta^4 + 5.1846\,\delta^5$$

for $\delta < 1$,

$$\eta = 1.9094 - 1.2295\delta + 0.39629\delta^2 - 6.9868\times10^{-2}\,\delta^3 + 6.5028\times10^{-3}\,\delta^4 - 2.4813\times10^{-4}\,\delta^5$$

for $1 \le \delta \le 7$, and

$$\eta = 0.199$$

for $\delta > 7$. The factor δ is given by

$$\delta = \sqrt{\frac{1010}{f_0}}\,10^{\left[\log(H)-1.328924+3.179768\times10^{-2}T\right]} \times 10^{\left[-2.173716\times10^{-4}T^2+8.42994\times10^{-6}T^3\right]}, \qquad \text{(C-11)}$$

where T is the temperature in °C,

H is the relative humidity in percent, and

f_0 is the tertsband center frequency in Hz.

C.2.2.2 Excess Ground Attenuation

When the sound source forms a shallow angle with respect to the observation point, the sound travels nearly parallel to ground of changing impedance. *Excess ground attenuation is the term used to represent the attenuation caused by the difference in the ground effect between the source and observation point.* Excess ground attenuation is a function of the distance between the source and the angle of the sound source with respect to the observation point. The total excess ground attenuation in decibels is given by A_d+A_θ., as defined next. The distance dependency A_d is given by [SAE, 1986]

$$A_d = 15.09\left(1 - e^{-0.00274\,d}\right)$$

for $d \leq 914m$, and

$$A_d = 13.86$$

for $d > 914m$., where d is the distance between the source and the observer. The angle dependency A_θ is given by

$$A_\theta = \frac{\left(3.96 - 0.066\,\theta + 9.9 \times e^{-0.13\theta}\right)}{13.86}$$

for $\theta \leq 60°$, and

$$A_\theta = 0$$

for $\theta > 60°$, where θ is the angle measured from the horizontal.

C.2.2.3 Human Frequency Response

The response of the human ear to sound depends on frequency. The sound pressure levels reported in this thesis use the A-Weighting scheme to account for this response. The A-weighting for a given tertsband is given in decibels by [Ruijgrok, 1993]

$$-145.528 + 98.262\log(f_0) - 19.509\left[\log(f_0)\right]^2 + 0.975\left[\log(f_0)\right]^3.$$

The weighting is added to the sound pressure level in each tertsband before they are summed to determine the total sound pressure level.

C.2.3 Noise Footprint

The algorithm to determine the noise impact around the airport was designed to minimize computational time, random access memory, and disk storage. In the algorithm, the surface around the airport is first divided into a grid aligned with the runway axis. In this discussion, a series of cells perpendicular to the runway axis will be referred to as rows, and a series of cells parallel to the runway axis will be referred to as columns. A grid size of 100m was used for all calculations, but the size of the grid cells may be specified by the user. The center of the grid is the threshold of the active runway. Each grid cell contains noise bins which span the range from the threshold noise level of 60 dBA to a maximum level of 140 dBA. The number stored in each bin is the number of times the noise exceeds the minimum level of that bin. Eight noise bins were used for all calculations, and they spanned the range from 60 dBA to 140 dBA.

At each aircraft location along a trajectory, the surface below the aircraft is searched by quadrants. The following description of the search algorithm applies to the front-right quadrant relative to the aircraft heading. The search begins with the grid cell below the aircraft. The search then goes to the cell that is right of that cell. If the noise level is greater than the threshold level, the number of hits in all the noise bins between the threshold level and the actual noise level is incremented, and the search then goes to the cell that is above the current cell. If the noise level is greater than the threshold level, the bins are incremented and the search continues along the column. The search continues until the noise level falls below the threshold. When this occurs, the search moves on to the first cell of the column that is right of the current column. This search pattern continues until the noise level in the first cell of the new column is below the threshold.

To account for instance where the noise levels directly below the aircraft are below the threshold while noise levels further out may exceed the threshold, a noise gradient constraint is placed on the search. If a cell has a noise level below the threshold but the noise gradient is positive (search is moving towards an area of higher noise levels) the search will continues until the noise level reaches the threshold or the noise gradient

becomes negative (the maximum noise level in that search direction is less than the threshold)

No memory is allocated for the grid cells at compilation. If the noise level in a cell is above the minimum threshold value, memory is allocated for that cell and it is added to a linked list. Therefore, although the grid structure is in place at the beginning of the search algorithm, no memory is allocated for any grid cell until it is determined that that cell experiences noise exposure greater than the threshold level. This dynamic allocation of memory restricts the total memory used, and allows the search algorithm to continue in whatever directions it needs to go without the restriction that would be encountered if memory for the entire grid was allocated during compilation.

D. Noise Boundaries

Certain noise sensitive communities have established maximum noise levels for aircraft operation. Once the maximum noise level is set, it is the job of the procedure designer to guarantee that the noise impact of aircraft operating near that community does not exceed the maximum allowed level. One method of incorporating these restrictions into the design of a noise abatement procedure is to simulate the noise impact of a wide range of trajectories and then determine which trajectories meet these noise restrictions. Another approach to the problem is to define a virtual region around the noise sensitive community, such that if an aircraft is outside this region, the noise level at all points in the noise sensitive community will not exceed the maximum allowed level. The surface of this region is the "Noise Boundary" for that noise sensitive community. This boundary is determined *a priori*, and defines the region in space (similar to terrain) from which aircraft must be excluded (Figure D-1). Since aircraft cannot penetrate the noise boundary, trajectories must either climb or turn to avoid the region.

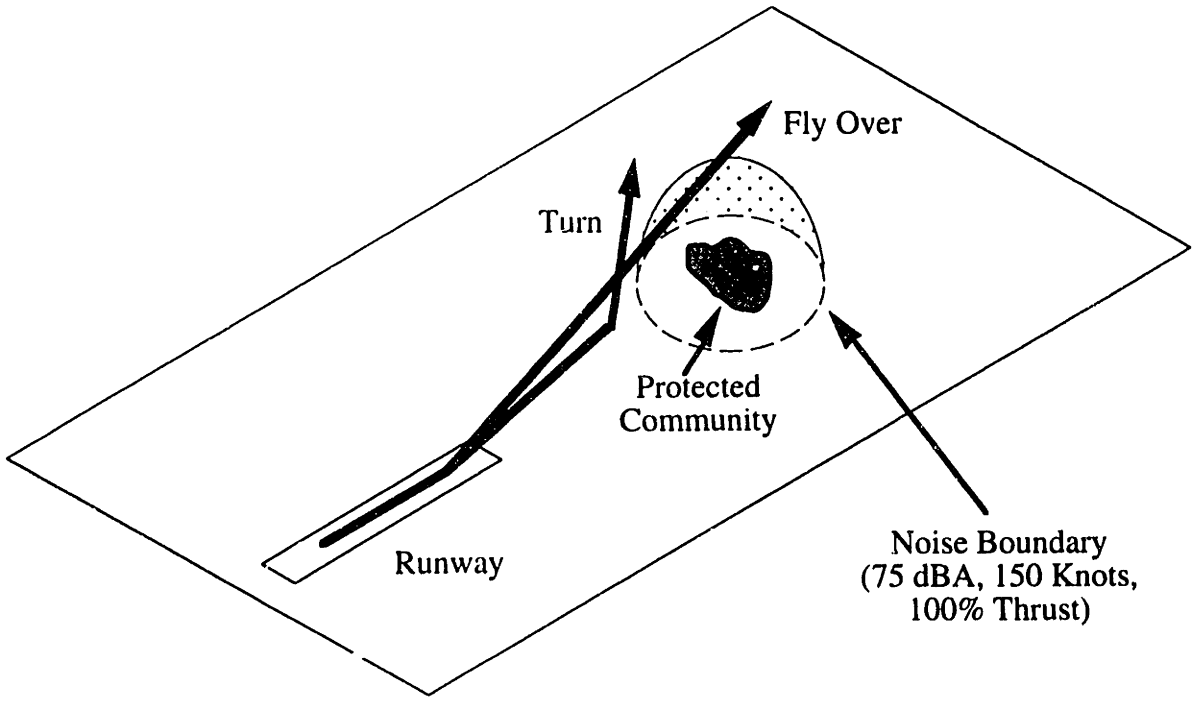

Figure D-1: Example of Noise Boundary

D.1 Direct Method

The direct method to determine the noise boundary for a community is to simulate the noise source at several locations in the region around the community and determine the points where the noise level in the community is equal to the maximum allowed level. The surface which includes all such points is the noise boundary. Since terrain can focus or diffuse sound, the noise level at any point in the community is a function of the source noise intensity, the distance from the source to the community, and the shape of the terrain around the community. The solution for a source over terrain of known shape is outlined below. The geometric constraints imposed on the sound by the terrain are combined with the temporal constraint implicit with the combination of two sound waves, into a delta function which is used to determine the points on the terrain which focus sound at the location of the receiver. For simplicity, the amplitude and phase of the reflected wave are assumed to be unchanged during reflection. This assumption does not change the results however, as the geometric and temporal constraints are unchanged. Corrections for amplitude and phase changes may be included in the algorithm that is derived.

Figure D-2 shows the geometry for a source moving at velocity v in air with ambient speed of sound c. In the figure, the source emits two sound waves, which interact at a given receiver location. The first wave emitted is reflected by the terrain, while the second wave travels directly to the receiver. In the figure, d is the distance the source travels between the instant it emits the reflected sound wave and the instant it emits the direct sound waves, R_I is the path length of the direct sound wave, R_{II} is the path length of the reflected sound wave from the source to the terrain, and R_T is the path length of the reflected sound wave from the terrain to the receiver. The angle γ is the flight path angle of the aircraft, θ_T is the angle between R_I and the horizon, θ_{II} is the angle between R_{II} and the horizon, and θ_T is the angle between R_T and the horizon. Similarly, ψ is the heading of the aircraft, ψ_I is the heading of R_I, ψ_{II} is the heading of R_{II}, and ψ_T is the heading of R_T. In this development, all reflections are assumed to be specular.

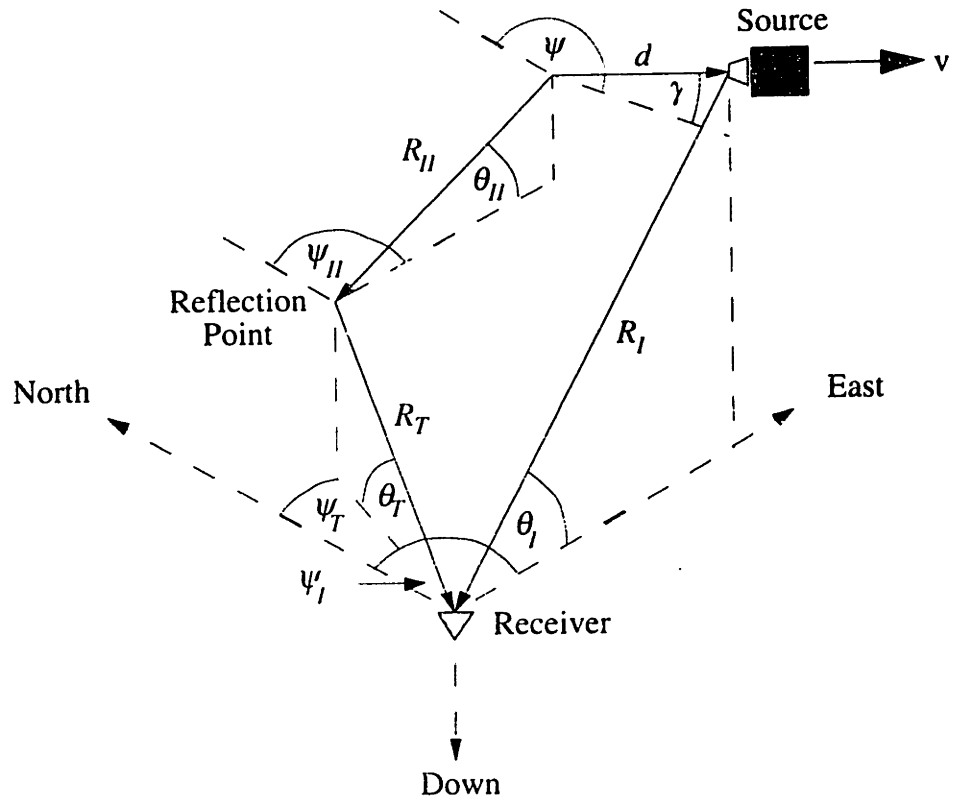

Figure D-2: Geometry of a moving source with sound reflections from the terrain.

The relationship between (ψ_T, θ_T) and (ψ_{II}, θ_{II}) must be consistent with the local gradient of the terrain. In the vertical plane, this relationship is given by

$$\theta_{II} = \theta_T + \pi - 2 \cdot \tan^{-1}\left(\frac{1}{R_T(\theta_T, \psi_T)} \frac{\partial R_T(\theta_T, \psi_T)}{d\theta_T} \right), \tag{D-1}$$

and in the horizontal plane

$$\psi_{II} = \psi_T + 2 \cdot \tan^{-1}\left(\frac{1}{R_T(\theta_T, \psi_T)} \frac{\partial R_T(\theta_T, \psi_T)}{d\psi_T} \right). \tag{D-2}$$

In the case for a stationary source, the time of origin of the sound does not matter since a reflected sound wave may interact with a direct sound wave which is produced at some later time. In the general case of a moving continuous source however, the motion of the source causes it to behave like a series of impulse sources at different locations. In order for two sound waves to interact at the same instance in time, they must meet the constraint imposed by the assumption of specular reflection as well as the temporal constraint which

is imposed by the velocity of the source. The temporal constraint requires that the difference in travel time of the direct and reflected sound must be equal to the time it takes the source to travel from the point of origin of the reflected sound to the point of origin of the direct sound, i.e.,

$$d = \frac{v}{c}\left(R_{II} + R_T - R_I\right) \tag{D-3}$$

When the temporal constraint is substituted into the expressions (in Cartesian Coordinates) for the difference between the vector R_I and the vector sum $R_T+R_{II}+d$, the following is obtained:

$$\begin{aligned}\Delta x = \; & R_I\left(\cos\theta_I \sin\psi_I + \frac{v}{c}\cos\gamma\sin\psi\right) \\ & - R_T\left(\cos\theta_T \sin\psi_T + \frac{v}{c}\cos\gamma\sin\psi\right) \\ & - R_{II}\left(\cos\theta_{II} \sin\psi_{II} + \frac{v}{c}\cos\gamma\sin\psi\right),\end{aligned} \tag{D-4}$$

$$\begin{aligned}\Delta y = \; & R_I\left(\cos\theta_I \cos\psi_I + \frac{v}{c}\cos\gamma\cos\psi\right) \\ & - R_T\left(\cos\theta_T \cos\psi_T + \frac{v}{c}\cos\gamma\cos\psi\right) \\ & - R_{II}\left(\cos\theta_{II} \cos\psi_{II} + \frac{v}{c}\cos\gamma\cos\psi\right),\end{aligned} \tag{D-5}$$

$$\begin{aligned}\Delta z = \; & R_I\left(\sin\theta_I + \frac{v}{c}\sin\gamma\right) \\ & - R_T\left(\sin\theta_T + \frac{v}{c}\sin\gamma\right) \\ & - R_{II}\left(\sin\theta_{II} + \frac{v}{c}\sin\gamma\right).\end{aligned} \tag{D-6}$$

where Δx, Δy, and Δz are the components of the difference in the path length of the direct sound and the reflected sound corrected for the motion of the source. When all three components of the path difference are simultaneously equal to zero, the temporal constraints are satisfied. Points on the terrain that satisfy the reflection constraints in equations D-1 and D-2, and the temporal constraint in equations D-4 through D-6, have reflections which reach the receiver at the same instant in time. Thus, the acoustic field at

the receiver is the sum of the field along the direct path and the fields along secondary paths where these constraints are met. When $v = 0$, these constraints reduce to the geometric solution for a stationary source.

In the direct method θ_I, ψ_I, R_I, θ_{II}, ψ_{II}, R_{II}, θ_T, ψ_T, and R_T must be known to determine whether a point on the terrain meets all the constraints. Four of these variables (θ_{II}, ψ_{II}, R_{II}, and R_T) are not independent, so the solution algorithm must iterate five (5) independent variables (θ_I, ψ_I, R_I, θ_T, ψ_T) to determine the noise boundary.

D.2 Reciprocal Method

The Reciprocal Method combines the principles of acoustic reciprocity and linear superposition to develop a reciprocal system. Solving the reciprocal problem, reduces the number of independent variables required to determine the noise boundary. In this approach, the source is placed at the receiver location, and only four (4) independent variables (θ_I, ψ_I, θ_T, ψ_T) are iterated to determine the solution.

D.2.1 Theory

Acoustic reciprocity is the principle that the position of a source and receiver may be interchanged without changing the sound pressure level that is measured (Figure D-3).

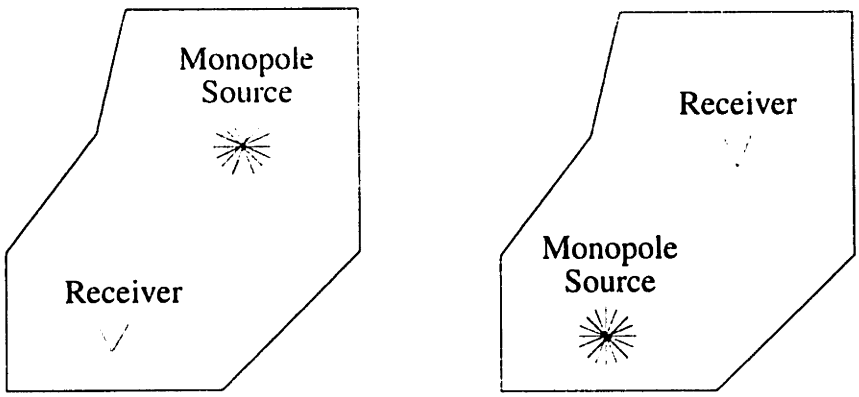

Figure D-3: Acoustic Reciprocity of a Monopole Source

Both systems shown are equivalent although the location of the source and the receiver are interchanged. Mathematically, the intensity of sound between any two points can be related by [Pierce, 1994]

$$\hat{p} = G_k(\mathbf{x}|\mathbf{x}_s)\,\hat{S}, \tag{D-7}$$

where

$$G_k(\mathbf{x}|\mathbf{x}_s)$$

is the Green's function for the surroundings, x is the receiver location and x_s is the source location. The Green's function is the same if source and receiver positions are interchanged. i.e.,

$$G_k(\mathbf{x}|\mathbf{x}_s) = G_k(\mathbf{x}_s|\mathbf{x}). \tag{D-8}$$

Therefore, switching the position of the source and receiver does not change the effects of the surroundings. Although the jet engine is not a single monopole source, at a sufficiently far distance it may be modeled as a compact collection of monopoles. The reciprocal method is most easily demonstrated for the case of a stationary continuous source over flat terrain (Figure D-4).

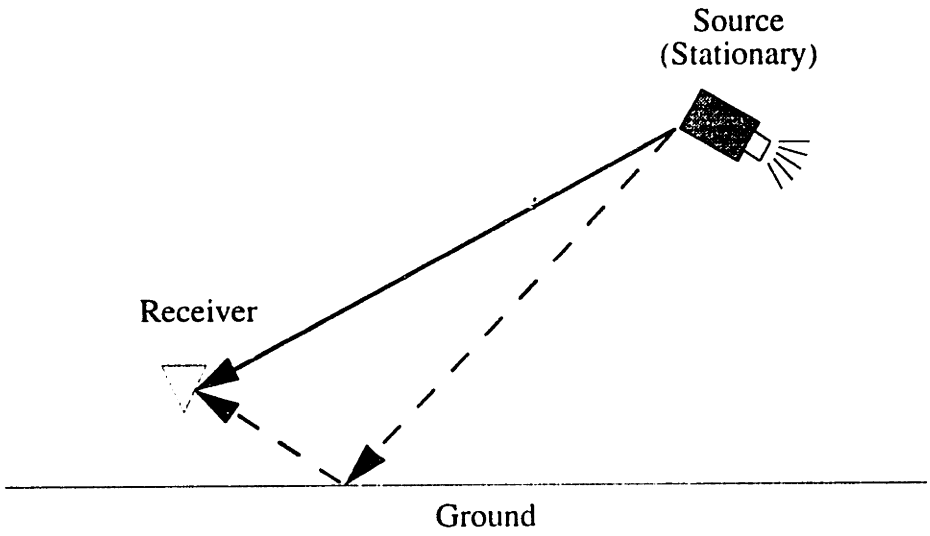

Figure D-4: Stationary Source Above Flat Ground Plane

The effect of the flat plane is modeled by an image receiver below the plane (Figure D-5a). This system is then split into two parts, a real part and an image part. The true measured signal is the sum of the two signals measured respectively at the real receiver location and at the image receiver location. This follows from the principle of linear superposition which guarantees that at any instant in time the pressure perturbation at the real receiver due to the source will be independent of the pressure perturbation at the image receiver due to the

source. The reciprocals of the real and image parts are determined by interchanging the position of the sources and receivers. Applying linear superposition for a second time to re-combine the reciprocals of the real and image parts gives the reciprocal for the entire system (Figure D-5b).

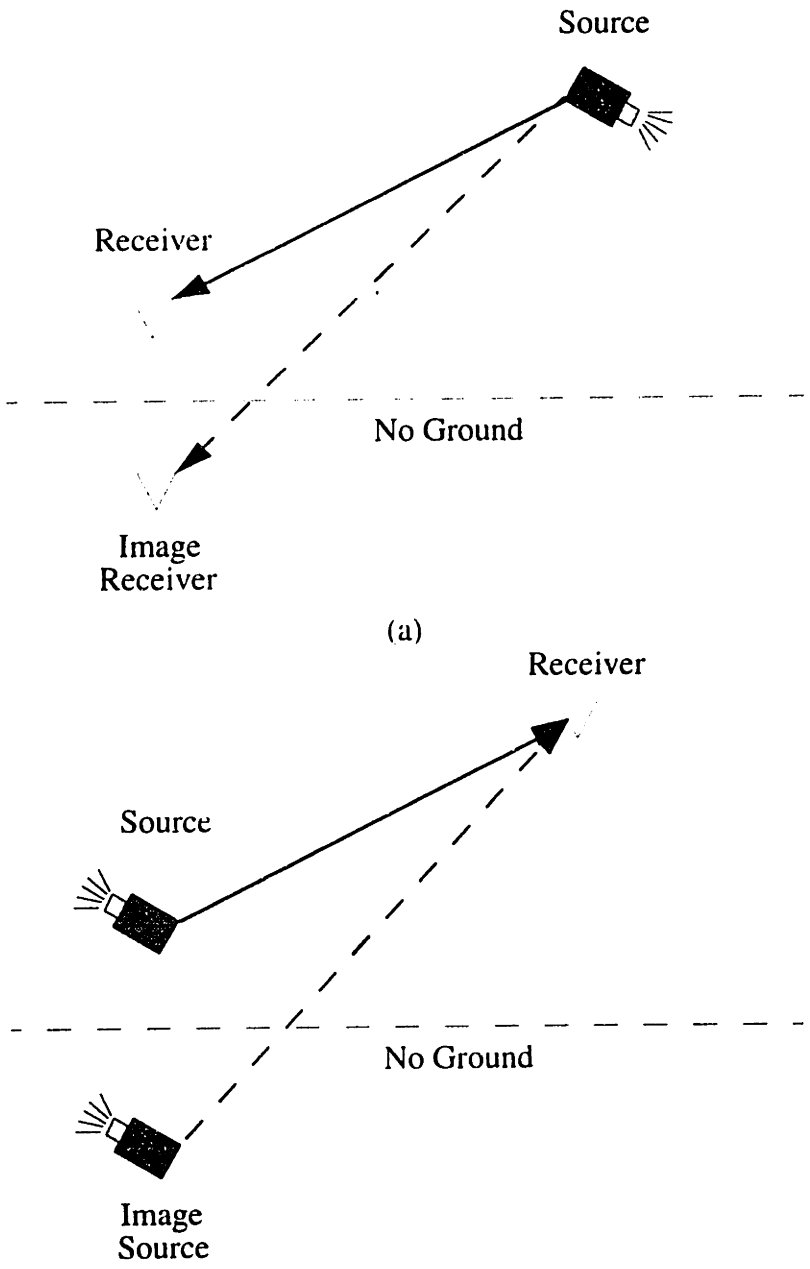

Figure D-5: (a) Direct System: Single Source with Real Receiver Above the Ground Plane and Image Receiver Below the Ground Plane. (b) Reciprocal System: Single Receiver with Real Source Above the Ground Plane and Image Source Below the Ground Plane.

D.2.2 Development

Returning to the problem addressed via the direct method: eliminating R_I and R_{II} by setting each of the three temporal constraints equal to zero, and combining these results with the condition that R_I and R_{II} must be positive gives six (6) inequalities with seven (7) variables. Three of those variables, θ_{II}, ψ_{II}, and R_T are functions of θ_T and ψ_T, therefore, the five (5) equalities that contain five (5) independent variables are transformed into six (6) inequalities containing four (4) independent variables. The inequalities are as follows:

$$R_T \frac{\left[\begin{array}{l}\left(\cos\theta_T \sin\psi_T + \frac{v}{c}\cos\gamma\sin\psi\right)\left(\sin\theta_I + \frac{v}{c}\sin\gamma\right) - \\ \left(\cos\theta_I \sin\psi_I + \frac{v}{c}\cos\gamma\sin\psi\right)\left(\sin\theta_T + \frac{v}{c}\sin\gamma\right)\end{array}\right]}{\left[\begin{array}{l}\left(\cos\theta_I \sin\psi_I + \frac{v}{c}\cos\gamma\sin\psi\right)\left(\sin\theta_{II} + \frac{v}{c}\sin\gamma\right) - \\ \left(\cos\theta_{II} \sin\psi_{II} + \frac{v}{c}\cos\gamma\sin\psi\right)\left(\sin\theta_I + \frac{v}{c}\sin\gamma\right)\end{array}\right]} > 0, \tag{D-9}$$

$$R_T \frac{\left[\begin{array}{l}\left(\cos\theta_T \sin\psi_T + \frac{v}{c}\cos\gamma\sin\psi\right)\left(\sin\theta_{II} + \frac{v}{c}\sin\gamma\right) - \\ \left(\cos\theta_{II} \sin\psi_{II} + \frac{v}{c}\cos\gamma\sin\psi\right)\left(\sin\theta_T + \frac{v}{c}\sin\gamma\right)\end{array}\right]}{\left[\begin{array}{l}\left(\cos\theta_I \sin\psi_I + \frac{v}{c}\cos\gamma\sin\psi\right)\left(\sin\theta_{II} + \frac{v}{c}\sin\gamma\right) - \\ \left(\cos\theta_{II} \sin\psi_{II} + \frac{v}{c}\cos\gamma\sin\psi\right)\left(\sin\theta_I + \frac{v}{c}\sin\gamma\right)\end{array}\right]} > 0, \tag{D-10}$$

$$R_T \frac{\left[\begin{array}{l}\left(\cos\theta_T \cos\psi_T + \frac{v}{c}\cos\gamma\cos\psi\right)\left(\sin\theta_I + \frac{v}{c}\sin\gamma\right) - \\ \left(\cos\theta_I \cos\psi_I + \frac{v}{c}\cos\gamma\cos\psi\right)\left(\sin\theta_T + \frac{v}{c}\sin\gamma\right)\end{array}\right]}{\left[\begin{array}{l}\left(\cos\theta_I \cos\psi_I + \frac{v}{c}\cos\gamma\cos\psi\right)\left(\sin\theta_{II} + \frac{v}{c}\sin\gamma\right) - \\ \left(\cos\theta_{II} \cos\psi_{II} + \frac{v}{c}\cos\gamma\cos\psi\right)\left(\sin\theta_I + \frac{v}{c}\sin\gamma\right)\end{array}\right]} > 0, \tag{D-11}$$

$$R_T \frac{\left[\begin{array}{l}\left(\cos\theta_T\cos\psi_T+\frac{v}{c}\cos\gamma\cos\psi\right)\left(\sin\theta_{II}+\frac{v}{c}\sin\gamma\right)- \\ \left(\cos\theta_{II}\cos\psi_{II}+\frac{v}{c}\cos\gamma\cos\psi\right)\left(\sin\theta_T+\frac{v}{c}\sin\gamma\right)\end{array}\right]}{\left[\begin{array}{l}\left(\cos\theta_I\cos\psi_I+\frac{v}{c}\cos\gamma\cos\psi\right)\left(\sin\theta_{II}+\frac{v}{c}\sin\gamma\right)- \\ \left(\cos\theta_{II}\cos\psi_{II}+\frac{v}{c}\cos\gamma\cos\psi\right)\left(\sin\theta_I+\frac{v}{c}\sin\gamma\right)\end{array}\right]} > 0, \tag{D-12}$$

$$R_T \frac{\left[\begin{array}{l}\left(\cos\theta_T\sin\psi_T+\frac{v}{c}\cos\gamma\sin\psi\right)\left(\cos\theta_I\cos\psi_I+\frac{v}{c}\cos\gamma\cos\psi\right)- \\ \left(\cos\theta_I\sin\psi_I+\frac{v}{c}\cos\gamma\sin\psi\right)\left(\cos\theta_T\cos\psi_T+\frac{v}{c}\cos\gamma\cos\psi\right)\end{array}\right]}{\left[\begin{array}{l}\left(\cos\theta_I\sin\psi_I+\frac{v}{c}\cos\gamma\sin\psi\right)\left(\cos\theta_{II}\cos\psi_{II}+\frac{v}{c}\cos\gamma\cos\psi\right)- \\ \left(\cos\theta_{II}\sin\psi_{II}+\frac{v}{c}\cos\gamma\sin\psi\right)\left(\cos\theta_I\cos\psi_I+\frac{v}{c}\cos\gamma\cos\psi\right)\end{array}\right]} > 0, \tag{D-13}$$

$$R_T \frac{\left[\begin{array}{l}\left(\cos\theta_T\sin\psi_T+\frac{v}{c}\cos\gamma\sin\psi\right)\left(\cos\theta_{II}\cos\psi_{II}+\frac{v}{c}\cos\gamma\cos\psi\right)- \\ \left(\cos\theta_{II}\sin\psi_{II}+\frac{v}{c}\cos\gamma\sin\psi\right)\left(\cos\theta_T\cos\psi_T+\frac{v}{c}\cos\gamma\cos\psi\right)\end{array}\right]}{\left[\begin{array}{l}\left(\cos\theta_I\sin\psi_I+\frac{v}{c}\cos\gamma\sin\psi\right)\left(\cos\theta_{II}\cos\psi_{II}+\frac{v}{c}\cos\gamma\cos\psi\right)- \\ \left(\cos\theta_{II}\sin\psi_{II}+\frac{v}{c}\cos\gamma\sin\psi\right)\left(\cos\theta_I\cos\psi_I+\frac{v}{c}\cos\gamma\cos\psi\right)\end{array}\right]} > 0. \tag{D-14}$$

The algorithm used to determine the noise boundary iterates the four independent variables outlined above. The algorithm is presented below.

1. Set the azimuth angle ψ_I and the elevation angle θ_I to the noise boundary.
2. Divide the radial in that direction into segments of equal length.
3. Create an array with a cell for each radial segment.
4. Populate each cell with the mean square acoustic pressure at that distance along the direct path from the source (now at the receiver location).
5. Search the terrain $\left(0 \le \psi_T < 2\pi, \quad -\infty < \theta_T < +\infty\right)$ for points which satisfy all six inequalities.

6. If a point is found, evaluate R_I and R_{II}, then add the mean square acoustic pressure for a sound wave that is reflected by that point to the array cell corresponding to that distance.

7. Return to step 1 and increment the respective angles.

D.2.3 2D Solution

When an aircraft is flying directly towards a sensitive location, and the terrain around the location is such that the noise emitted to either side of the aircraft track is not reflected towards the receiver, the problem reduces to two dimensions. In this case, $\psi_I = \psi_{II} = \psi_T = \psi + \pi$, and the inequalities reduce to

$$R_T \frac{\left[\left(\cos\theta_T - \frac{v}{c}\cos\gamma\right)\left(\sin\theta_I + \frac{v}{c}\sin\gamma\right) - \left(\cos\theta_I - \frac{v}{c}\cos\gamma\right)\left(\sin\theta_T + \frac{v}{c}\sin\gamma\right)\right]}{\left[\left(\cos\theta_I - \frac{v}{c}\cos\gamma\right)\left(\sin\theta_{II} + \frac{v}{c}\sin\gamma\right) - \left(\cos\theta_{II} - \frac{v}{c}\cos\gamma\right)\left(\sin\theta_I + \frac{v}{c}\sin\gamma\right)\right]} > 0, \quad \text{(D-15)}$$

$$R_T \frac{\left[\left(\cos\theta_T - \frac{v}{c}\cos\gamma\right)\left(\sin\theta_{II} + \frac{v}{c}\sin\gamma\right) - \left(\cos\theta_{II} - \frac{v}{c}\cos\gamma\right)\left(\sin\theta_T + \frac{v}{c}\sin\gamma\right)\right]}{\left[\left(\cos\theta_I - \frac{v}{c}\cos\gamma\right)\left(\sin\theta_{II} + \frac{v}{c}\sin\gamma\right) - \left(\cos\theta_{II} - \frac{v}{c}\cos\gamma\right)\left(\sin\theta_I + \frac{v}{c}\sin\gamma\right)\right]} > 0. \quad \text{(D-16)}$$

When an aircraft is flying directly away from a sensitive location, and the terrain does not reflect noise emitted to either side towards the receiver, then $\psi_I = \psi_{II} = \psi_T = \psi$ and the inequalities reduce to

$$R_T \frac{\left[\left(\cos\theta_T + \frac{v}{c}\cos\gamma\right)\left(\sin\theta_I + \frac{v}{c}\sin\gamma\right) - \left(\cos\theta_I + \frac{v}{c}\cos\gamma\right)\left(\sin\theta_T + \frac{v}{c}\sin\gamma\right)\right]}{\left[\left(\cos\theta_I + \frac{v}{c}\cos\gamma\right)\left(\sin\theta_{II} + \frac{v}{c}\sin\gamma\right) - \left(\cos\theta_{II} + \frac{v}{c}\cos\gamma\right)\left(\sin\theta_I + \frac{v}{c}\sin\gamma\right)\right]} > 0, \quad \text{(D-17)}$$

$$R_T \frac{\left[\left(\cos\theta_T + \frac{v}{c}\cos\gamma\right)\left(\sin\theta_{II} + \frac{v}{c}\sin\gamma\right) - \left(\cos\theta_{II} + \frac{v}{c}\cos\gamma\right)\left(\sin\theta_T + \frac{v}{c}\sin\gamma\right)\right]}{\left[\left(\cos\theta_I + \frac{v}{c}\cos\gamma\right)\left(\sin\theta_{II} + \frac{v}{c}\sin\gamma\right) - \left(\cos\theta_{II} + \frac{v}{c}\cos\gamma\right)\left(\sin\theta_I + \frac{v}{c}\sin\gamma\right)\right]} > 0. \quad \text{(D-18)}$$

The algorithm that is employed in the 2D case is presented below.

1. Set the elevation angle θ_I to the noise boundary.

2. Divide the radial in that direction into segments of equal length.

3. Create an array with a cell for each radial segment.

4. Populate each cell with the mean square acoustic pressure that would be felt at that distance if the source was at the receiver location.

5. Search the terrain $(-\infty < \theta_T < +\infty)$ for points which satisfy both inequalities.

6. If a point is found, evaluate R_I and add the mean square acoustic pressure for a sound wave that is reflected by that point to the array cell corresponding to that distance.

7. Return to step 1 and increment the elevation angle.

If the terrain can be described by an analytic function $R_T(\theta_T)$, then $\theta_{//}$ will be described by an analytic function. For example, flat terrain is described by the function

$$R_T = \frac{-h}{\sin\theta_T} \text{ for } -\pi < \theta_T < 0, \tag{D-19}$$

where h is the height of the receiver above the terrain. In this case, the analytic function relating $\theta_{//}$ and θ_T is

$$\theta_{//} = 2 \cdot \tan^{-1}\left(\frac{1}{\tan\left(\frac{\theta_T - \pi}{2}\right)}\right). \tag{D-20}$$

In most cases, however, the values of $\theta_{//}$ must be derived numerical from a terrain database.

D.3 Parameters

The parameters which define the noise boundary are the maximum noise level allowed in the noise sensitive community, the thrust of the aircraft, the speed of the aircraft, the attitude of the aircraft, and the shape of the terrain around the community. If the maximum noise level is fixed, as is the shape of the terrain, there exists a family of noise boundaries corresponding to different combinations of thrust level, speed, and attitude (Figure D-6). Therefore, an aircraft can change the dimensions of the noise boundary by varying its thrust level, speed, and/or attitude. This physical representation is useful to the procedure designer in deciding the minimum climb gradients, maximum speeds, and thrust levels during a noise abatement procedure. For example, a procedure may require an aircraft to

lower its thrust or speed and make a closer approach to the noise sensitive community, while still not exceeding the noise limit.

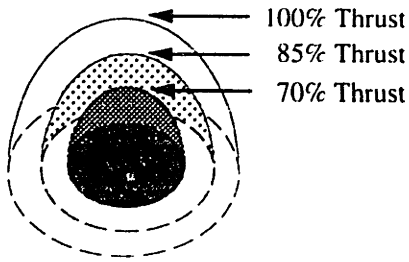

Figure D-6: Family of Exclusion Zones for 70%, 85%, and 100% Thrust.